Electrostatic Trapping as a Self-consistent Phenomenon in Plasmas and Other Collective Systems

Von der Universität Bayreuth
zur Erlangung des Grades eines
Doktors der Naturwissenschaften (Dr. rer. nat.)
genehmigte Abhandlung

vorgelegt von

Alejandro Luque Estepa
geboren am 23. Oktober 1978 in Sevilla, Spanien

1. Gutachter:	Prof. Dr. H. Schamel
2. Gutachter:	Prof. L. Kramer PhD.

Tag der Einreichung:	22.10.2004
Tag des Kolloquiums:	17.2.2005

Deutsche Zusammenfassung

Diese Doktorarbeit beschäftigt sich mit selbstkonsistenten elektrostatischen Strukturen in Plasmen und verwandten kollektiven Systemen. Damit sind kohärente Strukturen gemeint, für die der Einfang von Teilchen bzw. Pseudoteilchen im Potenzial der Welle verantwortlich ist. Die Phänomene, um die es geht, benötigen eine kinetische Beschreibung, d.h. eine Beschreibung, in der die Geschwindigkeitsverteilung der Teilchen voll berücksichtigt wird. Sie erweitern dadurch den Spielraum, den ein Plasma hat, um instabil zu werden.

Das zentrale Anliegen und Ergebnis der Arbeit, um es gleich vorweg zunehmen, ist es, dass es Störungen eines Plasmagleichgewichtes der genannten Art gibt, die das Plasma destabilisieren, obwohl eine lineare Stabilitätstheorie stabile Verhältnisse vorhersagt. Der in der Plasmatheorie übliche Weg, die Stabilität eines Plasmas anhand linearisierter Gleichungen zu charakterisieren, wird deshalb in Frage gestellt. Teilcheneinfang ist ein grundsätzlich nichtlinearer Prozess, der auch dann vorliegt, wenn die Wellenanregung schwach ist.

Der Einfluss des Teilcheneinfangs ist deshalb nicht an die Bedingung endlicher Amplitude, wie oft angenommen, geknüpft und muss deshalb von Anfang an berücksichtigt werden, will man zu allgemein gültigen Aussagen über Stabilität und assozierten anomalen Transport gelangen. Es ist deshalb nicht verwunderlich, dass das Problem des anomalen Transports ein bisher nicht abgeschlossenes Kapitel der Plasmatheorie darstellt, belegt durch viele Beispiele aus der Fusions- und Weltraumforschung, wo nahezu stoßfreie, stromgetriebene Plasmen vorliegen.

Teilcheneinfang ist jedoch nicht beschränkt auf klassische Plasmen. Ein weiteres Anliegen dieser Arbeit ist es, zu zeigen, dass der gewählte Formalismus auch auf andere Systeme, die kollektives Verhalten zeigen, übertragen werden kann. Insbesondere ist eine quantenmechanische Erweiterung möglich, die es uns gestattet, quanten-artige Systeme zu untersuchen und eine Verbindung zwischen elektrostatischem Teilcheneinfang in Plasmen und Enveloppe-Solitonen in nichtlinearen optischen Medien, wie z.B. in Glasfasern, herzustellen. Das longitudinale Verhalten von Teilchenstrahlen in zirkularen Beschleunigern und Speicherringen stellt ein weiteres Beispiel kollektiver Systeme dar, in denen das Phänomen des Teilcheneinfangs eine wesentliche Komponente der Dynamik darstellt.

Die Arbeit besteht aus fünf Kapiteln. In der Einführung (Kapitel 1) präsentieren wir eine Motivation zum Thema, geben einen kurzen Überblick über den theoretischen

Hintergrund und stellen das Vlasov-Poisson System, die gültige nichtlineare kinetische Beschreibung im Falle vernachlässigbarer Stöße, vor. In Kapitel 2 untersuchen wir die Auswirkungen des Teilcheneinfangs auf klassische Plasmen, die wir in Kapitel 3 auf Quantenplasmen und andere quanten-artige Systeme übertragen. In Kapitel 4 beschäftigen wir uns mit der Beschreibung solitärer Strukturen, wie sie experimentell in Teilchenbeschleunigern gefunden wurden. Zum Schluß, in Kapitel 5, geben wir eine kurze Zusammenfassung und Schlussfolgerungen der Arbeit, nachdem eine ausführlichere Zusammenfassung der Ergebnisse bereits am Ende eines jeden Kapitels vorgelegt wurde.

Klassische Plasmen

Dieser Abschnitt befasst sich mit dem Einfluss gefangener Teilchen auf die Dynamik eines zweikomponentigen, stromführenden Plasmas. Wir stellen die von Schamel(1972) in das Vlasov-Poisson System eingeführte Pseudo-Potenzialmethode vor, die gegenüber der in der Literatur üblichen BGK (Bernstein-Greene-Kruskal)-Methode u.a. den Vorteil hat, dass physikalisch nicht vertretbare Verteilungsfunktionen von vornherein ausgeschlossen werden können. Danach beschäftigen wir uns mit einer systematischen Erforschung bisher unbekannter Strukturen und finden z.B. eine alternierende Kette von Elektronen- und Ionenlöchern. Wir untersuchen dann die Energie solcher Strukturen und leiten dafür eine analytische Formel her, sowie vereinfachte Ausdrücke für solitare Elektronen- und Ionenlöcher und für harmonische Potenziale. Wir finden, dass es in einem großen Bereich des Parameterraumes strukturierte Plasmen gibt, die eine niedrigere Energie aufweisen als Plasmen ohne Struktur. Solche Strukturen werden der Kürze halber Strukturen mit negativer Energie genannt. Wir zeigen beispielsweise, dass Ionenlöcher negativer Energie für jede ausgewählte Driftgeschwindigkeit zwischen Elektronen und Ionen und für jedes Temperaturverhältnis existieren. Dies hat, wie sich später zeigen wird, wichtige Konsequenzen für die Stabilität eines stromführenden Plasmas.

Wir beschreiben dann einen numerischen Code, mit dem wir die zeitliche Entwicklung des Systems verfolgen können. Dieser Code basiert auf einer kinetischen Beschreibung beider Teilchensorten, Elektronen und Ionen, und verwendet eine Fourier-Hermite-Zerlegung der Verteilungsfunktionen, anhand derer das Vlasov-Poisson System aufintegriert werden kann. Die Evolutionsgleichungen für die Koeffizienten dieser Zerlegungung werden mittels eines Runge-Kutta Verfahrens vierter Ordnung gelöst. Auch schwache Stöße können im Rahmen einer Fokker-Planck Gleichung berücksichtig werden. Dieser Code wird dann benützt, um elektrostatische Strukturen in schwach dissipativen Plasmen aufzusuchen, nachdem wir uns durch eine Reihe von Tests von der Zuverlässigkeit des Codes überzeugen konnten. Wir finden, dass elektrostatische Gleichgewichtstrukturen mit gefangenen Teilchen auch bei schwachen Stößen dauerhaft existieren können, sobald ein äußeres homogenes elektrisches Feld dazu geschaltet wird.

Dann wenden wir uns dem Stabilitätsproblem des Plasmas zu und stellen die Hypothese auf, dass eine nichtlineare Instabilität mit der Existenz und dem spontanen Auftreten einer Struktur negativer Energie verknüpft ist. Wir zeigen, dass eine lineare Theorie die Plasmastabilität nicht vollständig beschreiben kann, insbesondere dann nicht, wenn es im linear stabilen Bereich zu einer Instabilität des Plasmas kommt. Wir zeigen dies numerisch durch zwei verschiedene Läufe mit dem Code, beide im linear stabilen Bereich. Einmal verwenden wir als Anfangsbedingung ein Ionenloch mit negativer Energie, ein zweites Mal ein solches mit positiver Energie. In beiden Fällen erscheint spontan eine

neue, ionenlochartige Struktur, die explosionsartig anwächst und sich schneller als das ursprüngliche Ionenloch bewegt. Das System ist trotz linearer Stabilität nichtlinear instabil. Es ist anzunehmen und wir haben erste Belege dafür, dass diese neue Struktur eine solche negativer Energie ist. Wir kommen deshalb zu einem neuen Paradigma der Plasmastabilität, in dessen Mittelpunkt Phasenraumstrukturen negativer Energie stehen.

Im Anhang A verwenden wir zusätzlich einen PIC (Particle-In-Cell) Code und zeigen auf eine zweite unabhängige Weise, dass sich kohärente elektrostatische Strukturen auch aus dem thermischen Rauschen heraus entwickeln können, selbst im Bereich linearer Stabilität.

Quantenplasmen

In Kapitel 3 der Arbeit wird die Theorie elektrostatischer Strukturen auf Quantenplasmen erweitert. Aus diesem Grunde wählen wir die Wigner-Beschreibung der Quantenmechanik. Sie beruht auf Pseudo-Verteilungsfunktionen im Phasenraum, die sich gemäß der von Neumann Gleichung zeitlich entwickeln. Wir bringen eine kurze Einführung in diesen Formalismus und erwähnen die unterschiedliche Interpretation für reine und gemischte Zustände. Danach berechnen wir analytisch die Quantenkorrekturen für nichtpropagierende Elektronenlöcher und machen dabei Gebrauch von der Kleinheit des dimensionslosen Verhältnisses von de Broglie- und Debye-Wellenlänge. Das Ergebnis ist, dass Quantenkorrekturen eine Annäherung des Systems an das thermische Gleichgewicht bringen.

Diese Methode wird dann auf andere physikalische Systeme übertragen, die durch eine nichtlineare Schrödinger Gleichung bzw. durch eine kinetische Gleichung für Pseudoteilchen, wie Photonen, beschrieben werden. So können wir durch eine Abwandlung der Potenzialmethode eine Verbindung zwischen der Existenz von Solitonen in nichtlinearen optischen Medien und dem Teilcheneinfang in Plasmen herstellen. Wir präsentieren eine Näherungslösung zur exakt lösbaren kubischen Schrödinger Gleichung und erweitern sie auf beliebige Nichtlinearitäten.

Teilchenstrahlen

Schließlich untersuchen wir in Kapitel 4 die Existenz kohärenter Strukturen in Strahlen geladener Teilchen in zirkularen Beschleunigern und Speicherringen. Zuerst referieren wir über die Existenz von lokalisierten Strukturen („Solitonen“) in einem homogenen und damit den gesamten Ring umfassenden Teilchenstrahl (coasting beam) und geben auch eine verbesserte Fokussierungsbedingung für den Teilchenstrahl an. Dann beschäftigen wir uns mit Teilchenpaketen (bunched beams) und erwähnen eine gängige Beschreibung, die auf Vereinfachungen in der transversalen Strahlgeometrie und in den Feldern beruht. Basierend auf diesem Modell, entwickeln wir ein iteratives Verfahren zur numerischen Bestimmung zeitunabhängiger Lösungen und finden erstmalig Lösungen, die eine lokale, dem Teilchenpaket aufgeprägte Verdichtung beschreiben im Einklang mit neueren Messungen. Auch Lösungen mit lokalen, den Löchern in Plasmen analogen Verdünnungen werden gefunden, deren experimentelle Bestätigung jedoch noch aussteht.

Zusammenfassend können wir sagen, dass die Arbeit die hohe Bedeutung des Teilcheneinfangs in der nichtlinearen Dynamik kollektiver Systeme belegt, für den wir eine, über

das klassische Plasma hinausgehende Beschreibung vorgelegt und untersucht haben. Damit wurde eine Basis gelegt zum verbesserten Verständnis von Plasmen und verwandten Systemen insbesondere im Hinblick auf Stabilität und anomalen Transport.

Contents

List of Figures

CHAPTER 1

Introduction

Little flower— but if I could understand
What you are, root and all, and all in all...

Lord Alfred Tennyson

This work investigates electrostatic trapping in plasmas and related systems. Plasmas are characterized by the non negligible presence of charged particles and commonly estimated to compose up to 99% of the apparent universe. In a plasma, the long-range Coulomb force exerted on the particles by the many distant ones is a factor in determining their statistical properties, usually much more important than the interaction with near neighbors. Due to this character, collective phenomena, which are the main subject of plasma physics, strongly influence the behavior of the system. The interior of stars and gas planets, the magnetosphere and ionosphere layers of our atmosphere, the electric discharges of lightnings and light arcs, large experimental setups like particle accelerators and tokamaks and also a small flame are common examples of systems studied in plasma physics. Needless to say, such a huge range of physical conditions can be modeled by many different descriptions and choosing the appropriate one under each circumstance is already an important and nontrivial issue in plasma physics.

The earliest theoretical developments were made from a macroscopic point of view and by means of a fluid like (hydrodynamical) description which disregards the velocity spread of particles at a given position. However, it became soon evident that there exists an interesting spectrum of phenomena that can only be described if one takes also into account the velocity distribution. A kinetic theory was hence developed by Vlasov [1] and Landau [2] based on the Vlasov-Poisson or more generally the Vlasov-Maxwell system of equations that introduced into the discipline a rich world of waves. Although initially the theory was based on a linearization of the equations, it was later supplemented by investigations on wave-particle resonances which brought nonlinearity into play.

The relevance of nonlinear kinetic models is also underlined by one of the most challenging practical applications of modern plasma physics, namely the development of a

controlled fusion reactor. In order to sustain the high temperatures and densities needed inside such a device, the importance of a deep understanding of transport processes and current- and gradient-driven instabilities, which are the main obstacles for the desired increase in confinement times, can be hardly overemphasized. However, since the fluid model considers only average quantities in velocity space, it is not capable of properly describing instabilities or damping phenomena. The kinetic model, on the other hand, provides an accurate description of energy-exchange processes between particles and waves, which are proved to be important especially in a collisionless plasma and which play important roles in plasma heating by waves and in the mechanisms of instabilities.

Inside kinetic models, many of the studies on transport phenomena are based on a linearization of the governing equations, from which *anomalous transport* models, such as quasilinear theories and weak or strong plasma turbulence theories are developed ignoring fundamental nonlinearities such as particle trapping. Among the observed phenomena that essentially escape from a linear treatment are magnetic reconnection processes, found in the solar dynamics as well as in the magnetotail in the Earth's magnetosphere, in which they are thought to be the precursors of auroral sub-storms. But also purely electrostatic structures, which are the main topic of the present work, such as double layers and phase space vortices are commonly observed nonlinear phenomena in the outer layers of the atmosphere, in the ionosphere and in the magnetosphere. The nonlinear world of collective trapping, hence, will be the focus of this thesis.

1.1 Theoretical background

In the following chapters we will deal with different systems from classical plasmas to quantum plasmas to particle beams in accelerators. For all of them we will study phenomena that require a kinetic description that will always be based on the Vlasov-Poisson system of equations or an analogue thereof, which we may call Vlasov-Poisson-like system. It is therefore appropriate to review some properties of such equations.

1.1.1 The Vlasov equation

In classical plasmas, the Vlasov equation, which is sometimes also called *collisionless Boltzmann equation*, can be easily derived if we think of a statistical system being described by a distribution function in phase space $f(\mathbf{x}, \mathbf{p}; t)$, in which every particle *carries* with it the value of f or, to speak in a more formal way, the distribution function is constant along the trajectory of any particle: $df/dt = 0$. The total derivative can be decomposed in a local and a convective term:

$$\frac{d}{dt} = \frac{\partial}{\partial t} + \frac{d\mathbf{x}}{dt} \cdot \frac{\partial}{\partial \mathbf{x}} + \frac{d\mathbf{p}}{dt} \cdot \frac{\partial}{\partial \mathbf{p}}. \tag{1.1}$$

On the other hand, if the single-particle Hamiltonian of the system is H, the evolution equations can be written as

$$\frac{d\mathbf{x}}{dt} = \frac{\partial H}{\partial \mathbf{p}}, \qquad \frac{d\mathbf{p}}{dt} = -\frac{\partial H}{\partial \mathbf{x}}. \tag{1.2}$$

This leads to a Liouville equation for the evolution of the distribution function

$$\frac{\partial f}{\partial t} + \{f, H\} = 0, \tag{1.3}$$

where $\{\cdot,\cdot\}$ denotes the Poisson bracket defined by

$$\{f,g\} := \frac{\partial f}{\partial \mathbf{x}} \cdot \frac{\partial g}{\partial \mathbf{p}} - \frac{\partial g}{\partial \mathbf{x}} \cdot \frac{\partial f}{\partial \mathbf{p}}. \tag{1.4}$$

If we assume that each particle has charge q and mass m and is affected by an electrostatic potential $\Phi(\mathbf{x};t)$, the Hamiltonian would read $H = \mathbf{p}^2/2m + q\Phi(\mathbf{x};t)$, where $\mathbf{p} = m\mathbf{v}$, and (1.3) would be written as

$$\frac{\partial f}{\partial t} + \frac{\mathbf{p}}{m} \cdot \frac{\partial f}{\partial \mathbf{x}} - q\nabla\Phi \cdot \frac{\partial f}{\partial \mathbf{p}} = 0. \tag{1.5}$$

This is the most known form of the nonrelativistic Vlasov equation in electrostatic approximation, which we use throughout this thesis, mainly in chapter 2. In principle, there will exist one Vlasov equation for each species in the plasma. However, it is often appropriate to use a mixed description of the system, which includes a kinetic treatment for one or several species while the others are described by fluid equations or are even considered as immobile.

In addition to (1.5), there are some other similar equations that may play a similar role as the Vlasov equation in different systems. In section 2.4.1 we study how to include the effects of weak collisions by means of the Fokker-Planck operator. In chapter 3 we use the quantum analogue to the Vlasov equation, the von Neumann equation. This one can also be applied to the study of systems very different from plasmas, namely nonlinear optical fibers. Finally, in chapter 4 we retake the form of Vlasov equation represented by (1.3) when dealing with the longitudinal dynamics of charged particle beams in particle accelerators and storage rings. We call all these equations *Vlasov-like equations*.

1.1.2 The Poisson and Poisson-like equations

The electrostatic potential $\Phi(\mathbf{x};t)$ introduced in (1.5) may have several sources: (a) an external one, which the experimenter imposes and over which he has (supposedly) complete control and (b) the field that the charged particles of the plasma create themselves. The overall effect of external fields is usually a drift between species with different charges (electron and ions), making the plasma carry a current. We concern ourselves with current-carrying plasmas in chapter 2. The internal field, on the other hand, will be called *self-consistent* field. The equation governing the self-consistent potential is Poisson's equation:

$$\nabla^2\Phi(x;t) = -\frac{\rho(\mathbf{x};t)}{\epsilon_0}, \tag{1.6}$$

where ρ is the local charge density which is in turn determined by the distribution functions. For a two-species plasma of electrons and single charged ions we can write it as

$$\rho(\mathbf{x};t) = en_i - en_e = \int d^3\mathbf{p}\, ef_i(\mathbf{x},\mathbf{p};t) - \int d^3\mathbf{p}\, ef_e(\mathbf{x},\mathbf{p};t). \tag{1.7}$$

Equation (1.6), usually merged with (1.7), is the equation governing the formation of a self-consistent field in classical plasmas and it is intensively studied in chapter 2. But the phenomena we deal with in this thesis are by no means restricted to these equations. In general, any equation that lets us determine the field Φ in (1.5) from the distribution

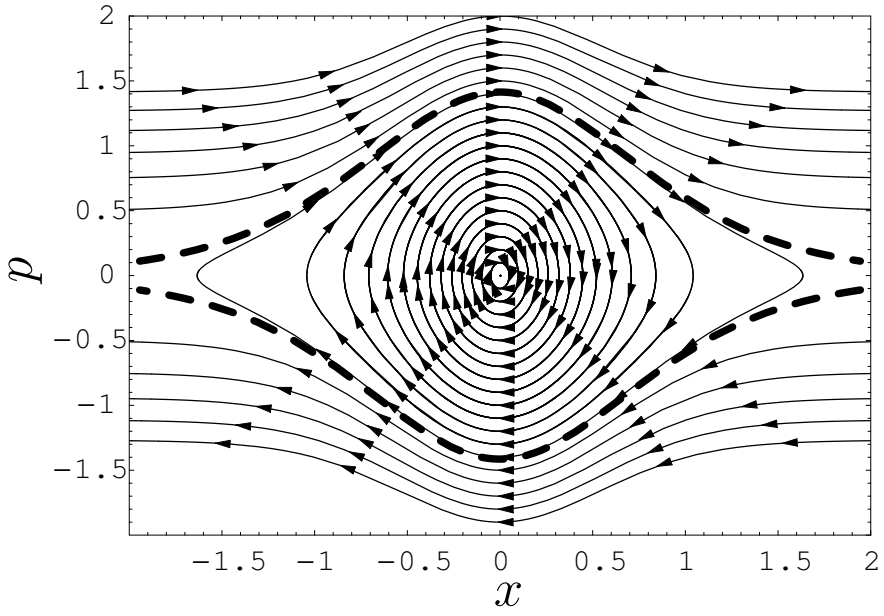

Figure 1.1: Possible trajectories in phase space of free and trapped particles. The dashed lines represent the separatrix, which is the boundary between the zones of trapped (inside) and free (outside) particles. Due to its shape, this kind of separatrix is commonly called O-type separatrix.

functions will be called *Poisson-like* equation. For example, in section 3.3 we study systems in which Φ does not stand for an electrostatic potential but instead represents the refractive index of a nonlinear optical medium and is coupled with the distribution function through an equation quite different from (1.7).

Finally, note that though the Vlasov equation is linear if the electrostatic potential is given, it forms a nonlinear system when it is coupled with (1.6) and (1.7). The nonlinearity of our system plays a crucial role in the kind of phenomena that we treat in this work.

1.2 Trapping in Vlasov-Poisson-like systems

The concept of trapping in plasmas came out when the resonant interaction between waves and particles was treated rigorously and nonlinearly. Trapping means that some of the plasma particles are confined to a finite region of the phase space where they bounce forth and back, describing closed trajectories. Figure 1.1 pictures a schematic phase space map that corresponds to this kind of state in a one dimensional plasma. Another possibility is that some particles come from far away and are reflected at some point, as shown in Fig. 1.2.

The first analytical method to construct equilibrium electrostatic structures involving particle trapping was given by Bernstein, Greene and Kruskal (BGK) [3]. Phase space holes, a particular case of trapping, became first evident in numerical simulations [4, 5]. Then some analytical treatments were developed which at first were based on very simple distributions such as waterbags [6, 7, 8]. A different method of constructing equilibrium solutions, called *pseudo-potential method* was introduced by H. Schamel in Ref. 9 and

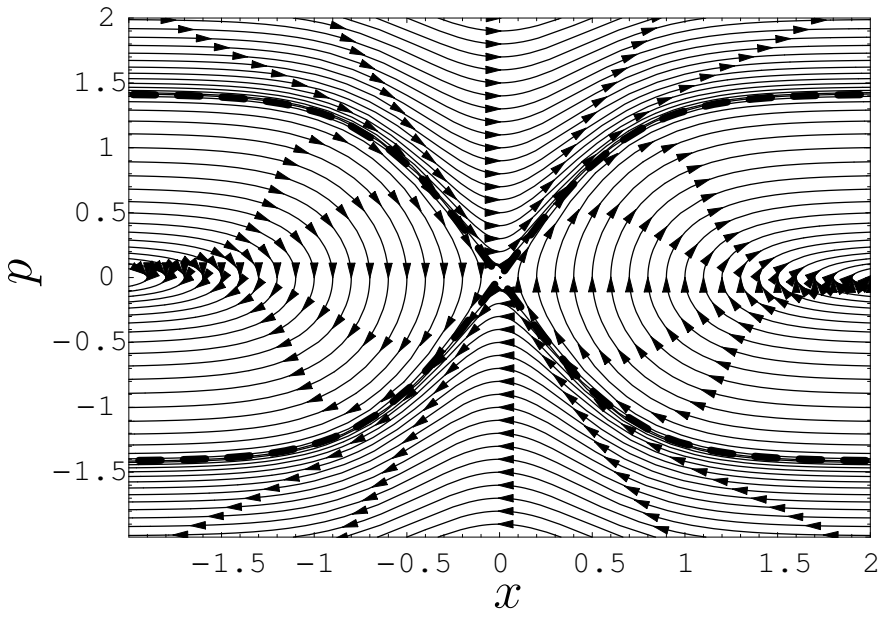

Figure 1.2: Another possible configuration of the phase space. This kind of separatrix is called X-type separatrix.

further developed in Refs. 10, 11, 12 (see also Ref. 13 for a review). The BGK approach and the pseudo-potential method, on the latter of which this thesis heavily relies, are explained with some detail in chapter 2.

1.3 Overview

The main aim of this thesis is to show the important role which self-consistent trapping is playing in the description of many different physical systems.

Chapter 2 is devoted to the study of trapping in classical two-species current-carrying plasmas. We perform an analytical study to systematically search for all kinds of structures involving trapping that can appear in such plasmas, thereby finding a nonlinear spectrum of waves that complements the linear one. We will also rigorously calculate the energies of electrostatic structures. Afterwards, by means of a numerical code developed with this aim, we will show that trapping structures survive when small collisional effects are introduced and that they play an essential role in the stability of current-carrying plasmas. This latter fact is also discussed in appendix A, in which we use another numerical code to repeat some previous results that brought into light an important connection between trapping and nonlinear stability. Namely, they showed that electrostatic structures can spontaneously develop out of thermal noise.

In the third chapter, trapping phenomena in weakly quantum systems are investigated. There we develop an analytical procedure to correct some equilibrium solutions of classical plasmas in order to include the effects of a finite de Broglie wavelength of the electrons. We also point out the theoretical connections that exist between trapping in plasmas and the propagation of solitons in nonlinear optical media. We show how the application of the pseudo-potential method can be extended to the trapping of pseudo-particles in the

framework of a Nonlinear Schrödinger Equation.

Finally, in chapter 4 we analyze trapping in charged particle beams in accelerators and storage rings. We review some results concerning trapping in coasting beams and then concentrate ourselves on the formation of solitons on the top of bunched beams, a phenomenon which we study numerically by means of a code developed for this purpose.

Chapter 5 contains a summary of all the investigations presented in the preceding chapters as well as some general conclusions we can extract from them.

CHAPTER 2

Trapping in classical plasmas

Let every student of nature take this as his rule that whatever the mind seizes upon with particular satisfaction is to be held in suspicion.

Francis Bacon

2.1 Description

In this section we will review some of the most widely used theories to describe trapped particles in classical plasmas. Then we will focus on the pseudo-potential method which we will use in the rest of this thesis.

2.1.1 Collisionless plasmas

We deal with a one dimensional, globally quasi-neutral, two-species plasma formed by electrons and single charged ions which eventually may also collide with a neutral background. We will also assume that the plasma is hot and dilute enough that the kinetic approach must be used and therefore leave aside the hydrodynamical approach. Except for Sect. 2.4, where a collision operator is taken into account, we also neglect second and higher order correlations between particles. This leads us to a pair of Vlasov equations as evolution equations for the electron and ion distribution functions, respectivley f_e and f_i :

$$\partial_t f_e + v\partial_x f_e + \partial_x \Phi \partial_v f_e = 0, \tag{2.1a}$$

$$\mu\partial_t f_i + u\partial_x f_i - \theta\partial_x \Phi \partial_u f_i = 0. \tag{2.1b}$$

In these equations electron (ion) velocities are normalized with the electron (ion) thermal velocity $v_{th} = \sqrt{\frac{kT_e}{m_e}}$ ($u_{th} = \sqrt{\frac{kT_i}{m_i}}$) and lengths are normalized with the electron Debye

length $\lambda_D = \sqrt{\frac{\epsilon_0 k T_e}{n_0 e^2}}$. Charges and masses are adimensionalized with respect to the electron charge, e and mass, m_e. The temperature ratio between both species is denoted by $\theta = T_e/T_i$. Finally, μ represents the ratio between the typical time scales of electrons and ions, $\mu = \sqrt{\theta/\delta}$, with δ being the mass ratio $\delta = m_i/m_e$.

But electrons and ions are affected by the electric field inside the plasma. In a one dimensional system, and using our normalizations, the Poisson equation (1.6) reduces to

$$\partial_x^2 \Phi(x;t) = n_e - n_i = \int dv\, f_e(x,v;t) - \int du\, f_i(u,x;t). \tag{2.2}$$

The joint system of equations comprising (2.1a), (2.1b) and (2.2) presents a full kinetic treatment of both species and will be the main focus of this chapter.

2.1.2 Validity of the Vlasov-Poisson description

Before entering into the theoretical details of the Vlasov-Poisson system, let us shortly review some of the systems in which this description is appropriate. The assumptions on which the equations rely are

One-dimensionality. In (2.1) and (2.2) we assumed that only one dimension is relevant in the description of our system. The main example of a situation that guarantees the validity of this assumption is that a very strong homogeneous magnetic field is immersed in the plasma. Under this condition, the particles gyrate around the magnetic field lines with a small Larmor radius and we can apply the *guiding-center* approximation, in which the particles are replaced by pseudo-particles located at the center of the rotating orbits and which, to lowest order in ϵ, where ϵ is the ratio between gyroradius and inhomogeneity length, move along the magnetic field lines. Only in higher order in ϵ, guiding center drifts, such as $\mathbf{E} \times \mathbf{B}$ drift, ∇B drift and magnetic curvature drift have to be taken into account, but this is neglected here, assuming the absence of these drifts.

Negligible collisions. As already said, by completely disregarding the effect of collisions, we assume the plasma is hot and dilute enough that second and higher order correlation between the particles can be neglected. The validity of this assumption is checked by the plasma parameter, that measures the inverse of the average number of particles inside a Debye sphere, $g := \left(\frac{4}{3}\pi n \lambda_D^3\right)^{-1}$. The collisionless limit is valid as long as $g \ll 1$. Later on, in section 2.4.1, we will investigate also weak collisional effects.

These conditions are commonplace in the magnetosphere [14, 15] but are also relevant in laboratories (see e.g. Ref. 16) and in high-tech machines such as fusion machines and particle accelerators and storage rings.

2.1.3 Electrostatic modes

First we want to study equilibrium ($\partial_t \to 0$) solutions of the Vlasov-Poisson system. Equation (2.1a) is solved by any distribution function that depends only on the constants of motion of a single particle. The simplest case is a distribution function that depends only on the single particle energy $E = v^2/2 - \Phi(x)$. If in addition we set $\Phi(x) = 0$ we find

that any $f_e(x,v) = f_e(v^2/2)$ will solve (2.1a) and (2.2). The physically most meaningful (most probable) distribution is the one that maximizes Boltzmann's H function $H = \int f \log f d^3x d^3v$. This is the familiar Maxwell distribution function, which for electrons reads

$$f_{e0} = \frac{1}{\sqrt{2\pi}} e^{-v^2/2}. \tag{2.3}$$

Similarly, for ions we have

$$f_{i0} = \frac{1}{\sqrt{2\pi}} e^{-u^2/2}. \tag{2.4}$$

When we introduce a drift velocity v_D between electrons and ions in the unperturbed region and we select a frame moving at a velocity v_0 in electron velocity space ($u_0 = \sqrt{\frac{\theta}{\delta}} v_0$ in ion velocity space), the distribution functions appear as

$$f_{e0} = \frac{1}{\sqrt{2\pi}} e^{-\frac{1}{2}(v-\tilde{v}_D)^2}, \tag{2.5a}$$

$$f_{i0} = \frac{1}{\sqrt{2\pi}} e^{-\frac{1}{2}(u+u_0)^2}, \tag{2.5b}$$

where $\tilde{v}_D = v_D - v_0$. The state described by distribution functions (2.5a) and (2.5b) along with $\Phi(x) = 0$ will be our *homogeneous* or *unperturbed* state in the wave frame, i.e. where the wave we are looking for is at rest.

Of course, we are not very much interested in such a simple, almost-trivial state. We are looking for electrostatic modes that may disturb the homogeneous state. The approach most often taken in the literature is to look for distribution functions $f = f_0 + \epsilon f_1$ where ϵ is a smallness parameter. This is inserted into (2.1a) and only terms of first order are maintained. Then an in depth analysis of the Vlasov equation can be performed which includes a wide spectrum of linear waves experiencing more or less Landau damping or growth, depending on v_D. It is often argued that the validity of this linearization relies on the smallness of the perturbation (ϵf_1) only and that for small enough amplitudes it can always be done safely enough. However, we will deal in this thesis with modes that even for infinitesimal amplitudes cannot be treated by a linearized Vlasov equation. The reason is that when linearizing (2.1a) we are in fact neglecting terms that depend on $\partial_v f_1$. This can be done only if not only the perturbation is small, but also its derivative (which is of course not implied by the first). In general we will study modes with very large (sometimes infinite) velocity derivatives, which render any linearization completely void. We will treat this with more detail in section 2.4.3.

A first approach for finding electrostatic trapped-particle modes is the BGK method (after Bernstein, Greene and Kruskal [3]). In this method one starts with a given potential $\Phi(x)$ and the distribution function of free particles f_{ef} and from it one is able to find the distribution function for trapped particles f_{et} that satisfies the Vlasov-Poisson system. The problem of this method is, however, that it does not guarantee that the obtained distribution function will be physically meaningful. In fact it is often negative or has undesired singularities. We therefore take a more suitable procedure, introduced in Ref. 9, to solve our equations in a more physical way.

2.1.4 The pseudo-potential method

To overcome the difficulties of the BGK method we can proceed in an inverse way. We can impose a physically meaningful distribution function from the beginning that solves Vlasov equation (2.1a) letting it depend only on the constants of motion of a single particle. Then we integrate it and insert it into Poisson equation to find a consistent potential. If we want to allow a drift velocity we have to use distribution functions asymmetric in velocities. Therefore we have to introduce a further constant of motion for free particles, apart from the energy, on which f_e will depend on. This new constant of motion will be

$$\sigma = \mathrm{sgn}(v). \tag{2.6}$$

We will use the following distribution functions [9, 12]:

$$f_e(x,v) = \frac{1+K}{\sqrt{2\pi}} \begin{cases} \exp\left[-\frac{1}{2}\left(\sigma_e\sqrt{2E_e} - \tilde{v}_D\right)^2\right], & E_e > 0, \\ \exp\left(-\tilde{v}_D^2/2 - \beta E_e\right), & E_e \leq 0, \end{cases} \tag{2.7a}$$

$$f_i(x,u) = \frac{1+A}{\sqrt{2\pi}} \begin{cases} \exp\left[-\frac{1}{2}\left(\sigma_i\sqrt{2E_i} + u_0\right)^2\right], & E_i > 0, \\ \exp\left(-u_0^2/2 - \alpha E_i\right), & E_i \leq 0, \end{cases} \tag{2.7b}$$

where K and A are normalization constants which allow us to find periodic waves and which disappear in the limit of a vanishing amplitude of the perturbation. The coefficients α and β are called *trapping parameters*, and set the relationship between the free and the trapped particles distribution functions allowing to control the status of trapped particles. When $\beta < 0$ ($\alpha < 0$) the electron (ion) distribution function will have a superimposed hole. Inversely, when $\beta > 0$ ($\alpha > 0$), a hump will be present in the distribution function. The energies in (2.7) are defined as

$$E_e = \frac{v^2}{2} - \Phi, \tag{2.8a}$$

$$E_i = \frac{u^2}{2} + \theta(\Psi - \Phi). \tag{2.8b}$$

Here Ψ is the amplitude of the potential (i.e. its maximum value). Later on in the analytical part we will assume $\Psi \ll 1$ to simplify the analysis. Otherwise a numerical evaluation of the expressions (namely the nonlinear dispersion relation and the pseudo-potential; see below) would be neccesary. The form that the distribution functions (2.7) take in velocity space is plotted in Fig. 2.1. The trajectories in phase space of the particles are as already shown in the introduction, Figs. 1.1 and 1.2.

Once we use this ansatz for the distribution functions and assume $\Psi \ll 1$, we arrive at the following expression for the electron and ion densities as functionals of the potential Φ [12]:

$$n_e(\Phi) = (1+K)\left\{1 - \frac{1}{2}\mathrm{Z}_r'\left(\frac{\tilde{v}_D}{\sqrt{2}}\right)\Phi - \frac{4}{3}b(\beta,\tilde{v}_D)\Phi^{3/2} + \dots\right\}, \tag{2.9a}$$

$$\begin{aligned} n_i(\Phi) = (1+A)\Bigg\{1 &- \frac{1}{2}\mathrm{Z}_r'\left(\frac{u_0}{\sqrt{2}}\right)\theta(\Psi-\Phi) \\ &- \frac{4}{3}b(\alpha,u_0)\left[\theta(\Psi-\Phi)\right]^{3/2} + \dots\Bigg\}, \end{aligned} \tag{2.9b}$$

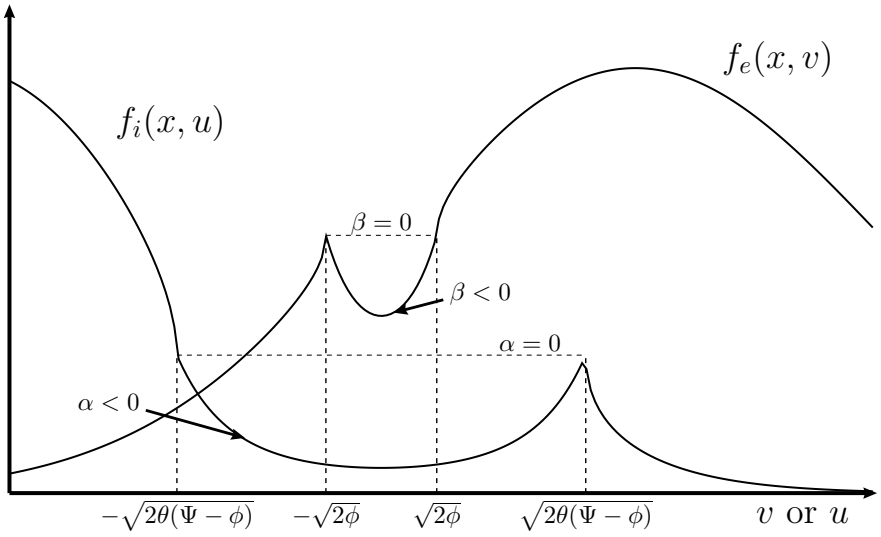

Figure 2.1: Shape of the distribution functions given by (2.7) in velocity space. Note the different scales for electron and ions.

where $Z_r'(x)$ represents the derivative of the real part of the plasma dispersion function and $b(\beta, v)$ is a function that in the most general case is defined as

$$b(\beta, v) = \frac{1}{\sqrt{\pi}} \left(1 - \beta - v^2\right) e^{-v^2/2}. \tag{2.10}$$

Using expressions (2.9), the Poisson equation (2.2) yields

$$\Phi'' = n_e(\Phi) - n_i(\Phi) =: -V'(\Phi), \tag{2.11}$$

with

$$\begin{aligned} -V(\Phi) = (1+K) &\left\{ \Phi - \frac{1}{4} \mathrm{Z}_r'\big(\frac{\tilde{v}_D}{\sqrt{2}}\big) \Phi^2 - \frac{8}{15} b(\beta, \tilde{v}_D) \Phi^{5/2} + \dots \right\} \\ - (1+A) &\left\{ \Phi - \frac{1}{4} \mathrm{Z}_r'\big(\frac{u_0}{\sqrt{2}}\big) \theta \left[\Psi^2 - (\Psi - \Phi)^2\right] \right. \\ &\left. - \frac{8}{15} b(\alpha, u_0) \theta^{3/2} \left[\Psi^{5/2} - (\Psi - \Phi)^{5/2}\right] + \dots \right\}. \end{aligned} \tag{2.12}$$

To integrate (2.11) we multiply both sides by Φ' and arrive at

$$\frac{\Phi'^2}{2} + V(\Phi) = 0. \tag{2.13}$$

This equation resembles strongly the energy conservation of a single classical particle; accordingly, we will call $V(\Phi)$ also the *classical potential*.

Some conditions are imposed upon $V(\Phi)$ in order to achieve physical solutions. First of all is clear that $\Phi'^2(x) \geq 0$. This means

$$V(\Phi) \leq 0 \quad \text{if} \quad 0 \leq \Phi \leq \Psi. \tag{2.14}$$

On the other side $\Phi = \Psi$ should correspond to a maximum in the potential, this is, $\Phi' = 0$. This condition may be written as

$$V(\Psi) = 0. \tag{2.15}$$

If we insert $V(\Psi)$ (2.12) into (2.15), a relationship arises between amplitude and velocity and that will be furtheron termed *nonlinear dispersion relation* (NDR).

As an example of how to solve equation (2.13) we can take the case of nonpropagating (standing) *solitary electron holes* with immobile ions. Taking $\theta \to 0$ (i.e. infinitely hot ions), $A = K = 0$, $\tilde{v}_D = 0$, the distribution function for electrons reads

$$f(x,v) = \frac{1}{\sqrt{2\pi}} \begin{cases} \exp(-E) & E > 0 \\ \exp(-\beta E) & E \leq 0 \end{cases}, \tag{2.16}$$

and (2.12) simplifies to

$$-V(\Phi) = \frac{\Phi^2}{2}\left(1 - \frac{16}{15} b(\beta,0)\sqrt{\Phi}\right) + \ldots, \tag{2.17}$$

Applying the NDR (2.15), we find

$$\frac{16}{15} b\sqrt{\Psi} = 1, \tag{2.18}$$

where we used $b := b(\beta, 0)$ to simplify the notation. This lets us further simplify the classical potential to yield

$$-V(\Phi) = \frac{\Phi^2}{2}\left(1 - \sqrt{\frac{\Phi}{\Psi}}\right). \tag{2.19}$$

With this expression we can integrate (2.13) and arrive at a bell-shaped localized potential

$$\Phi(x) = \Psi \mathrm{sech}^4\left(\frac{x}{4}\right). \tag{2.20}$$

The NDR together with the smallness condition $\Psi \ll 1$ implies

$$b = \frac{1-\beta}{\sqrt{\pi}} = \frac{15}{16\sqrt{\Psi}} \gg 1. \tag{2.21}$$

i.e. $-\beta$ is a large positive number. Therefore, a noticeable notch appears in the distribution function for trapped electrons.

Note the following advantages of the pseudo-potential method:

1. The solution is determined completely in its shape and velocity.

2. A standing solitary electron hole requires a specific electron trapping parameter β. Therefore, the family of solutions has only one parameter.

3. The ansatz (2.7) for the distributions functions guarantees that they will always be continuous and positive and therefore physically meaningful. There exist, however, a nonphysical property of such distribution functions, namely that for finite propagating velocities, an infinite jump in $\partial_v f$ is found at the separatrix.

2.2 Different kinds of electrostatic structures

The pseudo-potential method can predict and explain a wide range of potential electrostatic structures. Now that we have sketched the main features of this method, we can proceed to a systematic search for all those available structures. In doing this we will closely follow Ref. 17.

For simplicity, we define a normalized potential as

$$\phi := \frac{\Phi}{\Psi}, \tag{2.22}$$

and a normalized classical potential as

$$\mathcal{V}(\phi) := \frac{V(\Phi)}{\Psi^2}. \tag{2.23}$$

Then, (2.13) appears as

$$\frac{\phi'(x)^2}{2} + \mathcal{V}(\phi) = 0, \tag{2.24}$$

and $\mathcal{V}(\phi)$ is given in the weak amplitude limit by [12, 18]

$$\begin{aligned} -2\mathcal{V}(\phi) := -2\frac{V(\Phi)}{\Psi^2} &= \left(k_0^2 - \frac{B_i}{2}\right)\phi(1-\phi) \\ &\quad + B_e\phi^2(1-\sqrt{\phi}) \qquad (2.25) \\ &\quad + B_i(1-\phi)^2(1-\sqrt{1-\phi}), \qquad (2.26) \end{aligned}$$

where B_e, B_i and k_0 are defined [18] as

$$B_e := \frac{16}{15}b(\beta, \tilde{v}_D)\sqrt{\Psi}, \tag{2.27a}$$

$$B_i := \frac{16}{15}b(\alpha, u_0)\theta^{3/2}\sqrt{\Psi}, \tag{2.27b}$$

$$k_0^2 := \frac{2K}{\Psi}. \tag{2.27c}$$

Thus B_e (B_i) is a measure of the status of trapped electrons (ions), as explained in more detail in Refs. 12, 18, 19, while k_0 gives us a measure of the curvature of the potential as $\phi \to 0$ and is related with the actual wavenumber [9]. The parameter $\tilde{v}_D$ is again defined by $\tilde{v}_D := v_D - v_0$ where v_D is the drift velocity between electrons and ions; v_0 (u_0) is the phase velocity of the structure in the electron (ion) phase space and it holds $u_0 = v_0\sqrt{\theta m_i/m_e}$, where $\theta = T_{ef}/T_{if}$, in which T_{sf}, $s = e, i$, is the temperature of species s defined by the Maxwellian at the location in space where trapped particles of this species are absent.

In the following, we shall search in the three-dimensional parameter space spanned by k_0^2, B_e and B_i for areas where (2.26) gives physically meaningful solutions. Our aim is to obtain a complete picture of the allowed potential structures. As a result, several new structures will be detected.

In (2.26) ϕ is normalized by (2.22) in such a way that it is confined to the interval $0 \le \phi \le 1$. Therefore, we will start considering the behavior of $\mathcal{V}(\phi)$ at both boundaries

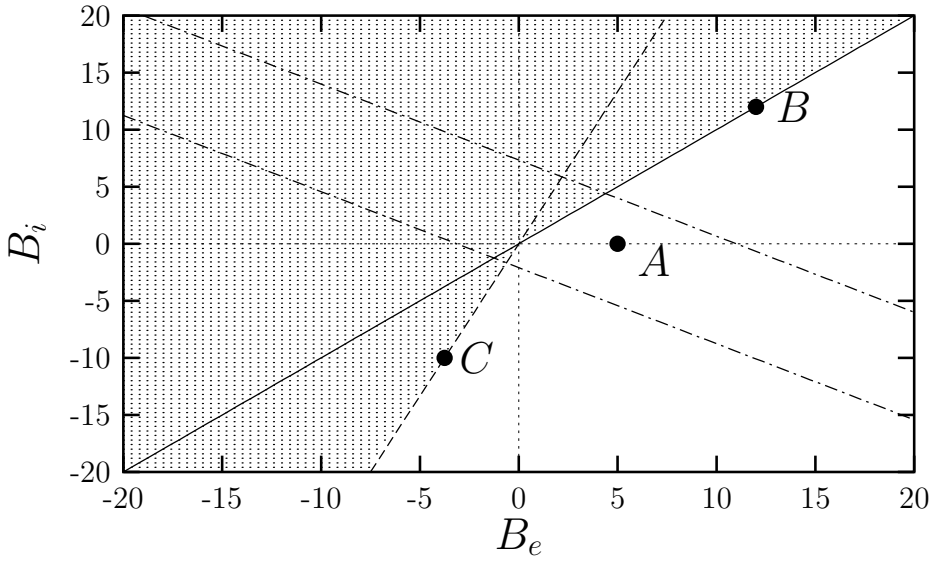

Figure 2.2: Existence region in parameter space for $k_0^2 = 0$. The non-shaded area represents the allowed region of the parameter space where the classical potential is meaningful. The solid line is given by eq. (2.31) whereas the dashed line represents the limit given by (2.33) in the text. Locations of three typical structures, denoted by **A**, **B** and **C** are pointed out. The two dash-dotted lines bound the area permitted by the nonlinear dispersion relation (NDR) for the particular value $\theta = 10$.

of this interval. In the proximity of each of these points we are allowed to use a Taylor expansion and, as long as the first derivative is nonzero, neglect terms of higher order:

$$\mathcal{V}(\delta\phi) \approx -\frac{1}{2}k_0^2\delta\phi, \tag{2.28}$$

$$\mathcal{V}(1-\delta\phi) \approx \frac{1}{2}\left(\frac{B_i - B_e}{2} - k_0^2\right)\delta\phi. \tag{2.29}$$

As $\mathcal{V}(\phi)$ must be negative for solutions $\phi(x)$ to exist, the first constraints in our parameter space are, therefore,

$$k_0^2 \geq 0, \tag{2.30}$$

$$k_0^2 \geq \frac{B_i - B_e}{2}. \tag{2.31}$$

2.2.1 Generalized electron holes and double layers ($k_0^2 = 0$)

If the equality holds in (2.30), i.e. if $k_0^2 = 0$, we have to look into higher order terms of the expansion:

$$\mathcal{V}(\delta\phi) \approx \frac{1}{2}\left(\frac{3}{8}B_i - B_e\right)\delta\phi^2 + \frac{1}{2}B_e\delta\phi^{5/2}, \tag{2.32}$$

from which a new restriction arises:

$$B_e \geq \frac{3}{8}B_i, \tag{2.33}$$

where the equality is admissible if and only if B_e is negative. Along with (2.31), this equation defines the region in the parameter space for $k_0^2 = 0$ where physically meaningful classical potentials exist (see Fig. 2.2).

For all the possible classical potentials with $k_0^2 = 0$, the derivative $\mathcal{V}'(\phi)$ is zero at $\phi = 0$. This implies that $\phi(x)$ goes asymptotically to zero for $x \to \infty$, for $x \to -\infty$ or for both. It hence represents a localized solution. Three characteristic types of localized solutions can be distinguished, labeled by **A**, **B**, and **C** (see Fig. 2.2).

A: $B_i = 0$**,** $B_e > 0$**.** In this case one has

$$-2\mathcal{V}(\phi) = B_e\phi^2(1 - \sqrt{\phi}), \tag{2.34}$$

and therefore, by solving (2.24), we obtain

$$\phi(x) = \operatorname{sech}^4\left(\frac{\sqrt{B_e}}{4}x\right), \tag{2.35}$$

which is a bell-shaped solitary pulse, whose width scales like $B_e^{1/2}$. This is the ordinary solitary electron hole, found earlier [12, 13, 20], being essentially characterized by electron trapping.

B: $B_i = B_e$**,** $B_e > 0$**.** For these values we obtain

$$\begin{aligned} -2\mathcal{V}(\phi) = B_e\Big[&\phi^2(1 - \sqrt{\phi}) + (1-\phi)^2\left(1 - \sqrt{1-\phi}\right) \\ &-\frac{1}{2}\phi(1-\phi)\Big], \end{aligned} \tag{2.36}$$

which is symmetric with respect to $\phi = 1/2$. Its behavior near $\phi = 0$ (or $\phi = 1$) is given by $-2\mathcal{V}(\phi) \approx \frac{5}{8}B_e\phi^2$ (resp. $\frac{5}{8}B_e(1-\phi)^2$). As $\mathcal{V}'(\phi) = 0$ for $\phi = 0$ and $\phi = 1$ this is a new type of a double layer solution representing therefore a monotonic potential $\phi(x)$. It supplements the three double layer solutions described in the literature [13, 21, 22, 23, 24], namely the strong double layer, the slow electron acoustic and the slow ion acoustic double layer.

C: $B_e = \frac{3}{8}B_i$**,** $B_i < 0$**.** Now we find

$$\begin{aligned} -2\mathcal{V}(\phi) = -B_i\Big[&\frac{1}{2}\phi(1-\phi) - \frac{3}{8}\phi^2\left(1 - \sqrt{\phi}\right) \\ &-(1-\phi)^2\left(1 - \sqrt{1-\phi}\right)\Big]. \end{aligned} \tag{2.37}$$

Near $\phi = 0$ we get

$$-2\mathcal{V}(\delta\phi) = -\frac{3}{8}B_i\delta\phi^{5/2} + \ldots, \tag{2.38}$$

whereas near $\phi = 1$ we find

$$-2\mathcal{V}(1 - \delta\phi) = -\frac{5}{16}B_i\delta\phi + \ldots, \tag{2.39}$$

which is again a solitary wave, however one with a larger width in comparison with that of **A**. To the best of our knowledge also this solitary wave solution is new. It needs both the effect of trapped ions and electrons for its existence.

Note that near the origin of Fig. 2.2, these solutions cease to be valid, as higher order effects become important.

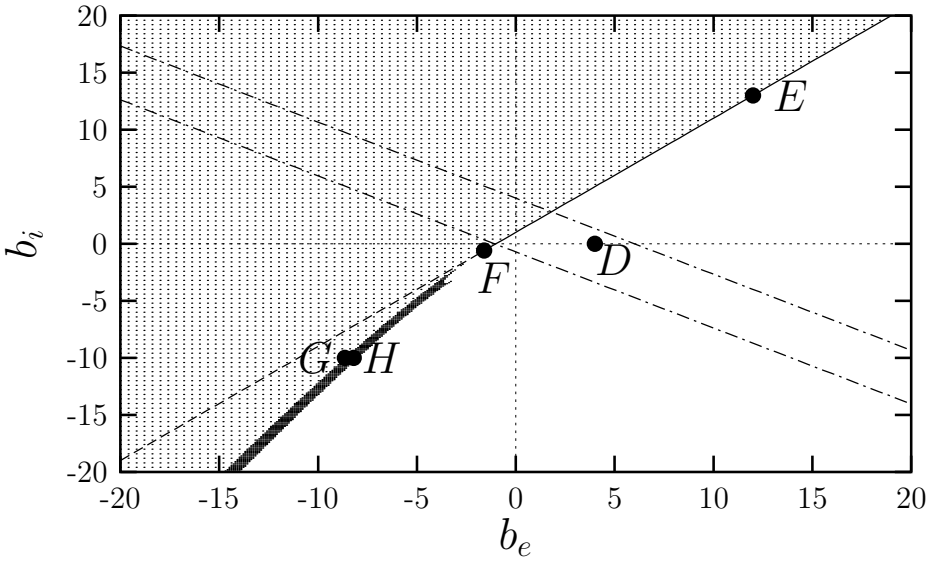

Figure 2.3: Existence region of the parameter space for $k_0^2 > 0$. As in Fig. 2.2, the lightly shaded area represents the region where physical solutions do not exist. The solid line represents the constraint imposed by (2.42); as can be seen, below the point marked with **F**, the forbidden area is further extended. Besides **F**, four characteristic structures are discussed in the text, whose locations are labeled by **D**, **E**, **G** and **H**. The dark shaded area marks the region where the classical potential has an intermediate maximum and, therefore, corresponds to two-shoulder structures (see text). The two dash-dotted lines bound the area allowed by the NDR for the particular value $\tilde{\theta} = 11$ (see text).

2.2.2 Periodic solutions and generalized ion holes ($k_0^2 > 0$)

Now we turn to the case $k_0^2 > 0$. In this case it is convenient to rescale our equations once more. We define the new dimensionless quantities

$$b_e := \frac{B_e}{2k_0^2}, \tag{2.40a}$$

$$b_i := \frac{B_i}{2k_0^2}, \tag{2.40b}$$

$$\tilde{\mathcal{V}}(\phi) := \frac{\mathcal{V}(\phi)}{k_0^2}, \tag{2.40c}$$

and rewrite the classical potential (2.26) and the constraint (2.31) respectively as

$$\begin{aligned} -2\tilde{\mathcal{V}}(\phi) =& (1-b_i)\phi(1-\phi) + 2b_e\phi^2\left(1-\sqrt{\phi}\right) \\ &+ 2b_i(1-\phi)^2\left(1-\sqrt{1-\phi}\right), \end{aligned} \tag{2.41}$$

$$1 \geq b_i - b_e. \tag{2.42}$$

Fig. 2.3 shows the allowed area of solutions (non-shaded region) in the b_e,b_i plane. In the upper part this area is restricted by the solid line which represents (2.42) with the equality sign. In the lower part (more precisely, below the point **F**) a new constraint enters, which

will be discussed below. Again, several typical structures are pointed out, labeled by **D**, **E**, **F**, **G** and **H**.

D: $b_i = 0$**,** $b_e > -1$**.** In this case we get

$$-2\tilde{\mathcal{V}}(\phi) = \phi(1-\phi) + 2b_e\phi^2\left(1-\sqrt{\phi}\right), \tag{2.43}$$

which near the boundaries behaves as

$$-2\tilde{\mathcal{V}}(\delta\phi) \approx \delta\phi, \tag{2.44}$$

for $\phi = \delta\phi \ll 1$, and

$$-2\tilde{\mathcal{V}}(1-\delta\phi) \approx (1+b_e)\delta\phi \tag{2.45}$$

for $\delta\phi = 1-\phi \ll 1$. As $\tilde{\mathcal{V}}'(\phi)$ is negative for $\phi = 0$ and $\phi = 1$ it represents, therefore, a periodic solution, which is mainly controlled by electron trapping.

E: $b_e = b_i - 1$**,** $b_i > -3/5$**.** Here we obtain

$$\begin{aligned} -2\tilde{\mathcal{V}}(\phi) =& (1-b_i)\left[\phi(1-\phi) - 2\phi^2\left(1-\sqrt{\phi}\right)\right] \\ &+ 2b_i(1-\phi)^2\left(1-\sqrt{1-\phi}\right). \end{aligned} \tag{2.46}$$

Near $\phi = 0$ and $\phi = 1$ we find

$$-2\tilde{\mathcal{V}}(\delta\phi) \approx \delta\phi, \tag{2.47}$$

when $\phi = \delta\phi \ll 1$, and

$$-2\tilde{\mathcal{V}}(\delta\phi) \approx \frac{1}{4}(3+5b_i)\delta\phi^2 - 2b_i\delta\phi^{5/2}, \tag{2.48}$$

if $\delta\phi = 1-\phi \ll 1$. This represents a generalized solitary ion hole being characterized by an inverted bell-shaped potential. For $b_i = 1$, $\tilde{\mathcal{V}}(\phi)$ is especially simple, becoming

$$-\tilde{\mathcal{V}}(\phi) = (1-\phi)^2(1-\sqrt{1-\phi}). \tag{2.49}$$

This represents the classical solitary ion hole (Refs. 25, 12 and references therein)

$$\phi(x) = 1 - \operatorname{sech}^4\left(\frac{x}{2\sqrt{2}}\right), \tag{2.50}$$

in which x is rescaled and stands for $k_0 x$.

This solution, which is predominantly determined by ion trapping, has a limit marked by **F** in Fig. 2.3.

F: $b_e = -8/5$**,** $b_i = -3/5$**.** Inserting these values into (2.41) we get the corresponding classical potential $\tilde{\mathcal{V}}(\phi)$. From (2.48) we learn that the first term on the rhs vanishes such that near $\phi = 1$ we obtain

$$-2\tilde{\mathcal{V}}(1-\delta\phi) \approx \frac{6}{5}\delta\phi^{5/2}, \tag{2.51}$$

similar to the previous case **C**. This represents a solitary potential structure that shows a larger width in comparison with (2.50), but still having the same inverted bell-shaped form. Again we have found a new kind of structure, namely a new solitary ion hole.

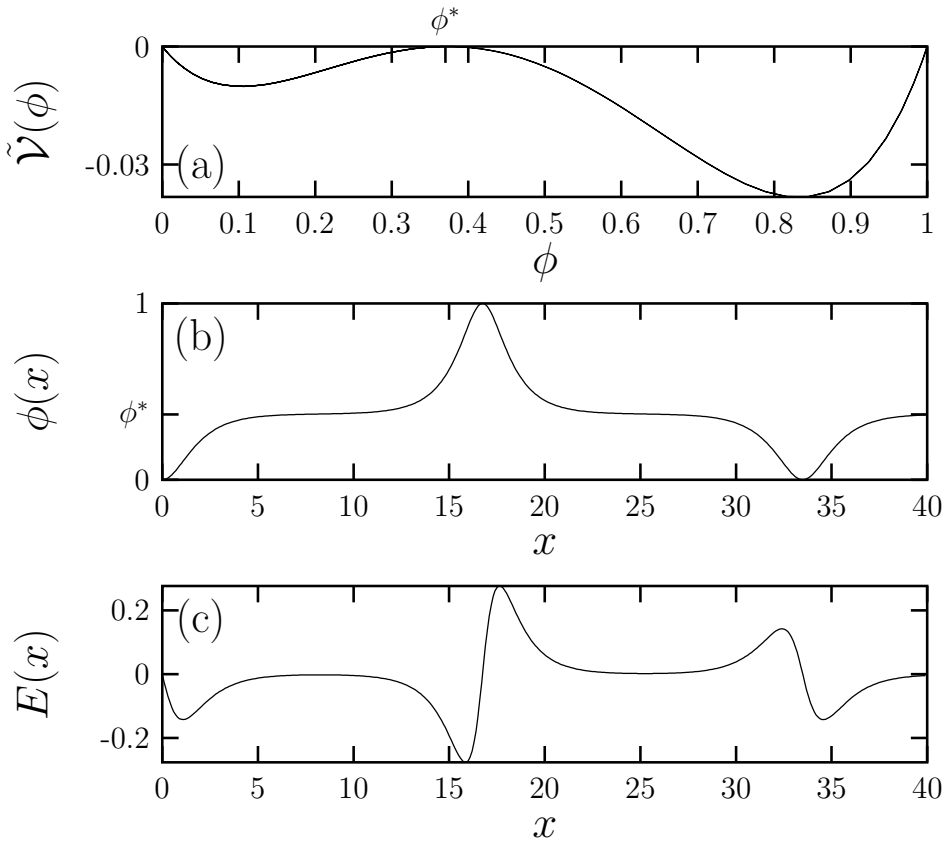

Figure 2.4: Classical potential $\tilde{\mathcal{V}}(\phi)$ (a), potential $\phi(x)$ (b) and electric field $E(x)$ (c) for a typical example of the structure referred as **G** in the text and in Fig. 2.3 ($b_e = -8.640$,$b_i = -10$).

Going below $b_i = -3/5$ along the line $b_e = b_i - 1$ (dashed line in Fig. 2.3) we see from (2.48) that $\tilde{\mathcal{V}}(\phi)$ behaves wrongly near $\phi = 1$ since it becomes positive. This can be avoided at fixed $b_i < -3/5$ by increasing b_e starting from $b_e = b_i - 1$. At a certain value of b_e, denoted by b_e^*, $\tilde{\mathcal{V}}(\phi)$ is again nonpositive but assumes a third zero at some ϕ^* in the interval $0 < \phi^* < 1$ where $\tilde{\mathcal{V}}(\phi)$ touches the $\tilde{\mathcal{V}} = 0$ axis from below.

G: $b_i < -3/5$**,** $b_e \gtrsim b_e^* > -8/5$**.** Very close to this point, where the classical potential deviates only slightly from being tangential to the zero axis, the corresponding potential $\phi(x)$ is periodic but with an intermediate plateau of arbitrary large size at $\phi = \phi^* < 1$, as seen in Fig. 2.4 for $b_i = -10$ and $b_e = -8.640$. This structure may be viewed as an alternating train of electron and ion holes.

H: $b_i < -3/5$**,** $b_e > b_e^* > -8/5$**.** If we further increase b_e the new maximum detaches from the zero line and becomes more negative. This gives rise to a periodic structure having now two shoulders in each period replacing the two plateaus. A typical example of this new type of periodic structure with imposed shoulders is shown in Fig. 2.5 for $b_i = -10$, $b_e = -8.600$. Fig. 2.5a shows the classical potential $\tilde{\mathcal{V}}(\phi)$ and Figs. 2.5b,c the corresponding potential $\phi(x)$ and the electric field $E(x)$. It is noteworthy to point out that near b_e^* a small change of either b_e or b_i (such as the variation between **G** and **H** may dramatically change the period of the structure).

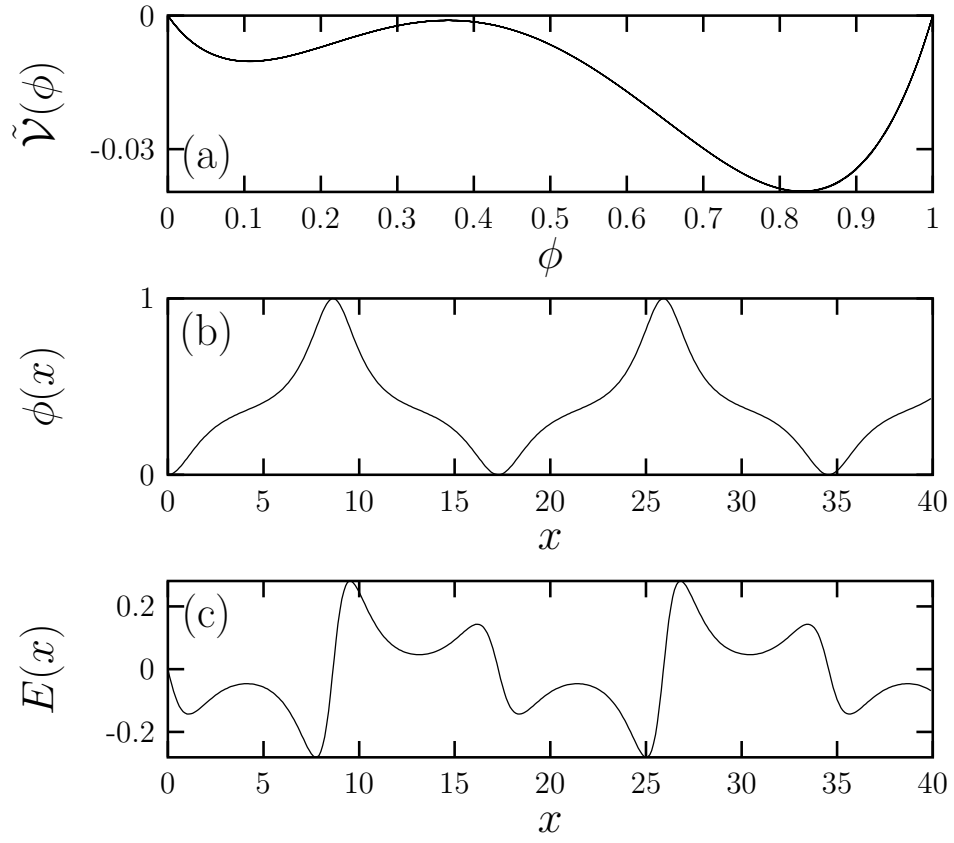

Figure 2.5: Classical potential $\tilde{\mathcal{V}}(\phi)$ (a), potential $\phi(x)$ (b) and electric field $E(x)$ (c) for a typical example of the structure referred as **H** in the text and in Fig. 2.3 ($b_e = -8.600$, $b_i = -10$). Note that although the points **G** and **H** are very close in Fig. 2.3, the period of the potential in **G** is almost double of that in **H**.

Again, structures **G** and **H** have not been discussed before in the literature.

2.2.3 Nonlinear dispersion relation

But not every set of parameters that produces a physically meaningful classical potential is valid. The nonlinear dispersion relation (2.15) has also to be fulfilled. In Ref. 12 it was shown that the NDR can be written as:

$$-\frac{1}{2}Z_r'\left(\frac{\tilde{v}_D}{\sqrt{2}}\right) - \frac{\theta}{2}Z_r'\left(\frac{u_0}{\sqrt{2}}\right) = B_e + \frac{3}{2}B_i - k_0^2. \tag{2.52}$$

The real part of the plasma dispersion function, $Z_r(x)$, satisfies $-0.285 \leq -\frac{1}{2}Z_r'\left(\frac{x}{\sqrt{2}}\right) \leq 1$. Hence, solutions for (2.52) will exist as long as

$$-0.285(1+\theta) \leq B_e + \frac{3}{2}B_i - k_0^2 \leq (1+\theta). \tag{2.53}$$

For $k_0 = 0$, the equality sign in this expression gives us two straight lines in Fig. 2.2, drawn for $\theta = 10$. They generally depend on θ and further restrict the area of the parameter

space where our structures are allowed. Only in the limit $\theta \to \infty$, when the two lines tend to $\pm\infty$, respectively, the whole non-shaded area of Fig. 2.2 becomes available for solutions.

For $k_0^2 > 0$, we use the rescaled form of (2.53)

$$-0.285\frac{1+\theta}{k_0^2} \leq 2b_e + 3b_i - 1 \leq \frac{1+\theta}{k_0^2}. \tag{2.54}$$

This time the location of the two restricting lines (given by the equality sign in (2.54)) depends on the parameter $\tilde{\theta} = (1+\theta)/k_0^2$, which is determined by two parameters now. In Fig. 2.3 the two limiting lines are drawn for $\tilde{\theta} = 11$. As in the previous case, the whole non-shaded area becomes available if $\tilde{\theta} \to \infty$ ($\theta \to \infty$).

In summary, in this section, a systematic evaluation of the classical potential and of the nonlinear dispersion relation has brought to light several new electrostatic equilibrium structures obeying the Vlasov-Poisson system for a two-component, current-carrying plasma. As described earlier [12, 18, 19], these equilibria have to supplement the linear wave spectrum of the Vlasov-Poisson system to arrive at a more complete description of low amplitude electrostatic plasma dynamics and turbulence.

We would also like to point out the possibility of finding two structures simultaneously in a current-carrying plasma, as seen *e.g.* by the FAST (Fast Auroral SnapshoT) satellite observations in the downward current regime [26]. For instance, a solitary electron hole **A** ($B_e^A \neq 0$, $B_i^A = 0$) and a double layer **B** ($B_e^B = B_i^B$) may both satisfy the same nonlinear dispersion relation and thus have the same phase velocity, namely when $B_e^A = \frac{5}{2}B_e^B$. Within our approach, such a coincidence in the measured wave spectrum comes out maturally, giving us confidence on the underlying model.

2.3 Energy deficit and negative energy structures

2.3.1 Renormalization of the solutions

An important issue that, as was suggested in Refs. 19, 18 and will be discussed later, may be related with the stability of a current-carrying plasma, is the total energy of the structured plasma compared with that of the homogeneous, unstructured system. In this section we will perform such a calculation and leave the stability problem to be further investigated by means of a numerical code in Sec. 2.6. At this point it suffices to say that strong evidences exist that link the presence of negative energy structures with unstable regimes.

However, before calculating the perturbed state energies, we must take into account that the average particle density that arises from (2.7) may differ from the unperturbed Maxwellian and therefore it would make no sense to directly compare the energies of both states. This problem can be overcome by a slight modification of the solution. For this purpose we define the average density of the electrons before modification as

$$M = \frac{1}{2L}\int_{-L}^{+L} n_e\, dx, \tag{2.55}$$

where L is the spatial periodicity of the solution, while for localized (solitary) solutions we take the limit $L \to \infty$.

For the homogeneous plasma n_e is independent of x and one has $M = n_e = 1$. In the inhomogeneous case, the dimensional distribution functions have to be multiplied by an additional factor $1/M$. Poisson's equation then allows us to find the new dimensional spatial coordinate: it is equal to the old one multiplied by $\sqrt{M}$. To be able to keep the distribution functions (2.7) and all results calculated from these, the corrected dimensional quantities are renormalized in such a way that the dimensionless quantities (f_e and x) are exactly as those given above. This is the case if the spatial coordinate is renormalized using the new Debye length $\lambda_D^{(n)}$ and the distribution function is renormalized by the new average density $n_{e0}^{(n)}$ given by

$$\lambda_D^{(n)} = \lambda_D \sqrt{M} \tag{2.56}$$

$$n_{e0}^{(n)} = \frac{n_{e0}}{M}. \tag{2.57}$$

Due to charge neutrality f_i can be treated exactly as f_e. Thus it is now possible to keep all results obtained above. It has to be kept in mind, however, that for different wave structures the same dimensionless quantity can have a different physical meaning, depending on the value of M.

2.3.2 Energy density of the plasma

Now we want to examine how large the energy density associated with the plasma structures presented in Sec. 2.1.4 is. This energy density will then be compared to the energy density of the corresponding homogeneous plasma. The following calculation is based on that of Ref. 12, but it takes into account the facts that the perturbed state has to be renormalized before it can be compared to the homogeneous state and that it has to be calculated in a new frame of reference. The result obtained in this section was first presented in Refs. 19 and 18.

When the energy density is calculated in the frame of reference in which the homogeneous state has minimum energy, the Vlasov-Poisson system is said to possess potentially usable free energy if the perturbed state has an energy which is lower than that of the uniform state. The homogeneous state has minimum energy in the frame moving with the center of mass velocity $v_{\mathrm{CM}} = \frac{\delta}{1+\delta} v_D$. However, for the sake of simplicity, we will prefer the laboratory frame in which the ions are assumed to be at rest, thus ignoring effects of order $\mathcal{O}(\delta)$.

To find the energy density w of a plasma wave in the laboratory frame we now assume a stationary wave with periodicity $2L$ and phase velocity v_0:

$$w = \frac{1}{4L} \int_{-L}^{+L} dx' \left[\int_{-\infty}^{+\infty} dv\, v^2 f_e(x', v) + \frac{1}{\theta} \int_{-\infty}^{+\infty} du\, u^2 f_i(x', u) + \Phi'(x')^2 \right], \tag{2.58}$$

where $x' \equiv x - v_0 t$. L is infinity for the solitary limits. The distribution functions $f_e(x', v)$ and $f_i(x', u)$ in (2.58) when transformed to wave frame coincide with (2.7) renormalized by (2.56), (2.57). This means that w is equal to the dimensional energy density, normalized by $kT_e n_{e0}^{(n)}$, where $n_{e0}^{(n)}$ is given by (2.57).

In the unperturbed homogeneous state w in (2.58) is found to be

$$w_H = \frac{1}{2}\left(1 + v_D^2 + \frac{1}{\theta}\right) \tag{2.59}$$

which follows simply from the Maxwellian distribution functions. There is no contribution from the electric field.

If a hole structure is present, the distribution functions in the laboratory frame $f_e(x', v)$ and $f_i(x', u)$, which are related to the ones in the wave frame (2.7) by a Galilean transformation, have to be considered. The energy density can then be calculated as follows. First, we calculate the quantity

$$u_e(\Phi) = \int_{-\infty}^{+\infty} dv\, v^2 f_e(v) \tag{2.60}$$

which is twice the kinetic energy density of the electrons in the laboratory frame (we dropped the x'-dependence). Next, u_e is written in terms of $\tilde{v} = v - v_0$, the velocity in the wave frame:

$$\begin{aligned} u_e(\Phi) &= \int_{-\infty}^{+\infty} d\tilde{v}\, \tilde{v}^2 f_e(\tilde{v}) + 2v_0 \int_{-\infty}^{+\infty} d\tilde{v}\, \tilde{v} f_e(\tilde{v}) \\ &\quad + v_0^2 \int_{-\infty}^{+\infty} d\tilde{v}\, f_e(\tilde{v}) \\ &=: \widehat{u_e}(\Phi) + 2v_0 \int_{-\infty}^{+\infty} d\tilde{v}\, \tilde{v} f_e(\tilde{v}) + v_0^2\, n_e(\Phi) \end{aligned} \tag{2.61}$$

The quantity $\widehat{u_e}$ introduced in Eq. (2.61) is again twice the kinetic energy density of the electrons, this time measured in the wave frame. To find u_e we differentiate Eq. (2.61) by Φ, simplify and then integrate again. The differentiation yields

$$\frac{d}{d\Phi} u_e(\Phi) = \frac{d}{d\Phi} \widehat{u_e}(\Phi) + 2v_0 \frac{d}{d\Phi} \int_{-\infty}^{+\infty} d\tilde{v}\, \tilde{v} f_e(\tilde{v}) + v_0^2\, n_e'(\Phi). \tag{2.62}$$

The first term on the rhs of (2.62) is found in Ref. 12 to be $n_e(\Phi)$. The second term can be obtained by integrating the stationary Vlasov equation in the wave frame over the velocity $\tilde{v}$:

$$\partial_x \int_{-\infty}^{+\infty} d\tilde{v}\, \tilde{v} f_e(\tilde{v}) = -\Phi'(x) \int_{-\infty}^{+\infty} d\tilde{v}\, \partial_{\tilde{v}} f_e(\tilde{v}) = -\Phi'(x)\, f_e(\tilde{v})\Big|_{-\infty}^{+\infty} = 0 \tag{2.63}$$

On the left hand side of Eq. (2.63) the differentiation ∂_x is replaced by $\frac{d\Phi(x)}{dx}\frac{d}{d\Phi}$. Eq. (2.63) then reads

$$\Phi'(x) \frac{d}{d\Phi} \int_{-\infty}^{+\infty} d\tilde{v}\, \tilde{v} f_e(\tilde{v}) = 0. \tag{2.64}$$

As $\Phi'(x)$ is not generally zero, this implies that $\frac{d}{d\Phi}\int d\tilde{v}\, \tilde{v} f_e(\tilde{v}) = 0$, i.e. the second term of the rhs of (2.62) vanishes.

Eq. (2.62) can therefore be simplified to the following expression:

$$\frac{d}{d\Phi} w_e(\Phi) = n_e(\Phi) + v_0^2\, n_e'(\Phi). \tag{2.65}$$

Integration of (2.65) over Φ yields w_e:

$$w_e(\Phi) = \int_0^\Phi n_e(\Phi)\, d\Phi + v_0^2\,[n_e(\Phi) - n_e(0)] + w_e(0) \tag{2.66}$$

The only quantity which remains to be determined is $w_e(0)$. It is calculated using the definition (2.60), setting $\Phi = 0$ in (5a) of Ref. 12. The result is

$$w_e(0) = (1+K)\left(1 + v_D^2\right), \tag{2.67}$$

where $K = k_0^2\Psi/2$. The ionic term w_i can be calculated using similar arguments. In analogy to (2.65) one finds:

$$\frac{d}{d\Phi} w_i(\Phi) = -n_i(\Phi) + \frac{u_0^2}{\theta}\, n_i'(\Phi), \tag{2.68}$$

where w_i refers to the second integral in (2.58), including the factor $1/\theta$ (note that w_i was defined without this factor in Ref. 12).

In this case, however, it is easier to calculate $w_i(\Psi)$ than $w_i(0)$. For this reason the limits of integration are chosen as follows:

$$w_i(\Phi) = \int_\Phi^\Psi n_i(\Phi)\, d\Phi + \frac{u_0^2}{\theta}\,[n_i(\Phi) - n_i(\Psi)] + w_i(\Psi). \tag{2.69}$$

$w_i(\Psi)$ is again found from the definition analogous to (2.60), setting $\Phi = \Psi$ in the distribution function (5b) of Ref. 12:

$$w_i(\Psi) = \frac{(1+A)}{\theta}, \tag{2.70}$$

where A is given by (21) in Ref. 12. Thus the contribution of the kinetic energy terms to the total energy density is known.

We now insert the contribution of the kinetic energy of the electrons, given by (2.66) and (2.67), as well as the contribution of the kinetic energy of the ions, given by (2.69) and (2.70) into the expression for the total energy density (2.58). The contribution of the field energy is rewritten by replacing $\Phi'(x)^2$ by the classical potential $V(\Phi)$. Also, in the contribution of the ion kinetic energy, the integral $\int_\Phi^\Psi$ is replaced by $\int_0^\Psi - \int_0^\Phi$. This allows us to use Poisson's equation $n_e - n_i = \Phi''(x)$, which in turn can be expressed by $-V'(\Phi)$. After performing the (trivial) integration over Φ this contribution can be combined with the one from the field energy. Finally, the integration over x is performed for those terms not depending on space, and one gets an exact expression for the total energy density:

$$\begin{aligned} w = \quad & \frac{1}{2}\left[(1+K)\left(1+v_D^2\right) + \int_0^\Psi n_i(\Phi)\, d\Phi + \frac{(1+A)}{\theta}\right] \\ + \quad & \frac{1}{4L}\int_{-L}^{+L}\left\{v_0^2\,[n_e(\Phi) - n_e(0)] + \frac{u_0^2}{\theta}\,[n_i(\Phi) - n_i(\Psi)]\right\} dx \\ - \quad & \frac{3}{4L}\int_{-L}^{+L} V(\Phi)\, dx. \end{aligned} \tag{2.71}$$

Before the energy density (2.71) can be compared to the energy density of a homogenous plasma as given by (2.59), one has to make sure both expressions are given in the

same normalization. We remember that w is equal to the dimensional energy density, normalized by $kT_e n_{e0}^{(n)}$, with $n_{e0}^{(n)}$ given by (2.57). If the same standardized normalization $kT_e n_{e0}$ is to be used instead, w has to be divided by M (2.55). It is found by inspection that M can be written as

$$M =: 1 + \epsilon \tag{2.72}$$

with ϵ of order $\mathcal{O}(\Psi)$. As we will consider only the small amplitude limit we make use of $1/(1+\epsilon) \approx 1 - \epsilon$. Thus the total energy density of a structured plasma in the same normalization as was used for the homogeneous plasma is given by

$$\begin{aligned} w_S &\approx \frac{1-\epsilon}{2}\left[(1+K)\left(1+v_D^2\right) + \int_0^\Psi n_i(\Phi)\,d\Phi + \frac{(1+A)}{\theta}\right] \\ &+ \frac{1-\epsilon}{4L}\int_{-L}^{+L}\left\{v_0^2\left[n_e(\Phi) - n_e(0)\right] + \frac{u_0^2}{\theta}\left[n_i(\Phi) - n_i(\Psi)\right]\right\} dx \\ &- \frac{3(1-\epsilon)}{4L}\int_{-L}^{+L} V(\Phi)\,dx. \end{aligned} \tag{2.73}$$

Note that this renormalization was not taken into account in Ref. 12.

We now introduce the difference in the energy density, $\Delta\tilde{w}$ by

$$\Delta\tilde{w} := w_S - w_H. \tag{2.74}$$

We will show later that it is possible to find situations where $\Delta\tilde{w}$ is negative, which means that the perturbed state is then energetically lower than the unperturbed state. This is what we will call a negative energy state.

After insertion of (2.59) and (2.73) into the definition of $\Delta\tilde{w}$ the small amplitude limit, $\Psi \ll 1$, is taken, neglecting all contributions of order $\mathcal{O}(\Psi^2)$ and higher. The third part of Eq. (2.73) can be transformed using

$$\int_{-L}^{+L} V(\Phi)\,dx = -\int_0^\Psi \sqrt{-2V(\Phi)}\,d\Phi. \tag{2.75}$$

By inspection it can be seen that the contribution of (2.75) to (2.73) is of order $\mathcal{O}(\Psi^2)$ and can be neglected. Note that this implies that the contribution of the electrostatic energy is of higher order than that of the nonlinear trapping effect. Thus particle trapping obviously is not a small correction, but the dominant effect even at infinitesimal wave amplitude!

Note that A, K and ϵ are of order $\mathcal{O}(\Psi)$. By inserting $n_e(\Phi)$ and $n_i(\Phi)$, given by (20a,b) in Ref. 12, into (2.73) we then get the final expression for the energy density difference:

$$\begin{aligned} \Delta\tilde{w} &= \frac{1}{2}\left[\Psi + (K-\epsilon)\left(1+v_D^2\right) + \frac{A-\epsilon}{\theta}\right] \\ &+ \frac{v_0^2}{4L}\int_{-L}^{+L}\left\{-\frac{1}{2}Z_r'\left(\frac{\tilde{v}_D}{\sqrt{2}}\right)\Phi - \frac{4}{3}b(\beta,\tilde{v}_D)\Phi^{3/2}\right\} dx \\ &+ \frac{u_0^2}{4L\theta}\int_{-L}^{+L}\left\{-\frac{\theta}{2}Z_r'\left(\frac{u_0}{\sqrt{2}}\right)(\Psi-\Phi)\right. \\ &\qquad \left. -\frac{4}{3}b(\alpha,u_0)\left[\theta(\Psi-\Phi)\right]^{3/2}\right\} dx \end{aligned} \tag{2.76}$$

This expression was first presented in Ref. 19. It allows us to search for regions in the parameter space where $\Delta\tilde{w}$ is negative, i.e. where negative energy modes exist. This will be done in the following section.

2.3.3 Explicit evaluation of Δw

This section is devoted to an explicit evaluation of Δw, defined as $\Delta w := \Delta\tilde{w}/\Psi$ (see below) for certain classes of wave structures with emphasis on regions where Δw is negative. Before doing this, we summarize the formulas needed and simplify the notation by introducing new dimensionless parameters.

If we rewrite the expression for the energy difference (2.76) using the simplifying notation introduced at the beginning of section 2.2, we find

$$\begin{aligned}\Delta w := \frac{\Delta\tilde{w}}{\Psi} &= \frac{1}{2}\left[1+\left(\frac{k_0^2}{2}-\varepsilon\right)\left(1+v_D^2\right)+\frac{\mathcal{A}-\varepsilon}{\theta}\right] \\ &\quad +\frac{v_0^2}{4L}\int_{-L}^{+L}\left[-\frac{1}{2}Z_r'\left(\frac{\tilde{v}_D}{\sqrt{2}}\right)\phi-\frac{5}{4}B_e\phi^{3/2}\right]dx \\ &\quad +\frac{u_0^2}{4L\theta}\int_{-L}^{+L}\left[-\frac{\theta}{2}Z_r'\left(\frac{u_0}{\sqrt{2}}\right)(1-\phi)\right. \\ &\quad \left.-\frac{5}{4}B_i(1-\phi)^{3/2}\right]dx \end{aligned} \tag{2.77}$$

with

$$\begin{aligned}\varepsilon := \frac{\epsilon}{\Psi} &= \frac{k_0^2}{2}-\frac{1}{2}Z_r'\left(\frac{\tilde{v}_D}{\sqrt{2}}\right)\frac{1}{2L}\int_{-L}^{+L}\phi\,dx \\ &\quad -\frac{5}{4}B_e\frac{1}{2L}\int_{-L}^{+L}\phi^{3/2}dx \end{aligned} \tag{2.78a}$$

$$\mathcal{A} := \frac{A}{\Psi} = \frac{\theta}{2}Z_r'\left(\frac{u_0}{\sqrt{2}}\right)+\frac{5}{4}B_i. \tag{2.78b}$$

We emphasize that our rescaled energy expression Δw in (2.77) does not contain the amplitude Ψ as an independent parameter anymore: now it only appears through B_e and B_i, where it is used in conjunction with the trapping parameters α and β.

In terms of our new parameters, (2.30) and (2.31) are written as

$$k_0^2 \geq 0 \tag{2.79a}$$

$$k_0^2 \geq \frac{B_i-B_e}{2}. \tag{2.79b}$$

We must exclude the case $k_0^2 = B_e = B_i = 0$ that would lead to a null classical potential. In this case higher order terms that have been neglected would come into play.

At this point, the following cases are of interest:

- Generalized solitary electron holes, in which $k_0^2 = 0$ and $\mathcal{V}'(0) = 0$. The potential ϕ has a bell-like shape
- Generalized solitary ion holes, with $k_0^2 = \frac{B_i-B_e}{2}$, $\mathcal{V}'(1) = 0$. The potential has an inverted bell-shape.

- Harmonic (monochromatic) waves, in which $B_e = B_i = 0$, $k_0^2 > 0$.

The formalism allows other structures as well like cnoidal waves [27] and double layers [11, 13], but these will not be treated in this thesis.

Now we study the existence of negative energy solutions for the three cases mentioned.

Generalized solitary electron holes

We call generalized solitary electron hole the structure that appears when $k_0^2 = 0$, described in Sect. 2.2.1 This results in a bell-like shape potential $\phi(x)$; the term "generalized" comes from the fact that we allow B_i to be nonzero. In this case, (2.79b) reduces to $B_e \geq B_i$. In this section we will restrict ourselves to $B_e > B_i \geq 0$.

We are interested in finding the areas in the parameter space where negative energies can exist. These areas can be found by combining equations (2.52) and (2.77). Therefore, we will first look for values of our parameters that would give us negative energies and later we will restrict to those values allowed by the NDR.

Proceeding this way, we first look at (2.77) in order to find a simplified expression valid for electron holes. This has already been done in Ref. 19 for $B_i = 0$, where one could analytically integrate (2.24). When we allow for $B_i \neq 0$, it seems no longer possible to obtain such a quadrature. However, as $\phi(x)$ has a bell-like shape that becomes zero at both infinities, it is clear that

$$\lim_{L\to\infty} \frac{1}{2L} \int_{-L}^{+L} (1-\phi)^{3/2} dx = 1, \tag{2.80}$$

while $\frac{1}{2L}\int \phi(x)dx$ and $\frac{1}{2L}\int \phi^{3/2}(x)dx$ vanish in this limit $L \to \infty$.

Therefore, we can rewrite (2.77) as

$$\Delta w = \frac{1}{2}\left\{1 + \frac{1}{\theta}\left[\frac{\theta}{2} Z_r'\left(\frac{u_0}{\sqrt{2}}\right) + \frac{5}{4} B_i\right]\left(1 - u_0^2\right)\right\} \tag{2.81}$$

which is an extension of Eq. (8) in Ref. 19. Note that it has no explicit B_e-dependence, which means that essentially only ion trapping will affect its value and its sign. More precisely, B_e will enter implicitly through the back-door via the NDR where it influences v_0 resp. u_0.

An inspection of (2.81) shows us that in order to yield negative energies, u_0 has to be larger than some $u_0^\star$ which is defined by $\Delta w(u_0^\star) = 0$ and only depends on θ for given B_i. If $B_i = 0$, this value will be constant: we will find $\Delta w < 0$ whenever $u_0 > 2.124$. If $B_i > 0$, the limiting $u_0^\star$ will grow monotonically from 1 ($\theta = 0$) to 2.124 ($\theta \to \infty$). The θ-dependence of $u_0^\star$ is shown in the dotted and dash-dotted lines of Fig. 2.6 (for $B_i = 0$ and $B_i = 0.2$, respectively).

The second step in our procedure is to look at the nonlinear dispersion relation, which becomes

$$-\frac{1}{2} Z_r'\left(\frac{\tilde{v}_D}{\sqrt{2}}\right) - \frac{\theta}{2} Z_r'\left(\frac{u_0}{\sqrt{2}}\right) = B_e + \frac{3}{2} B_i. \tag{2.82}$$

Whether it has a solution with $\tilde{v}_D \geq 0$ depends on the values of θ and u_0. If we remember that $-0.285 \leq -\frac{1}{2} Z_r'\left(\frac{\tilde{v}_D}{\sqrt{2}}\right) \leq 1$, we can delimit the region of the θ, u_0 plane in which solutions exist by plotting the curves that correspond to $-\frac{1}{2} Z_r'\left(\frac{\tilde{v}_D}{\sqrt{2}}\right) = 1$ (i.e.

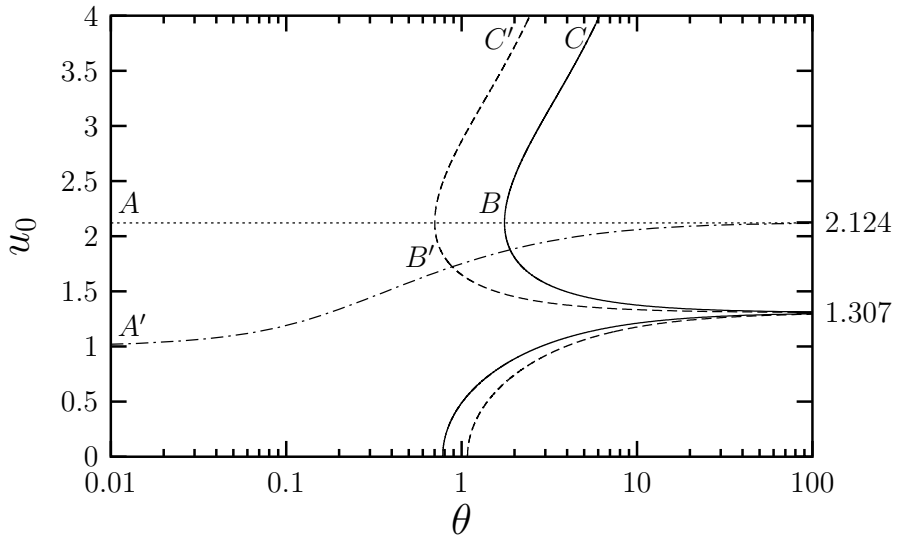

Figure 2.6: The dotted and dash-dotted curves represent the values $u_0^\star$ that would give $\Delta w = 0$ respectively for $B_i = 0$ and $B_i = 0.2$. Negative energies appear only above these curves. Also shown are the boundaries of the area where solutions of the NDR exist: for $B_i = 0$ (solid line) and $B_i = 0.2$ (dashed line) we have plotted the curves implicitly given by $-\frac{1}{2}Z_r'\left(\frac{\tilde{v}_D}{\sqrt{2}}\right) = 1$ (upper branch) and $-\frac{1}{2}Z_r'\left(\frac{\tilde{v}_D}{\sqrt{2}}\right) = -0.285$ (lower branch). Solutions of the NDR exist to the left of these curves. Both are made for $B_e = 0.5$.

$\tilde{v}_D = 0$, upper branch) and $-\frac{1}{2}Z_r'\left(\frac{\tilde{v}_D}{\sqrt{2}}\right) = -0.285$ (i.e. $\tilde{v}_D = 2.124$, lower branch). The allowed areas lie to the left and between these curves (solid and dashed lines in Fig. 2.6). Some remarks should be given:

1. As $\frac{1}{2}Z_r'\left(\frac{u_0}{\sqrt{2}}\right) = 0$ for $u_0 = 1.307$, the curves show an asymptotic behavior at this value of u_0. If $0 < B_e + \frac{3}{2}B_i < 1$, there will exist one and only one solution with $u_0 = 1.307$ for every value of θ.

2. We can easily see that for $B_e + \frac{3}{2}B_i > 1$ no solutions with $u_0 > 1.307$ can appear. As negative energies appear only above certain value of u_0 between 1 and 2.12, we will henceforth restrict ourselves to $B_e + \frac{3}{2}B_i \leq 1$, thus neglecting a relatively small number of negative energy solutions around $B_e + \frac{3}{2}B_i \approx 1$, $B_i \neq 0$ and $\theta \ll 1$.

Now we are able to combine (2.81) and (2.82) to find the negative energy modes which are allowed by the NDR. They will be above $u_0^\star$ and to the left of the upper branch of the NDR limit. In Fig. 2.6 they are bounded by ABC (for $B_i = 0$) and $A'B'C'$ (for $B_i = 0.2$). We call $\theta^\star$ the value of θ in which the curve $u_0^\star(\theta)$ intersects the upper branch of the NDR limit (points labeled B and B' in Fig. 2.6).

Now we move to the θ, v_D plane. There, we can obtain a first approach to a "nonlinear stability region" if we consider the case $B_i = 0$. Figure 2.7 shows the negative energy boundaries for this value of B_i and three values of B_e. We can understand the shape of these figures if we follow the path given by the points ABC ($B_e = 0.5$), that correspond also to those of Fig. 2.6 (all but C: see caption). From A to B we move along a line with fixed $u_0 = 2.124$ and $\Delta w = 0$. The NDR (2.82) shows that the θ dependence of v_D is

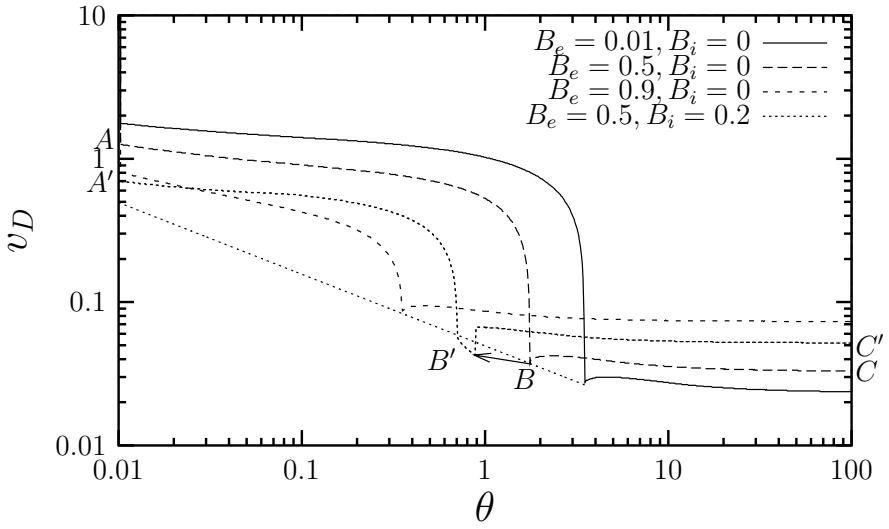

Figure 2.7: Regions of existence of negative energy electron holes for some values of B_e and B_i. Negative energy appears above the curves plotted. Points C and C' do not actually correspond to those of Fig 2.6, but both are intended to be just arbitrary points with $\theta > \theta^\star$ (see text).

implicitly given by

$$-\frac{1}{2}Z_r'\left(\frac{\tilde{v}_D}{\sqrt{2}}\right) = B_e + 0.285\theta \tag{2.83}$$

(remember that $\tilde{v}_D = v_D - v_0 = v_D - u_0\sqrt{\delta/\theta}$). We will reach B at $\theta = \theta^\star$, the point where the NDR allows no more solutions with $u_0 = 2.124$ ($\Delta w = 0$). From (2.83), we can obtain the exact value of $\theta^\star$ if we set $-\frac{1}{2}Z_r'\left(\frac{\tilde{v}_D}{\sqrt{2}}\right)$ to 1, its maximum value:

$$\theta^\star = \frac{1}{0.285}\left(1 - B_e\right). \tag{2.84}$$

From B to C we move in a range where $\Delta w = 0$ is not possible, although $\Delta w < 0$ is. The dependence of the minimum v_D on θ is depicted in the right part of each plot in Fig. 2.7.

As we increase B_e, the corner (B in Fig. 2.7) at $\theta^\star$ is shifted towards smaller values of θ and larger values of v_D following the equation

$$v_D = 2.124\sqrt{\frac{\delta}{\theta^\star}}, \tag{2.85}$$

that results from $u_0 = 2.124$, $\tilde{v}_D = 0$, that in turn follows from the NDR (2.82) making use of (2.84). Equation (2.85) gives us a kind of nonlinear stability limit for electron holes with $B_i = 0$. This limit (left part of solid line in Fig. 2.8) extends from $\theta^\star = 0$ (for $B_e = 1$) to $\theta^\star = \frac{1}{0.285} \approx 3.509$ (remember that (2.79b) implies $B_e > 0$). For larger θ we must use the right part of the negative energy limit for very small B_e, which is approximated by $B_e = 0.01$ in Fig. 2.7. Considering all of this, we obtain the continuous line of Fig. 2.8, which clearly lies below the linear stability limit of Refs. 28 and 29

If we now allow $B_i \neq 0$, we can see (Figs. 2.6, 2.7) that for a given B_e, the corner at $\theta^\star$ (B and B') is shifted to the left but *below* the negative energies limit found for $B_i = 0$ (see arrow in Fig. 2.7). We can find a new limit if we allow B_i to be as large as possible

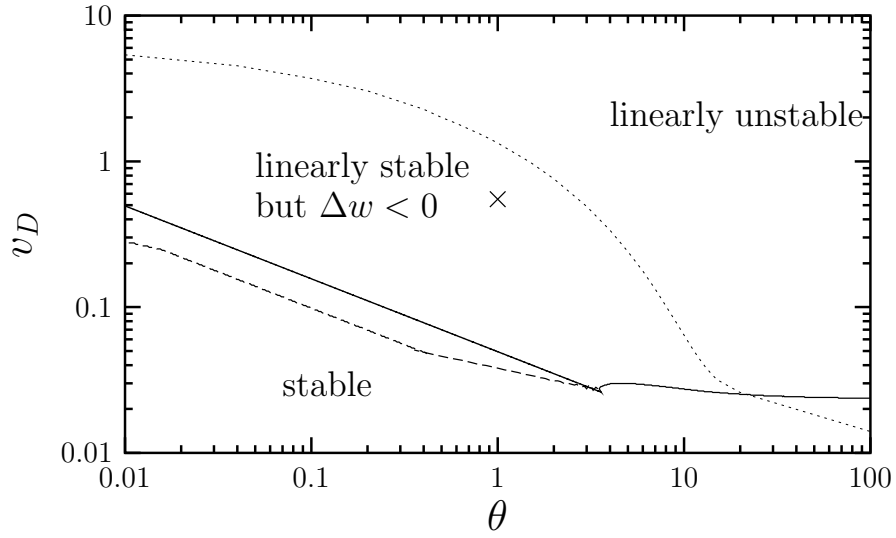

Figure 2.8: Expected stability regions for electron holes. The solid line represents the critical drift velocity $v_D(\theta)$ above which solitary electron holes with negative energy ($\Delta w < 0$) can be found for $B_i = 0$. The dashed line is the extension we can make if we allow $B_i \neq 0$. The dotted line represents the linear stability limit (after Refs. 28, 29).

for every value of B_e (i.e. we must impose $B_e > B_i$, and we require $B_e + \frac{3}{2}B_i \leq 1$). The corresponding corners give us the dashed line of Fig. 2.8.

We therefore conclude that the inclusion of B_i extends the region in the θ, v_D plane, albeit slightly, where negative energy generalized electron holes can be found.

Generalized solitary ion holes

Now we examine the generalized solitary ion hole case, in which $k_0^2 = \frac{B_i - B_e}{2}$, so that the potential has an inverted-bell shape. Now, (2.79a) requires $B_i \geq B_e$; we will treat only the case $B_i \geq B_e \geq 0$.

We will follow the same steps as we did in the electron holes case: first we examine the energy expression looking for negative energy states. Later we restrict ourselves to the solutions which are allowed by the NDR.

Only if $B_e = 0$ we know that (2.24) can be integrated by a quadrature [19]. However, in order to find the concrete energy expression, it is only necessary to notice that, with this shape of the potential,

$$\lim_{L\to\infty} \frac{1}{2L} \int_{-L}^{+L} \phi^{3/2} dx = 1, \tag{2.86}$$

whereas $\frac{1}{2L}\int(1-\phi)dx$ and $\frac{1}{2L}\int(1-\phi)^{3/2}dx$ vanish in the limit $L \to \infty$.

If we now insert these integrals into the general energy expression (2.77), we get

$$\Delta w = \frac{1}{2}\left\{1 + \left[\frac{1}{2}Z_r'\left(\frac{\tilde{v}_D}{\sqrt{2}}\right) + \frac{5}{4}B_e\right](1 + v_D^2 - v_0^2)\right\}. \tag{2.87}$$

Note that this expression does not explicitly depend on B_i, and a statement analogous to that for the electron hole case after (2.81) can be made.

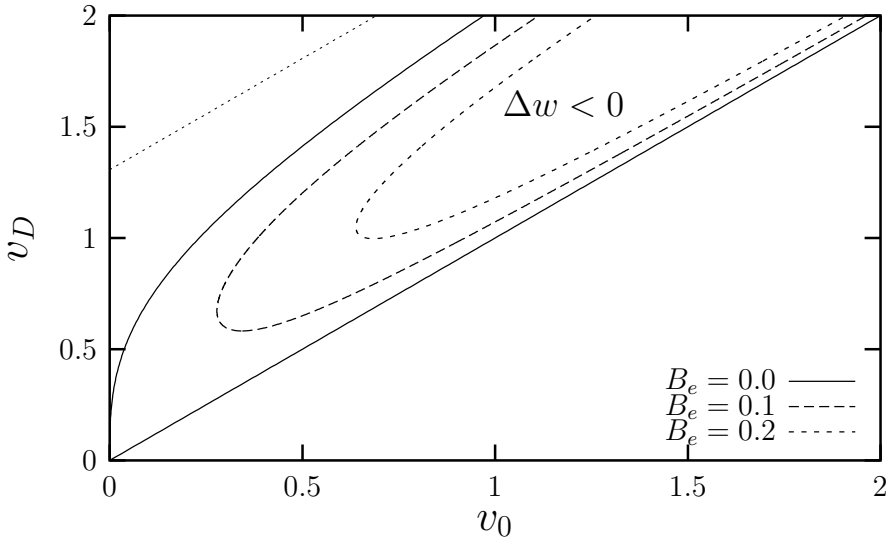

Figure 2.9: Areas of the v_0, v_D plane where negative energy ion holes appear for different values of B_e. The dotted line corresponds to $\tilde{v}_D = 1.307$: note that no negative energy modes are found above this line; therefore $-\frac{1}{2}Z_r'\left(\frac{\tilde{v}_D}{\sqrt{2}}\right) > 0$.

This time, the sign of the energy depends on two quantities, v_D and v_0. In Fig. 2.9 we can see the areas of the v_D, v_0 plane in which the energy becomes negative, depending on the value of B_e. No negative energy modes are found with $\tilde{v}_D > 1.307$.

For $B_e = 0$ these areas were already given in Ref. 19. Indeed, in this particular case, Δw vanishes for $\tilde{v}_D = v_D - v_0 = 0$ while another solution for $\Delta w = 0$ exists, which we call $v_\star$. Realistic values for ion hole velocities lie in the ion thermal range. This implies that $v_0 \leq O\left(\sqrt{\delta/\theta}\right)$. For θ not too small, v_0 is hence a small quantity and the negative energy condition for v_D becomes $v_0 < v_D < (3v_0)^{1/3} < 1$. We can also express this condition as

$$\frac{v_D^3}{3} < \sqrt{\frac{\delta}{\theta}} < v_D. \tag{2.88}$$

Remember that u_0 stands for the phase velocity of the hole structure normalized by the ion thermal velocity.

For $B_e > 0$, there exist minimal values of v_D and v_0 for negative energy solutions, as seen from Fig. 2.9.

Our second step is to look at the NDR (2.52), which for ion holes takes the form

$$-\frac{1}{2}Z_r'\left(\frac{\tilde{v}_D}{\sqrt{2}}\right) - \frac{\theta}{2}Z_r'\left(\frac{u_0}{\sqrt{2}}\right) = B_i + \frac{3}{2}B_e. \tag{2.89}$$

At this point, two different cases must be treated:

1. If $B_i + \frac{3}{2}B_e > 1$, which we may call strong ion trapping regime, there exists a distinguished value of θ, which we call θ_0, that satisfies $1 + \theta_0 = B_i + \frac{3}{2}B_e$. For this θ_0, $v_D = v_0 = u_0 = 0$ is a valid solution of the NDR (2.89). Note also that there can be no solutions for $\theta < \theta_0$.

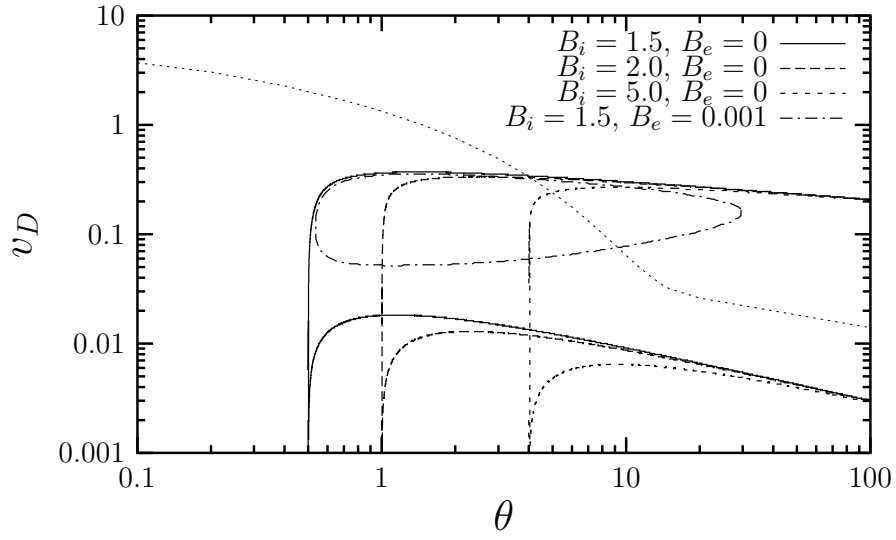

Figure 2.10: Negative energy areas of the θ, v_D plane for ion holes with different values of B_e and B_i satisfying $B_i + \frac{3}{2}B_e > 1$. The vertical lines where the curves for $B_e = 0$ abruptly cease are given by $\theta = \theta_0$. Note the shrunk area of $\Delta w < 0$ in case of $B_e = 0.001$. The dotted line represents the linear stability limit.

Using equations (2.87) and (2.89), we can plot the areas in the θ, v_D plane where negative energy solutions exist for given values of our parameters B_e and B_i. In Fig. 2.10 we have plotted the shapes of the negative energy areas for different values of B_i and B_e.

As can be seen, for $B_e = 0$ these curves extend down to $v_D = 0$ at θ_0.This is due to the fact that in this case the energy expression gives us $\Delta w = 0$ for $\tilde{v}_D = 0$, so that negative energy states will always exist in the proximity of these values. Hence, for each value of $v_0 \ll 1$, in the linearly stable region, a value of B_i can be found for which a negative energy ion hole exists. *Note that this implies no threshold velocity.*

Now we set $B_e > 0$. From (2.82) and $B_i + \frac{3}{2}B_e > 1$ we can see that $-\frac{1}{2}Z_r'\left(\frac{u_0}{\sqrt{2}}\right) > 0$ and therefore $u_0 < 1.307$. This can also be expressed as

$$\sqrt{\frac{\theta}{\delta}}v_0 < 1.307. \tag{2.90}$$

But, as we have already shown in Fig. 2.9, when $B_e > 0$, there exists a minimum v_0 for negative energy modes. If we call this v_0^{min}, we find that θ has to satisfy

$$\theta < \delta\left(\frac{1.307}{v_0^{min}}\right)^2. \tag{2.91}$$

Therefore we have constraints both in θ and in v_D. This explains why the negative energy areas are significantly diminished even for a very small value of B_e, as can be seen in Fig. 2.10.

2. If $B_i + \frac{3}{2}B_e < 1$, corresponding to a moderate or small ion trapping effect, the shape of the negative energy regions has a very different form, as can be seen in Fig. 2.11.

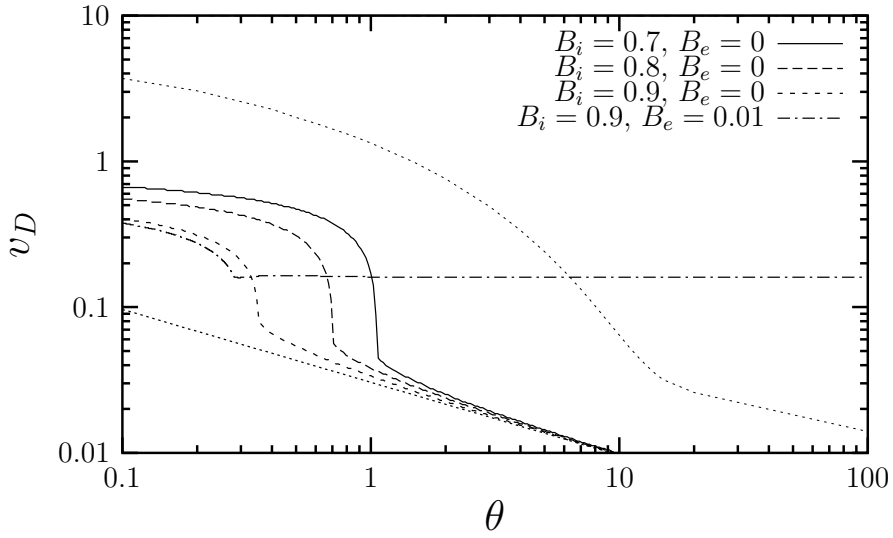

Figure 2.11: Negative energy areas of the θ, v_D plane for ion holes with different values of B_e and B_i satisfying $B_i + \frac{3}{2}B_e < 1$. The lower dotted line represents the asymptotic limit of negative energies for $B_e = 0$ and large θ, given by (2.92) in the text. The upper dotted line represents the linear stability limit.

Now for every θ, there exists a finite minimum drift velocity. If $B_e = 0$, as we increase B_i, the limiting curve is shifted downwards. Therefore, the largest negative area is the one given by $B_i \approx 1$. For large θ all of these curves can be approximated by letting $u_0 = 1.307$, $v_0 = v_D$ thus yielding (dotted line in Fig. 2.11)

$$v_D = 1.307\sqrt{\frac{\delta}{\theta}}. \tag{2.92}$$

When $B_e > 0$, we must consider again that a minimum v_D appears (Fig. 2.9) and the negative energy areas are reduced, as shown in Fig. 2.11.

Harmonic (monochromatic) waves

The third case we are considering here is that of harmonic waves, where $B_e = B_i = 0$ and k_0^2 is left arbitrary but larger than zero. In this case, the classical potential reduces to

$$-\mathcal{V}(\phi) = \frac{k_0^2}{2}\phi(1-\phi). \tag{2.93}$$

From this expression, we can integrate (2.24) and obtain a harmonic wave with wavenumber k_0 (and, therefore, half-period $L = \frac{\pi}{k_0}$):

$$\phi = \frac{1}{2}\left[1 + \cos(k_0 x)\right]. \tag{2.94}$$

This harmonic potential is an exact solution of our nonlinear equations. Note that $B_e = B_i = 0$ still implies that a certain amount of trapping is required (i.e. $\alpha = 1 - u_0^2$ and

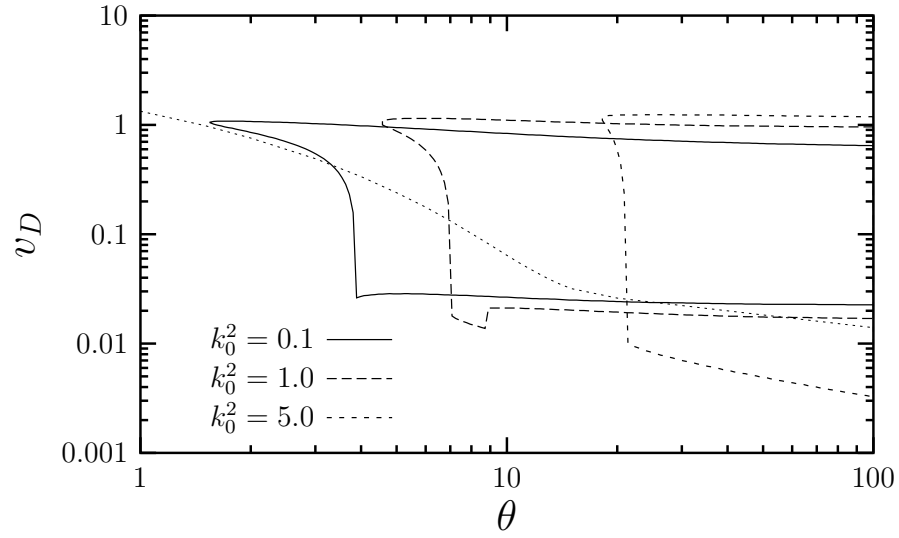

Figure 2.12: Negative energy areas of the θ, v_D plane for purely harmonic waves with different values of k_0^2. The dotted line represents the linear stability limit.

$\beta = 1 - \tilde{v}_D^2$). By inserting the potential (2.94) into the integrals that appear in the energy expression, and calculating the resulting trivial integrals, one gets

$$\begin{aligned}\Delta w =& \frac{1}{2}\left\{1 + \frac{k_0^2}{2}\left(1 + v_D^2\right) + \frac{1}{4}Z_r'\left(\frac{u_0}{\sqrt{2}}\right)\left[1 - \theta\left(1 + v_D^2\right) - u_0^2\right]\right. \\ & \left. - \frac{v_0^2}{4}Z_r'\left(\frac{\tilde{v}_D}{\sqrt{2}}\right)\right\},\end{aligned} \tag{2.95}$$

while the NDR (2.52) is in this case as simple as

$$k_0^2 - \frac{1}{2}Z_r'\left(\frac{\tilde{v}_D}{\sqrt{2}}\right) - \frac{\theta}{2}Z_r'\left(\frac{u_0}{\sqrt{2}}\right) = 0. \tag{2.96}$$

Combining (2.95) and (2.96) we obtain

$$\begin{aligned}\Delta w =& \frac{1}{2}\left\{1 + \frac{k_0^2}{2}\left(1 + v_D^2 - v_0^2\right) + \right. \\ & \left. \frac{1}{4}Z_r'\left(\frac{u_0}{\sqrt{2}}\right)\left[1 - \theta\left(1 + v_D^2 - v_0^2\right) - u_0^2\right]\right\}.\end{aligned} \tag{2.97}$$

Now we can proceed to scan the θ, v_D plane looking for negative energy states. Combining the condition $\Delta w < 0$ with the NDR one again obtains a region of allowed states with negative energy density. The boundary of this region is shown in Fig. 2.12 for different values of k_0^2. Negative energy states with given k_0^2 exist to the right of the corresponding curve. One can clearly see that *negative energy harmonic waves can be found in the linearly stable region;* at very low drift velocities v_D only negative energy harmonic waves with large wave number (i.e. short wavelength) exist, but for larger drift velocities the restriction on the allowed values of k_0 is less severe. Note that harmonic waves of negative energy are possible only for $\theta \gtrsim 1$.

2.4 Numerical simulation

This section will be devoted to the description and results of numerical simulations of the Vlasov-Poisson system[1]. These numerical simulations will allow us to (i) check the validity of the pseudo-potential method, (ii) include the eventual effects of small collisions which we disregarded up to this point and (iii) observe the temporal evolution of the system when the initial conditions are close but not exactly matching any of our solutions.

The main technical problems involved in the simulation of Vlasov systems are well known in the literature: they are related with the so-called *filamentation* of phase-space. As the Vlasov equation is conservative, the value of the distribution function is preserved along the trajectory of any particle. These trajectories are, if time steadiness is not granted, rather complex and lead to phase-mixing, i.e. the appearance of finer and finer structures in phase space which at some point become too small to be followed by the finite resolution of the numerics. This is an intrinsically unavoidable problem of integrating the Vlasov equation and can, therefore, never be completely overcome. We may try, however, to devise methods that allow us to minimize this difficulty and let us simulate the Vlasov equation for longer times.

Here we will use a method particularly suited for dealing with velocity distributions close to a Maxwellian. We will decompose the distribution functions into Hermite polynomials in velocity space and Fourier modes in coordinate space. But before we get into details, let us devote some words to the effect of dissipation in the Vlasov equation (2.1a).

2.4.1 Fokker-Planck collision operator

To include a certain degree of collisions in equation (2.1a) we should first remember that it comes from the Boltzmann equation where the term describing collisions was neglected. The Boltzmann equation for electrons in its full form stands

$$\partial_t f_e + v\partial_x f_e + \partial_x \Phi \partial_v f_e = \left(\frac{\partial f}{\partial t}\right)_c \tag{2.98}$$

where the term $\left(\frac{\partial f}{\partial t}\right)_c$, commonly called *collision integral*, represents the instantaneous change of f_e due to collisions. The explicit calculation of this term is rather involved and beyond the scope of this thesis. To deal with collisions integral, a collision model including some simplifications has to be used instead [30].

We define $\psi(v, \Delta v)$ as the probability that a particle, due to collisions, changes its velocity from v to $v + \Delta v$ in a given time interval Δt. The distribution function therefore satisfies

$$f(x, v, t) = \int d(\Delta v) f(x, v - \Delta v, t - \Delta t)\psi(v - \Delta v, \Delta v). \tag{2.99}$$

If we perform a Taylor expansion on $f\psi$ we obtain

$$\begin{aligned} f(x, v, t) = \int d(\Delta v) \Big\{ & f(x, v, t - \Delta t)\psi(v, \Delta v) - \Delta v \frac{\partial (f\psi)}{\partial v} \\ & + \frac{1}{2}\Delta v \Delta v \frac{\partial^2 (f\psi)}{\partial v^2} \Big\}. \end{aligned} \tag{2.100}$$

[1]The code described in this section can be downloaded from the internet at `http://www.phy.uni-bayreuth.de/~btpa16/downloads.html`.

But we can rewrite these integrals by taking into account

$$\int d(\Delta v)\psi(v,\Delta v) = 1, \tag{2.101a}$$

i.e., a particle must be found somewhere, and defining

$$\langle \Delta v\rangle := \int d(\Delta v)\Delta v\psi(v,\Delta v), \tag{2.101b}$$

$$\langle \Delta v\Delta v\rangle := \int d(\Delta v)\Delta v\Delta v\psi(v,\Delta v), \tag{2.101c}$$

and finally write

$$f(x,v,t) = f(x,v,t-\Delta t) - \frac{\partial\left(f\langle\Delta v\rangle\right)}{\partial v} + \frac{1}{2}\frac{\partial^2\left(f\langle\Delta v\Delta v\rangle\right)}{\partial v^2}. \tag{2.102}$$

Now all the physics of collisions is hidden in the factors $\langle\Delta v\rangle$ and $\langle\Delta v\Delta v\rangle$ and has not to be further considered, as it is found in many textbooks [31]. A more direct way of deriving the collision operator is to make use of the BBGKY hierarchy of correlations to get, for the plasma case and for shielded Coulomb interactions, the Lenard-Balescu collision operator [32] which can be cooked down to a Fokker-Planck type collision operator, involving the Coulomb logarithm. Finally, by assuming the presence of a neutral gas, we can further simplify the collision operator which can in that case be written as

$$\left(\frac{\partial f}{\partial t}\right)_c = \frac{\partial}{\partial v}\left(-\nu v f + D(v)\frac{\partial f}{\partial v}\right), \tag{2.103}$$

where ν is the collision rate between the given species and the neutral gas and $D(v)$ is a diffusion coefficient. As we may expect that collisions lead the particle distribution towards a Maxwellian as given in (2.3), we can set $D(v) = -\nu$ and then write the collisional term as

$$\left(\frac{\partial f}{\partial t}\right)_c = -\nu\frac{\partial}{\partial v}\left(vf + \frac{\partial f}{\partial v}\right) =: \nu\mathbf{F}f, \tag{2.104}$$

the operator $\mathbf{F} = \frac{\partial}{\partial v}\left(v + \frac{\partial}{\partial v}\right)$ being called *Fokker-Planck collisional operator*. Thus, to include collisions, equations (2.1) should be corrected, in the wave frame, as

$$\partial_t f_e + v\partial_x f_e + \partial_x\Phi\partial_v f_e = \nu_e\partial_v\left[\partial_v f_e + (v-\tilde{v}_D)f_e\right] \tag{2.105a}$$

$$\mu\partial_t f_i + u\partial_x f_i - \theta\partial_x\Phi\partial_u f_i = \nu_i\partial_u\left[\partial_u f_i + (u+u_0)f_i\right], \tag{2.105b}$$

with

$$\nu_i = \nu_e\sqrt{\frac{\theta}{\delta}}. \tag{2.106}$$

2.4.2 Fourier-Hermite decomposition

We can integrate equations (2.105) by performing a decomposition in Fourier modes and Hermite polynomials. The latter are given by the expression

$$\mathrm{He}_m(z) = (-1)^m e^{z^2/2}\frac{d^m}{dz^m}e^{-z^2/2}. \tag{2.107}$$

They satisfy the recursive relations

$$\mathrm{He}_{m+1}(z) = z\mathrm{He}_m(z) - \mathrm{He}'_m(z), \tag{2.108a}$$

$$m\mathrm{He}_{m-1}(z) = \mathrm{He}'_m(z), \tag{2.108b}$$

and the orthogonality relation

$$\int_{-\infty}^{+\infty} dz\, e^{-z^2/2}\mathrm{He}_n(z)\mathrm{He}_m(z) = m!\sqrt{2\pi}\delta_{nm}. \tag{2.109}$$

Now we can, in general, write the distribution functions for electrons and ions as

$$f_e(x,v,t) = \frac{1}{\sqrt{2\pi}}e^{-\frac{1}{2}(v-\tilde{v}_D)^2}\sum_{m=0}^{\infty}\frac{\mathrm{He}_m(v-\tilde{v}_D)}{(m-1)!!}\sum_{n=-\infty}^{\infty}k^e_{nm}(t)e^{\frac{in\pi x}{L}}, \tag{2.110a}$$

$$f_i(x,u,t) = \frac{1}{\sqrt{2\pi}}e^{-\frac{1}{2}(u+u_0)^2}\sum_{m=0}^{\infty}\frac{\mathrm{He}_m(u+u_0)}{(m-1)!!}\sum_{n=-\infty}^{\infty}k^i_{nm}(t)e^{\frac{in\pi x}{L}}, \tag{2.110b}$$

where L is the half-length of the system. Note that this decomposition implies that $f_s(x,v,t) = f_s(x+2L,v,t)$ and therefore limits us to periodic solutions or, if we use a large enough L, solitary solutions with identical conditions for $x \to +\infty$ and $x \to -\infty$. Double layers cannot, therefore, be simulated or found within this framework.

Note also that the coefficients $k^s_{nm}(t)$ are, in general, complex. However, the distribution functions are densities of probability and must therefore be always real. The condition $f_s(x,v,t) = f^*_s(x,v,t)$ imposes that

$$k^s_{nm}(t) = k^{s*}_{-nm}(t). \tag{2.111}$$

To obtain all the coefficients k^s_{nm} from the distribution functions themselves we can make use of the orthogonality properties of Fourier modes and Hermite polynomials (2.109) and find

$$k^e_{nm}(t) = \frac{1}{2L}\frac{1}{m!!}\int_{-L}^{+L}dx\int_{-\infty}^{+\infty}dv f_e(x,v,t)\mathrm{He}_m(v-\tilde{v}_D)e^{-\frac{in\pi x}{L}}, \tag{2.112a}$$

$$k^i_{nm}(t) = \frac{1}{2L}\frac{1}{m!!}\int_{-L}^{+L}dx\int_{-\infty}^{+\infty}du f_i(x,u,t)\mathrm{He}_m(u+u_0)e^{-\frac{in\pi x}{L}}. \tag{2.112b}$$

The decomposition given by (2.110) is exact but it would demand the use of an infinite number of coefficients which, of course, no computer can do. This means we have to truncate the expansion and limit the total number of coefficients to N Fourier modes ($-N < n < N$) and M Hermite polynomials ($0 \le m < M$). The selection of N and M is of course a tradeoff between accuracy (or maximum simulated time in which the results are still reliable) and computer use. There are however some limitations we have always to keep in mind.

Suppose we want to simulate a electrostatic structure of amplitude ψ and spatial extension l (typically several times an electron Debye length). Given the x-dependency in (2.110) it is clear that to have enough spatial resolution it must hold $\frac{L}{N\pi} \ll l$. This is,

$$N \gg \frac{L}{l\pi}. \tag{2.113}$$

On the other side, if the potential amplitude is ψ, the size of the structure in velocity space will be around $\sqrt{2\psi}$. For large m, Hermite polynomials may be approximated by

$$\mathrm{He}_m(z) = \begin{cases} (-1)^{m/2}(m-1)!!e^{z^2/4}\cos\left(z\sqrt{m+\frac{1}{2}}\right) & \text{if } m \text{ is even,} \\ (-1)^{(m-1)/2}\sqrt{\frac{1}{m}}m!!e^{z^2/4}\sin\left(z\sqrt{m+\frac{1}{2}}\right) & \text{if } m \text{ is odd.} \end{cases}$$

Then, if we use M polynomials, we achieve a resolution $\left(M+\frac{1}{2}\right)^{-1/2} \approx M^{-1/2}$. Therefore the condition to represent a structure of amplitude ψ yields $M^{-1/2} \ll \sqrt{2\psi}$ or

$$M \gg \frac{1}{2\psi}. \tag{2.114}$$

Densities and electrostatic potential

The Fourier-Hermite decomposition allow us to calculate the particle densities and the electrostatic potential without much computational effort. This is because, as a result of (2.109), when integrating in velocity space the contributions of all Hermite polynomials but $\mathrm{He}_0(z)$ vanish. Making use of this fact, we can calculate the densities of each species as

$$n_e(x,t) = \int_{-\infty}^{+\infty} dv f_e(x,v) = \sum_{n=-\infty}^{\infty} k^e_{n0}(t)e^{\frac{in\pi x}{L}}, \tag{2.115a}$$

$$n_i(x,t) = \int_{-\infty}^{+\infty} du f_i(x,u) = \sum_{n=-\infty}^{\infty} k^i_{n0}(t)e^{\frac{in\pi x}{L}}. \tag{2.115b}$$

These expressions determine also the electrostatic potential through the Poisson equation $\partial_x^2\phi(x,t) = n_e(x,t) - n_i(x,t)$. This results in

$$\phi(x,t) = \sum_{n\neq 0} \frac{L^2}{n^2\pi^2}\left(k^i_{n0} - k^e_{n0}\right)e^{\frac{in\pi x}{L}} + C, \tag{2.116}$$

where use was made of the necessary condition $\int_{-L}^{+L}\partial_x\phi = 0$ and C is an arbitrary constant that we will conventionally choose to assure $\phi(-L) = \phi(L) = 0$:

$$C = -\sum_{n\neq 0}(-1)^n \frac{L^2}{n^2\pi^2}\left(k^i_{n0} - k^e_{n0}\right). \tag{2.117}$$

For convenience we define also

$$c^s_{nm} := \frac{2L^2}{\pi^2 n^2}\mathrm{Re}(k^s_{nm}), \qquad s^s_{nm} := \frac{2L^2}{\pi^2 n^2}\mathrm{Im}(k^s_{nm}), \tag{2.118}$$

which allows us to rewrite (2.116) as

$$\phi(x,t) = \sum_{n=1}^{\infty}\left[(c^i_{n0} - c^e_{n0})\cos\left(\frac{n\pi x}{L}\right) + (s^i_{n0} - s^e_{n0})\sin\left(\frac{n\pi x}{L}\right)\right]. \tag{2.119}$$

In this way, as we choose an initially symmetric potential, we will often follow the evolution of the cosine coefficients c^e_{n0} and c^i_{n0}, which are usually enough to give us an idea of the involved processes.

2.4.3 Time integration

Once we have a suitable representation of the distribution functions, we can insert it into equations (2.105) and find out how the coefficients k^e_{nm} and k^i_{nm} evolve in time. The result reads

$$\begin{aligned}\frac{dk^e_{nm}}{dt} =& -\nu_e m k^e_{nm} + \frac{(m-1)!!}{(m-2)!!}\frac{iL\gamma^e_{nm-1}}{\pi} \\ & - \frac{in\pi}{L}\left[\tilde{v}_D k^e_{nm} + \frac{(m-1)!!}{(m-2)!!}k^e_{nm-1} + \frac{(m+1)!!}{m!!}k^e_{nm+1}\right],\end{aligned} \tag{2.120a}$$

$$\begin{aligned}\frac{dk^i_{nm}}{dt} =& \frac{1}{\mu}\left\{-\nu_e m k^i_{nm} - \frac{(m-1)!!}{(m-2)!!}\frac{i\theta L\gamma^i_{nm-1}}{\pi}\right. \\ & \left. -\frac{in\pi}{L}\left[-u_0 k^i_{nm} + \frac{(m-1)!!}{(m-2)!!}k^i_{nm-1} + \frac{(m+1)!!}{m!!}k^i_{nm+1}\right]\right\},\end{aligned} \tag{2.120b}$$

where the coupling coefficients γ^s_{nm} for any species s are defined as

$$\gamma^s_{nm} = \sum_{\bar{n}\neq 0}\frac{1}{\bar{n}}k^s_{n-\bar{n}\,m}\left(k^i_{\bar{n}0} - k^e_{\bar{n}0}\right). \tag{2.121}$$

Therefore, if we have an initial distribution function, we can decompose it as in (2.112) and then use (2.120) to integrate the evolution of each coefficient in time by using any numerical procedure, e.g. a fourth order Runge-Kutta [33].

Linear approximation

As we already mentioned, a large part of plasma kinetic theory has been developed in the framework of a linearization of Vlasov equations. We also said that the linear approach leaves out many important solutions of the full Vlasov-Poisson system, among them solutions constructed by the pseudo-potential method. Therefore, it would be interesting to compare the results of our fully non-linear code with those that an approximate linear code would yield. The Fourier-Hermite decomposition we have just described is also particularly well suited to perform this simplification.

The linearization of the Vlasov equation rests on the assumption that one is close enough to a homogeneous solution, in our case a Maxwellian as (2.5), which we may call f_0. Then we can write $f = f_0 + \epsilon f_1$, $\phi = \epsilon\phi_1$ with ϵ being a smallness parameter. If we insert this ansatz into Vlasov equation (2.1a) we get

$$\partial_t f_0 + \epsilon\partial_t f_1 + v\partial_x f_0 + \epsilon v\partial_x f_1 + \epsilon\partial_x\phi_1\partial_v f_0 + \epsilon^2\partial_x\phi_1\partial_v f_1 = 0. \tag{2.122}$$

Here the point is that if one were able to neglect the $\mathcal{O}(\epsilon^2)$ term, the resulting equation would appear as

$$\partial_t f + v\partial_x f + \partial_x\phi\partial_v f_0 = 0, \tag{2.123}$$

which is often referred to as the *linearized Vlasov equation*. The mistake here is to assume that whenever ϵf_1 is small, also $\epsilon\partial_v f_1$ is, which is, in general, false.

To test every result against linear theory we may still use (2.120) but now replace k^s_{nm} in (2.121) by certain k^0_{nm} which are the coefficients of the expansion of the homogeneous Maxwellian (2.5), simply

$$k^0_{nm} = \delta_{n0}\delta_{m0}. \tag{2.124}$$

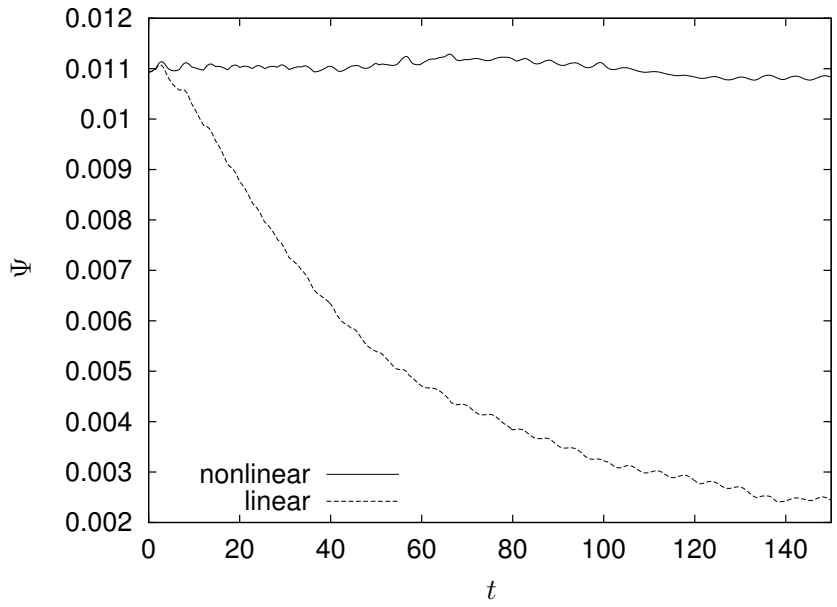

Figure 2.13: Evolution of the amplitude in linear and nonlinear runs of the Vlasov code with the same initial conditions corresponding to an electron hole. Note how the linear run damps out the structure where it remains stationary in the nonlinear run.

The linear expression for γ^s_{nm} yields

$$\gamma^s_{nm} = \delta_{m0} \frac{1}{n} \left(k^i_{n0} - k^e_{n0} \right) . \tag{2.125}$$

The utmost importance of the nonlinear terms in the trapping structures we are studying becomes apparent in Fig. 2.13. There the same initial conditions corresponding to an electron hole have been used for two different runs of the code and the evolution of the amplitude has been represented. If we keep the nonlinear terms, the electron hole, which is a solution of the full nonlinear Vlasov-Poisson system, remains rather stationary: only small oscillations due to inaccuracies in the initial conditions and truncation errors are visible. However, if we use a linear code, the structure is Landau-damped, as predicted by the linear theory. Note that we intentionally used a small amplitude electron hole to show that the linear theory fails even for arbitrarily small amplitudes.

2.4.4 Tests

To be sure that the code above described works correctly and produces accurate results, we have tested it against several known theoretical predictions as well as against the code used by Korn and Schamel in Refs. 34, 27, 35, where ions are either immobile or behave according to linearized fluid equations.

Two-stream instability

First of all, we will check that the code conforms to the theoretical predictions of linear stability on a two-stream electron-ion plasma [28]. For mass ratio $\delta = 1/100$ and equal

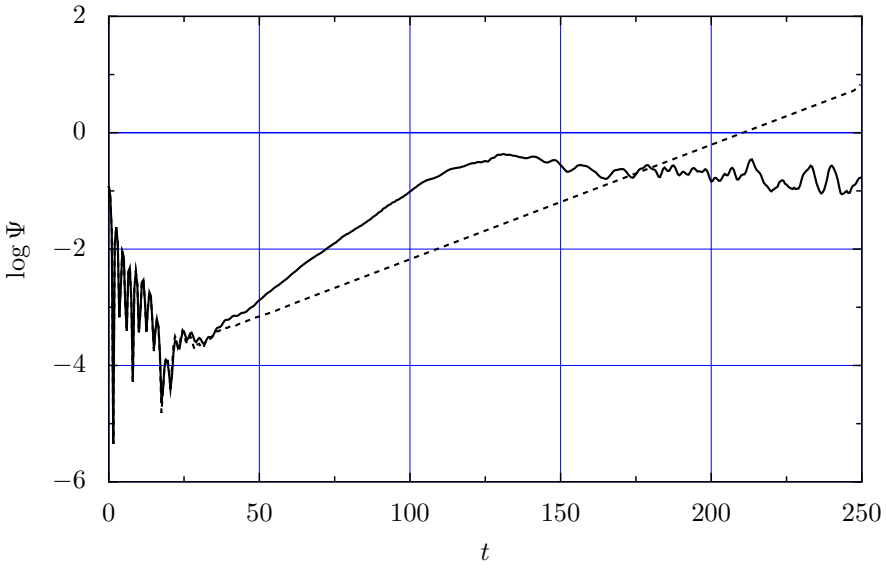

Figure 2.14: Evolution of the amplitude of the electrostatic potential in the linearly unstable regime of the two-stream instability, $\delta = 1/100$, $\theta = 1$, $v_D = 2.0$. The solid line represents the evolution of the fully nonlinear equation while the dashed one pictures the linear evolution. The simulation was performed with $M = 2000$, $N = 5$.

electron and ion temperatures, according to such theory, the plasma becomes unstable for drift velocities larger than $v_D^\star = 1.308(1 + \delta^{1/2}) = 1.4388$. To test the plasma stability we will introduce a perturbation in the electron distribution function. We set, at $t = 0$

$$f_e(x, v, t = 0) = \frac{1}{\sqrt{2\pi}} e^{-\frac{1}{2}(v-\tilde{v}_D)^2} \left(1 + \epsilon \cos(kx)\right), \tag{2.126a}$$

$$f_i(x, u, t = 0) = \frac{1}{\sqrt{2\pi}} e^{-\frac{1}{2}(u+u_0)^2}, \tag{2.126b}$$

where $k = \pi/L$, L being one half of the spatial periodicity imposed by the Fourier expansion. According to the decomposition given by (2.110a), this corresponds to the initial coefficients $k^e_{00} = 1$, $k^e_{10} = \epsilon/2$, $k^i_{00} = 1$ and all the remaining $k^s_{nm} = 0$. We will use here $\epsilon = 0.05$, $k = 1/2$. Note that the perturbed distribution function still has the shape of a *local Maxwellian* and therefore trapping and nonlinear effects play a negligible role for short evolution times, the distribution function experiencing no topological changes, e.g. no region will appear with $\partial_v f > 0$, $v > 0$.

A typical outcome of the code in the unstable regime is presented in Fig. 2.14, where the logarithm of the total potential amplitude is depicted as a a function of time for a linear as well as for a nonlinear run. Note how the linearized Vlasov equation leads to an exponential growth that does not saturate, while the full nonlinear equation drives a faster growth at the beginning but is finally saturated as the amplitude approaches a certain maximum.

On the other hand, a simulation ran with parameters inside the linearly stable regime produces the results showed in Fig. 2.15. In this case the linear and nonlinear runs first coincide but later the nonlinear evolution shows that, also in this case, and contrasting with the linear run, a certain saturation at low amplitude occurs which is a well-known

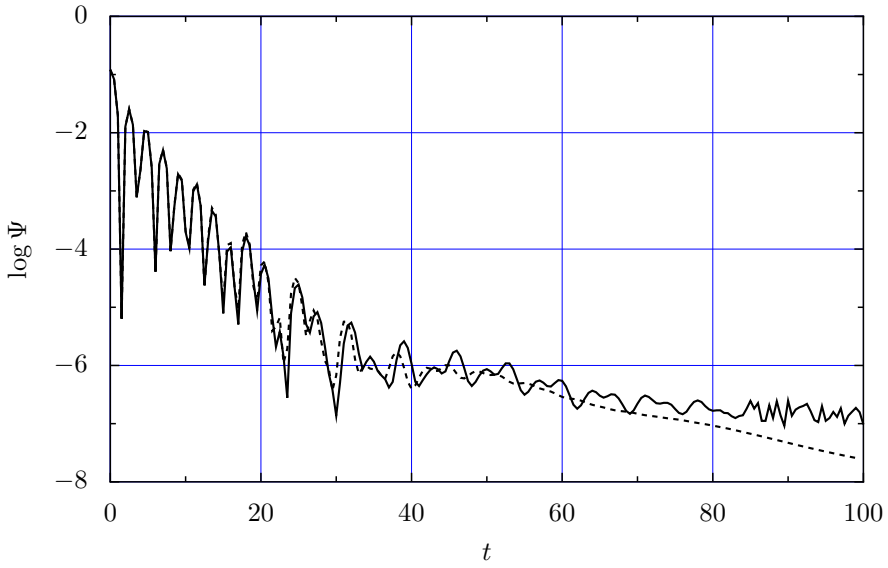

Figure 2.15: Same as in Fig. 2.14 but with $v_D = 1.0$, this is, in the linearly stable regime.

phenomenon associated with the so-called nonlinear Landau damping scenario [36]; this temporal evolution was also seen in numerical simulations by G. Manfredi [37].

Summarizing the outcomes of the code in the linearly stable and unstable regimes, one is tempted conclude that the result are in accordance with the linear stability theory and that the difference between a linear and a nonlinear treatment of the evolution equations rests only in quantitative differences and in the well-known effect of nonlinear saturation. However, as we will see later, we can find growing instabilities in regions where linear theory predicts stability. The reason that this qualitative differences between both treatments did not arise in these simulations is that we favoured linear theory by selecting an initial perturbed state which we are in fact able to write as $f = f_0 + f_1$, where f_0 is a homogeneous Maxwellian and f_1 satisfies $\partial_v f_1 \ll \partial_v f_0$, which, as already mentioned, is a necessary assumption of the linear stability theory. In section 2.6 we will introduce perturbations that, although small, violate this condition. Then we will see how the outcome of the nonlinear evolution strongly contradicts the predictions of linear theory.

Energy conservation

Another obvious test we can face the code against is the conservation of total energy in the non-dissipative regime. The total energy density of the plasma is divided into three components, as written in (2.58): kinetic energies of electrons and ions and the energy of the electrostatic field. The decomposition given in (2.110) allows us to easily calculate the kinetic energies of each species in the wave frame. For electrons it reads

$$w_e^{kin,wave} = \frac{1}{4L}\int_{-L}^{+L} dx \int_{-\infty}^{+\infty} dv\; v^2 f_e(x,v). \tag{2.127}$$

But we can write $v^2 = \mathrm{He}_2(v-\tilde{v}_D) + 2\tilde{v}_D\mathrm{He}_1(v-\tilde{v}_D) + \tilde{v}_D^2 + 1$ and then if we make use of the orthogonality property of the Hermite polynomials (2.109) we arrive at

$$w_e^{kin,wave} = \frac{1}{2}\left[2k_{02}^e + 2\tilde{v}_D k_{01}^e + (\tilde{v}_D^2+1)k_{00}^e\right], \tag{2.128a}$$

that in the laboratory frame is easily transformed into

$$w_e^{kin,lab} = \frac{1}{2}\left[2k_{02}^e + 2v_D k_{01}^e + (v_D^2+1)k_{00}^e\right]. \tag{2.128b}$$

On the other hand, a similar procedure can be followed to calculate the kinetic energy of the ions:

$$\begin{aligned} w_i^{kin,wave} =& \frac{1}{4L\theta}\int_{-L}^{+L} dx \int_{-\infty}^{+\infty} du\; u^2 f_i(x,u) \\ =& \frac{1}{2\theta}\left[2k_{02}^i + 2u_0 k_{01}^i + (u_0^2+1)k_{00}^i\right]. \end{aligned} \tag{2.129a}$$

But in this case the expression in the laboratory frame is greatly simplified because the center of mass of ions is resting:

$$w_i^{kin,lab} = \frac{1}{\theta}\left(k_{02}^i + \frac{k_{00}^i}{2}\right). \tag{2.129b}$$

The last component of the total energy density is the field energy, which is independent of the frame of reference:

$$w^{field} = \frac{1}{4L}\int_{-L}^{+L} dx\;\left(\partial_x\phi(x,t)\right)^2. \tag{2.130}$$

To find an explicit expression for this quantity in terms of our Fourier-Hermite coefficients, we make use of (2.116). The local energy density is

$$\frac{1}{2}\left(\partial_x\phi\right)^2 = \frac{1}{2}\sum_{n_1\neq 0}\sum_{n_2\neq 0}\frac{L^2}{n_1 n_2 \pi^2}\left(k_{n_1 0}^i - k_{n_1 0}^e\right)\left(k_{n_2 0}^{i\star} - k_{n_2 0}^{e\star}\right)e^{\frac{i(n_1-n_2)\pi x}{L}}. \tag{2.131}$$

If we integrate in space and take (2.111) into account, equation (2.131) yields

$$w^{field} = \sum_{n>0}\frac{L^2}{n^2\pi^2}\left|k_{n0}^i - k_{n0}^e\right|^2. \tag{2.132}$$

The conservation of the total energy of the system was carefully checked in every non-dissipative run of the code. As a representative example, we can select the run described above of a two-stream instability with $v_D = 2.0$ corresponding to Fig. 2.14. The variations in the three components of the energy in the laboratory frame as well as the sum of them is represented in Fig. 2.16.

Immobile ions. The bump-in-tail instability

We can also compare the results of our code with those of the one developed by Korn and Schamel [27, 35, 34]. That code was also based in a decomposition of the Vlasov-Poisson system into Fourier and Hermite coefficients but disregarded the kinetic behavior of ions, treating them by linearized fluid equations. This means that the results of both codes have to converge as we impose e.g. $\delta \to 0$, this is, as we fix the ion density to $n_i = 1$ (another agreement should be given if very large phase velocities, $u_0 \gg 1$ are involved, in which case trapping and other kinetic distortions of f_i are negligible).

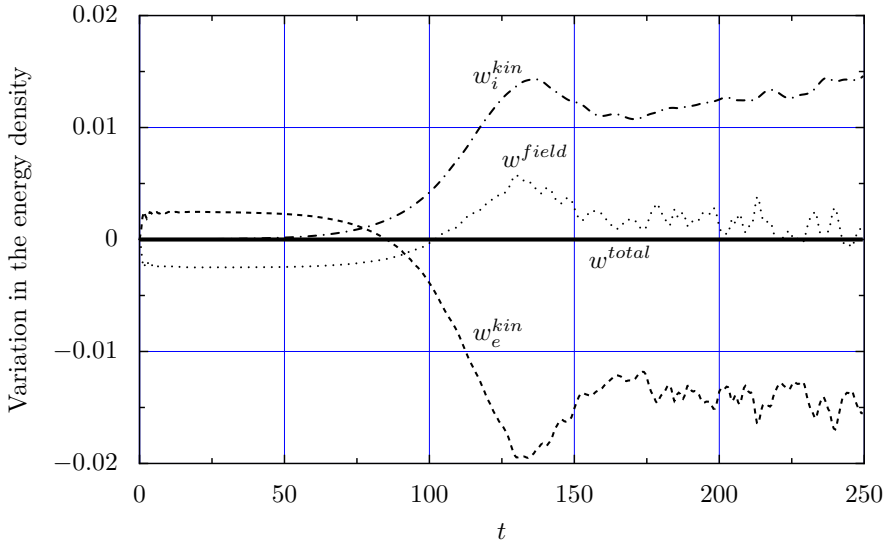

Figure 2.16: Temporal evolution of the kinetic energies of electrons (w_e^{kin}) and ions (w_i^{kin}) in the laboratory frame and field energy (w^{field}) as well as their sum ($w^{total} = w_e^{kin} + w_i^{kin} + w^{field}$). The scale is chosen such that all the energies are zero at $t = 0$.

To perform this comparison we choose as initial conditions those of a bump-in-tail instability [38], given by an initial distribution function for electrons [34, 38]

$$f_e(x, v, t = 0) = f_0(v) \left[1 + \epsilon \sum_{j=1}^{8} \cos\left(\frac{n\pi x}{L}\right) \right], \tag{2.133a}$$

where

$$f_0(v) = \frac{1}{\sqrt{2\pi}} \left[\mathrm{He}_0(v) + \frac{1}{6}\mathrm{He}_4(v) \right] e^{-\frac{1}{2}v^2}, \tag{2.133b}$$

and we chose $\epsilon = 0.006$, $L = 20.944$.

As both codes were Fourier-Hermite Vlasov codes, we should expect that the results are exactly the same out of numerical errors. This is in fact the case, as can be seen by comparing Figs. 2.17 and 2.18. The results are also compatible with those of T.P. Armstrong and D. Montgomery [38], who observed how, in contradiction to linear theory, the third Fourier mode of the potential was dominant over the other two growing modes, as can be observed in our figures (see also Ref. 34).

2.5 Existence of dissipative equilibria with kinetic ions

In section 2.4.1 we described how to correct the Vlasov equation to include the influence on the dynamics of electrons and ions of the dissipation due to collisions with a neutral background. We did so by adding to the evolution equations a new term of the form of a Fokker-Planck collisional operator. A natural question to ask now is what kind of solutions satisfy the time-independent Vlasov-Poisson-Fokker-Planck system, which are expected to last for long times in weakly collisional plasmas. First we note that the equations are trivially solved by homogeneous Maxwellian distribution functions; but we are interested

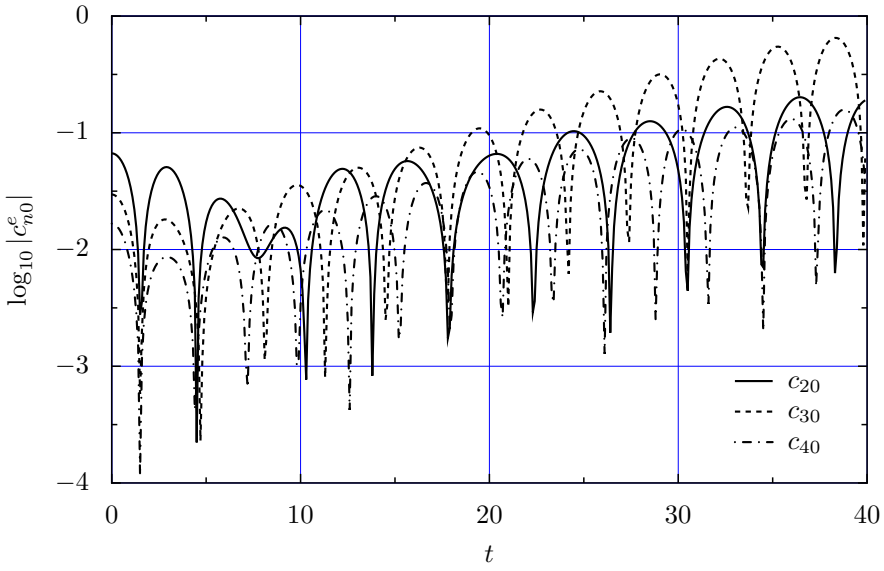

Figure 2.17: Time evolution of the three growing Fourier modes of the electrostatic potential when $\delta = 0$ and the initial distribution function is set as (2.133) in the text (following Ref. 38). The simulation was done with $N = 8$ Fourier modes and $M = 1000$ Hermite polynomials.

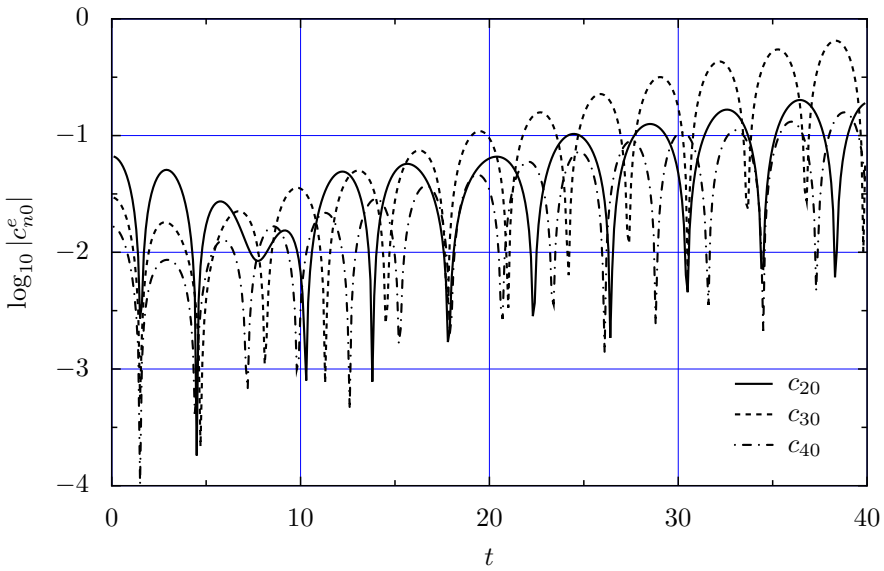

Figure 2.18: Same as in Fig. 2.17, but using the Korn-Schamel code for immobile/fluid ions.

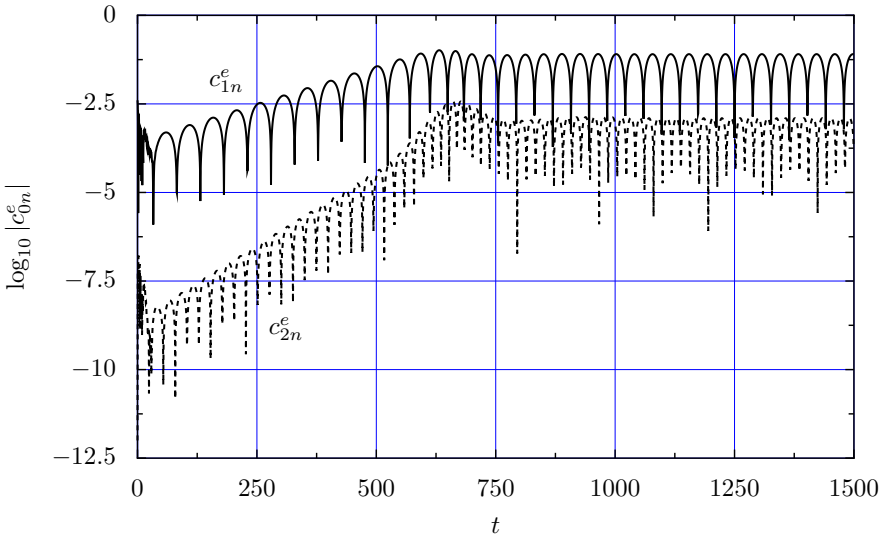

Figure 2.19: Evolution of the first two cosine Fourier modes of the contribution of electrons to the electrostatic potential. The starting distribution function was (2.126) with $\epsilon = 0.001$, $L = 2\pi$. Note that three different phases can be distinguished in the time evolution: (a) adaptation to self-consistency, until $t \approx 50$, (b) growth of the inhomogeneous structure, up to $t \approx 650$ and (c) saturation and persistence of the final structure.

in inhomogeneous solutions and also in how an initially homogeneous distribution in an unstable regime may be disturbed by small fluctuations and evolve into a inhomogeneous equilibrium.

A rigorous analytical treatment of such a problem remains out of the scope of this thesis and seems to present essential and up to this point unsurmounted difficulties. A numerical approach was performed by J.Korn and H.Schamel making use of the code described above [27, 35, 34]. The outcome was that self-consistent dissipative equilibria do exist but only as long as ions are allowed to move and adapt themselves to the equilibrium. No inhomogeneous solutions were found for immobile ions ($\delta = 0$).

With our code, that also includes the kinetic properties of ions we can perform similar investigations. If we start the code in a linearly unstable regime and use again (2.126) as initial distribution functions, but now including a small dissipation coefficient $\nu_e = 0.015$, we see an evolution of the first Fourier modes of the distribution functions as represented in Figs. 2.19 and 2.20. We can observe that for long times a inhomogeneous steady state is formed, the oscillations in the coefficients being due to an inappropriate reference frame [35]. This result may appear in some sense surprising at first sight, as one may expect that the introduction of energy dissipation would lead to a steady decrease of the total internal energy of the plasma and a damping out of any structure. A more careful look at the underlying model of equations (2.105) provides an answer to this ostensible paradox: by fixing the drift between both species we are in fact imposing an external electric field $E = v_D/\nu_e$. The plasma is therefore not a closed system and it can gain energy from this external field.

Dissipative inhomogeneous equilibria do not exist, however, for large dissipation coefficients. Following Refs. 34, 35 we can scan the parameter space of drift velocities and dissipation coefficients and find the existence region when ions are treated kinetically.

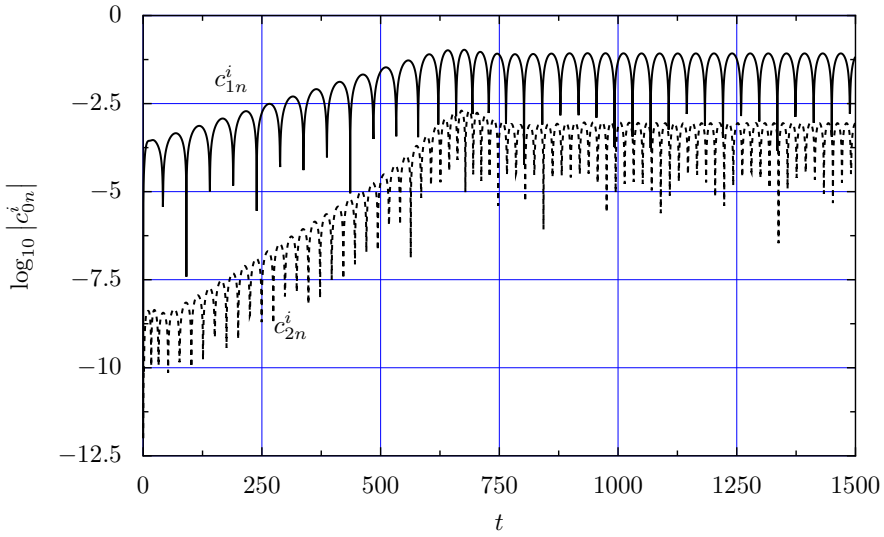

Figure 2.20: Same as Fig. 2.19, but here the ion contributions are plotted. Due to the slower reaction of ions, and the fact that their initial distribution function was a homogeneous Maxwellian, the phase of adaptation to self-consistency is absent here.

The results are shown in Fig. 2.21. A comparison with the diagram for fluid ions shows that for small v_D it is now much harder to obtain inhomogeneous equilibria. This is not surprising, as linear theory predicts that for fluid ions the instability begins at $v_D = 0.195$ while this limit is increased to $v_D = 1.318$ when the kinetics of ions is taken into account. On the other hand, for larger drift velocities, around $v_D = 3$, the maximum ν that allows the formation of inhomogeneous equilibrium is somewhat larger if we include the kinetics of ions. Note however that this diagram is obtained with initial distribution functions without any topological variation from the unperturbed state. Therefore, all these results do not take into account the possible appearance of perturbations involving trapping. In the next chapter we insert trapping structures as initial conditions and prove that in such cases instability and probably also dissipative equilibria exist for a broader region of parameter space.

2.6 Stability

2.6.1 Motivation

Probably the most important issue regarding phase-space structures is their relationship with the overall stability of the plasma, in particular the stability of current-carrying plasmas. The linear approximation provides analytical possibilities from which precise results can be extracted [28, 29] but on the other side, few analytical approaches are known to study the nonlinear stability of a two-species Vlasov-Poisson system. In section 2.4.3 we have shown how linear theory fails to predict the correct behavior of holes and other structures involving trapping. Furthermore, numerical experiments, such as those of Berman, Dupree and Tetreault (see Refs. 39, 40 and also appendix A) indicate that instability may exist far below the threshold predicted by linear theory and that it is related with the formation of phase-space vortices, i.e., collective trapping of particles.

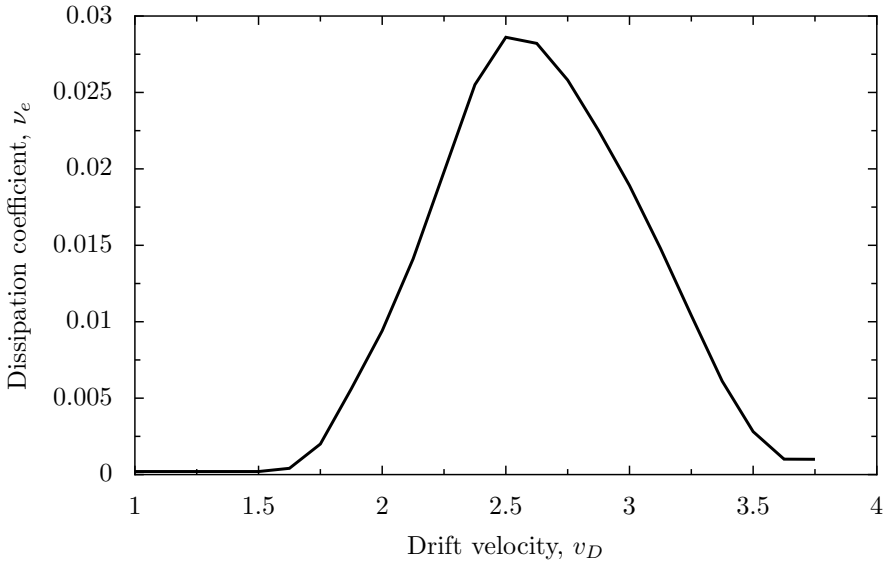

Figure 2.21: Limit of existence of inhomogeneous dissipative structures for kinetic ions. This diagram was obtained with (2.126) as initial distribution function, with $\epsilon = 0.001$, $M = 250$, $N = 4$.

Therefore, strong evidences exist that suggest that the theory of particle trapping should play a crucial role in an accurate study of nonlinear stability. In section 2.3.1 we pointed out the possibility that trapping structures might nonlinearly destabilize the plasma if they have a energy deficit, i.e. if the excited system has a smaller energy than the unperturbed system. This hypothesis, first exposed in Refs. 18, 19 was suggested by the analytical results of Refs. 12, 19 and the above mentioned numerical work of Berman, Dupree and Tetreault.

In the present section we will use the numerical code described in section 2.4 to further develop this hypothesis.

2.6.2 Numerical research

One of the main difficulties that arise when simulating a two-species plasma is the different time scales between electron and ions. A typical time of the electron evolution is given by $\omega_{pe}^{-1} = (n_e e^2/\epsilon_0 m_e)^{-1/2}$, which in our equations is normalized to unity. On the other hand, the typical time for ions is given by $\omega_{pi}^{-1} = (n_i e^2/\epsilon_0 m_i)^{-1/2} = (m_i n_e/m_e n_i)^{1/2}\omega_{pe}^{-1}$. If we assume quasineutrality, the ratio between both typical times is reduced to

$$\frac{\omega_{pe}^{-1}}{\omega_{pi}^{-1}} = \left(\frac{m_e}{m_i}\right)^{1/2} = \delta^{1/2}. \tag{2.134}$$

Typically, δ is assumed to be a very small quantity for natural electron-ion plasmas; for example, for hydrogen $\delta = 1/1836.2$. As in our numerical code time is normalized by ω_{pe}^{-1} this means that in order to take into account the effect of the ion mobility, we should go to times much larger than $\omega_{pi}^{-1} \approx 45$. But on the other side, if we want to resolve accurately enough the motion of electrons, the simulation timestep has to be $\Delta t \ll 1$. This

results in a severe difficulty in simulating plasma processes that involve simultaneously and essentially both electron and ion kinetic equations, as is our case.

The common way out of this problem was to choose larger "artificial" mass ratios and assume that the qualitative behavior of the plasma remains unchanged. Although formerly considered only as a numerical trick, finite mass ratios are becoming an important concern in modern plasma physics due to some recent laboratory experiments [41] with *pair plasmas*, composed by ionized fullerene (C_{60}), with mass ratio $\delta = 1$. A further equal mass plasma is an electron-positron plasma which could be produced in laboratories [42, 43, 44] and is believed to be the origin of high-energy processes found under most astrophysical conditions, such as pulsar magnetospheres [45], active galactic nuclei [46] and models of the early universe [47] [2]. Besides, most results, including our own, point in the direction that the kinetic treatment of ions plays a decisive role in plasma stability; it is, therefore, an appropriate idea to enhance this role by using relatively large mass ratios. However, to keep an asymmetry between both species we will here maintain $\delta < 1$. To compare with the results of Berman, Dupree and Tetreault, we will use the same mass ratio $\delta = 1/4$ and also the same temperatures for both species: $\theta = 1$. The latter is in fact a very good assumption, since the high momentum transfer at collision between unequal particles does not allow a difference in temperatures to survive. For these mass and temperature ratios the linear theory predicts stability for drift velocities smaller than $v_D^\star = 1.96$. For our simulations we choose $v_D = 1.75$.

As starting conditions we will use generalized solitary ion holes, as described in section 2.2, case **E**. The reason of choosing them is that the dynamics of the system is driven by electron reflection, and therefore we expect shorter reaction times. As we want to study the effects that trapping structures may have on the stability of a thermal plasma, we will select very small amplitudes, typically $\Psi = 0.05$. This selection has the additional advantage of emphasizing the failure of linear theory to predict the evolution even for very small amplitudes. The main drawback of this decision is that the number of Hermite polynomials required to resolve such small amplitudes has to be very large. We will here use $M = 5000$, although we observed that a smaller number may also be used, as the results are the same with $M \approx 1000$. The smallness of the amplitude of the electrostatic potential assures the validity of the expansions of the preceding sections. However, to avoid any influence of the inaccuracies involved in such expansions, we solved numerically all the density integrals without any smallness assumption.

Finally, we are simulating a solitary structure but the Fourier decomposition we are using imposes a certain periodicity on the system. The effects of this periodicity will be small and appear only for long times if we select a system length much larger than the typical length of the simulated structure, which is usually of the order of several Debye lengths. We choose a half-length of $L = 50$.

Note that, as mentioned in 2.3.1, ion holes with an energy deficit exist for *any* values of θ, v_D. As we are interested in testing the relationship between the concept of energy deficit and stability, we will make two different runs of the code: one with an energy deficit ($\Delta w < 0$) and another one in the range of a positive energy difference ($\Delta w > 0$). If we would insert an exact ion hole, which is a solution of the Vlasov-Poisson system, no time evolution would happen and the system would be stationary. Therefore, we introduce a small perturbation in the initial distribution functions. The best way to do this is to

[2] Note however that in e^--e^+ plasmas the anihilation time and the cooling time due to cyclotron emission can be too short to allow the excitation of measurable collective phenomena.

Parameter			Description
δ	=	1/4	Electron/ion mass ratio
θ	=	1	Electron/ion temperature ratio
v_D	=	1.75	Drift velocity of the electrons
Ψ	=	0.05	Initial amplitude of the electrostatic potential
L	=	50	Half-length of the system
v_0	=	0.8188735	Phase velocity of the structure
α	=	-5.948906	Ion trapping parameter
β	=	0.133544	Electron trapping parameter
N	=	35	Number of Fourier modes
M	=	5000	Number of Hermite polynomials

Table 2.1: Parameters of the simulation for negative energies. Note that α and β were perturbed and therefore the values here presented do not satisfy the nonlinear dispersion relation. The original values for the solitary ion hole were $\alpha = -5.93891$, $\beta = 0.132544$.

perturb them in the trapped particle range, which can be easily achieved just by changing the values of the trapping parameters α and β. Typically, these changes will be of order $\Delta\alpha/\alpha \sim \Delta\beta/\beta \sim 0.01$.

A. Negative energy range ($\Delta w < 0$)

The first of our runs was made with the parameters of table 2.1. Applying (2.87) we find $\Delta w = -0.00423914$. If we look at the evolution of the potential amplitude as plotted in Fig. 2.22, we see a sharp exponential increase around $t \sim 150$. This is an indication that the system is in fact explosively unstable, something that is confirmed if we take a look at the evolution of the energies (Fig. 2.23) where we can see that a large amount of energy is transferred from the electrons to the ions and, as a collateral result, the field energy is also increased. But what happened inside the plasma? Did the initial hole grow as Figs. 2.22 and 2.23 seem to suggest? To answer this question we have to look at the spatial distribution of the system. For example, Fig. 2.24 represents the temporal evolution of the electron and ion densities at different positions along the system length. In this plot we can see that the initial hole remains quite stationary while another structure is triggered that propagates with a larger phase velocity and which is at the end responsible of the growth of the potential amplitude and the onset of the instability. This new structure propagates with a velocity $v_0' \approx 1.0$.

The outcome of this simulation is that the plasma can be in fact destabilized by a ion hole with an initial energy deficit. Furthermore, the system reacts by creating another structure (or, from an equivalent point of view, by *splitting* the initial hole). As linear theory predicts stability in this regime, this result is already worth noting. However, the question of the relation between nonlinear instability and negative energies still has to be answered. Note in any case, that this hypothesis is favoured by the fact that newly created hole has a larger phase velocity and, according to (2.87) lies deeper in the negative energy range. In any case, we need more information, that could be provided by another run, now in the positive energy range.

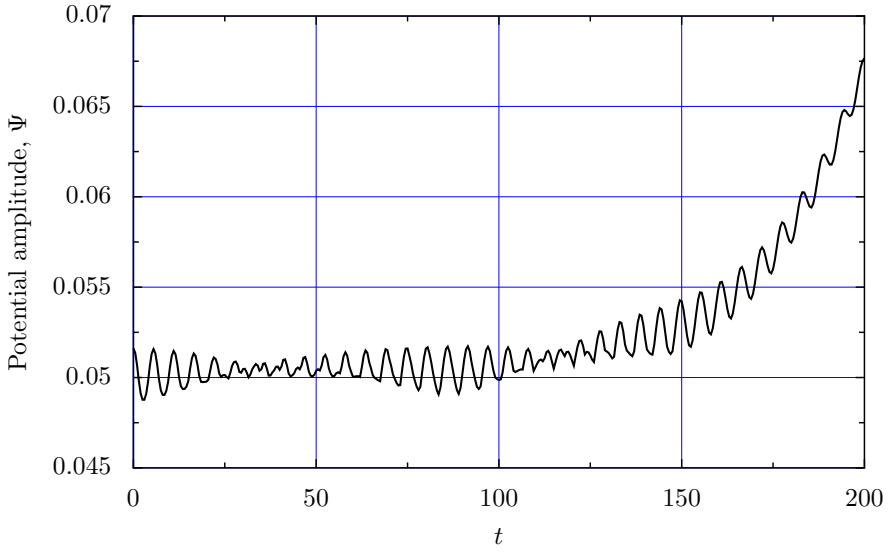

Figure 2.22: Evolution of the amplitude of the electrostatic potential in the run with the parameters of table 2.2 ($\Delta w < 0$)

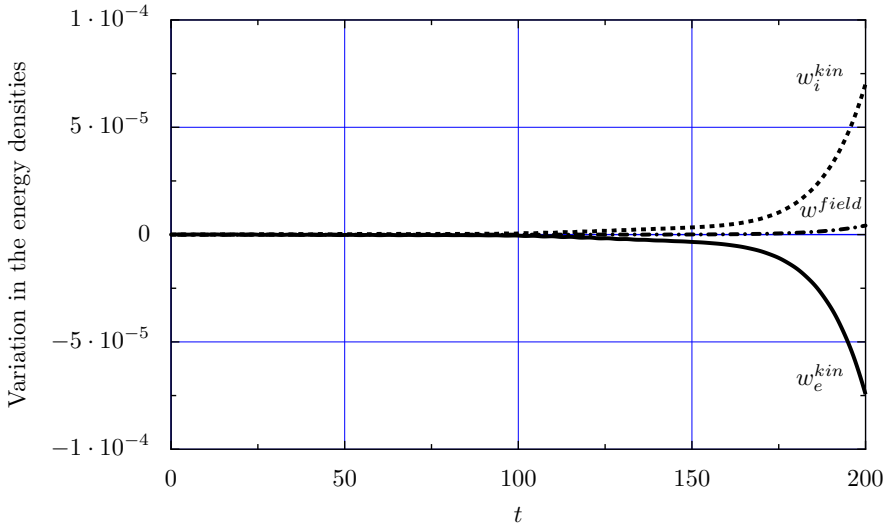

Figure 2.23: Evolution of the three energy components in the run with the parameters of table 2.2 ($\Delta w < 0$).

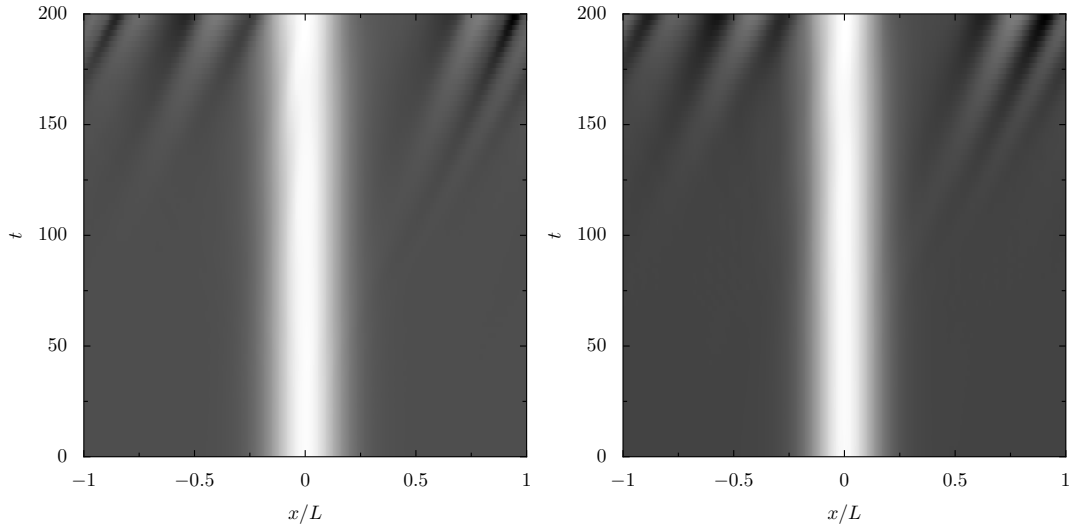

Figure 2.24: Evolution of the electron (left) and ion (right) densities in the run with the parameters of table 2.1 ($\Delta w < 0$). Darker means higher densities.

B. Positive energy range ($\Delta w > 0$)

In a second run we selected the parameters given in table 2.2. They yield an energy difference $\Delta w = 0.033268$. As plotted in Fig. 2.25, also a growing explosive instability appears that now develops around $t = 100$. Looking now at Fig. 2.26 we notice that the process of energy transfer is again very similar: the ion kinetic energy is increased at the expense of the electrons while this produces also a boost in the field energy. Figure 2.27 tells us that again a new structure is triggered which propagates faster than the initial hole.

Also in this case we can note that an increase in the phase velocity, according to (2.87) leads usually to smaller energies (if we keep β fixed). Therefore, we may ask ourselves whether the new structure has an energy deficit. If we measure the phase velocity of this generated structure, we find that it is $v_0' \approx 0.65$ i.e. this velocity does *not* lie in the negative energy domain as long as we assume $B_e = 0$, something which was used in Ref. 19 (see (2.77)) to simplify the calculations (note that in this particular case the boundary between positive and negative energies lies at the same v_0 also when we assume $\beta = 0$). There is, however, no physical necessity for this assumption. The issue of the connection between energy deficits and stability requires, therefore, a further discussion, which is presented in the next section.

2.6.3 Discussion. Are energy deficits related with instability?

In the past section we proved numerically that instability occurs in current-carrying plasmas far below the linear stability threshold and that this instability can be triggered by perturbed ion holes. We also showed that the response of the system to such holes was to create another structure that propagates faster and that quickly grows nonlinearly and explosively. The question of whether the energy deficits that we investigated in section 2.3.1 may give us a key to understand this nonlinear instability remains, however, a point to be clarified.

Parameter			Description
δ	=	1/4	Electron/ion mass ratio
θ	=	1	Electron/ion temperature ratio
v_D	=	1.75	Drift velocity of the electrons
Ψ	=	0.05	Initial amplitude of the electrostatic potential
L	=	50	Half-length of the system
v_0	=	0.35834	Phase velocity of the structure
α	=	-4.474941	Ion trapping parameter
β	=	-1.042535	Electron trapping parameter
N	=	35	Number of Fourier modes
M	=	5000	Number of Hermite polynomials

Table 2.2: Parameters of the simulation for positive energies. Note that α and β were perturbed and therefore the values here presented do not satisfy the nonlinear dispersion relation. The original values were $\alpha = -4.464941$, $\beta = -1.032535$.

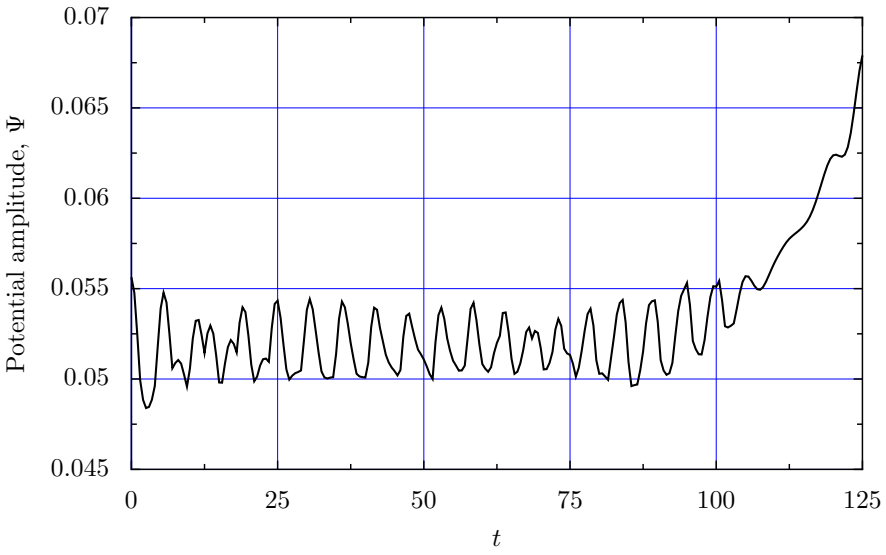

Figure 2.25: Evolution of the amplitude of the electrostatic potential in the run with the parameters of table 2.2 ($\Delta w > 0$)

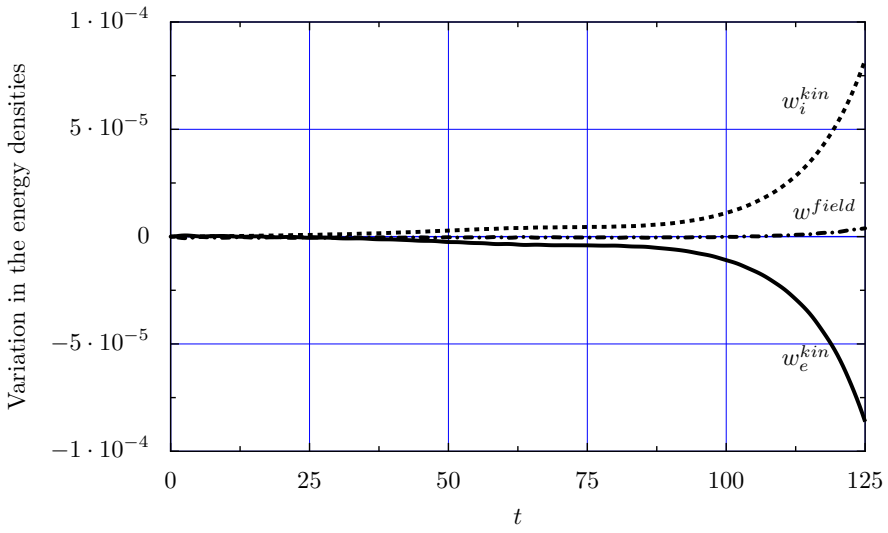

Figure 2.26: Evolution of the components of the energy in the run with the parameters of table 2.2 ($\Delta w > 0$). Compare with the plots of Fig. 2.23.

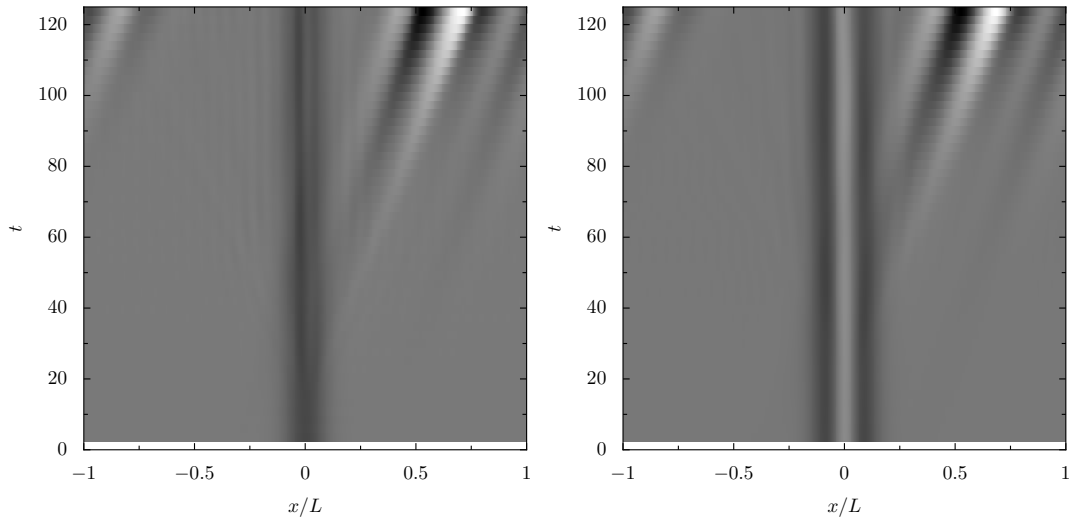

Figure 2.27: Evolution of the electron (left) and ion (right) densities in the run with the parameters of table 2.2 ($\Delta w > 0$). Darker means higher densities.

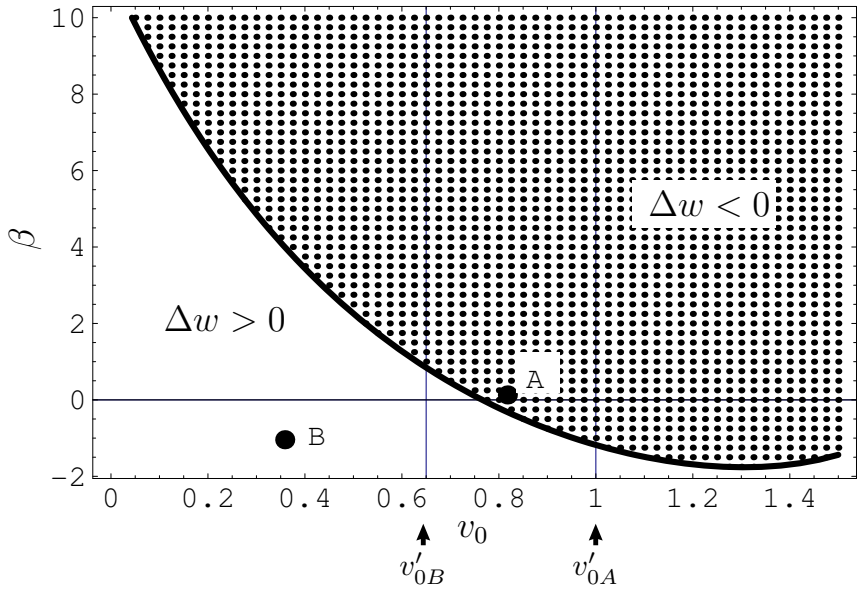

Figure 2.28: Area of energy deficits in the v_0, β plane for $\delta = 1/4$, $\theta = 1$, $v_D = 1.75$. The shaded region spans the parameters that yield negative energies according to (2.87) in the text. The points **A** and **B** represent, respectively, the initial holes selected for the runs of the code described in section 2.6.2 (Tables 2.1 and 2.2). The vertical lines v'_{0B} and v'_{0A} represent the phase velocities of the observed triggered structures on each run. See text for a discussion on this figure.

To shed some light on this issue, we can take a look at Fig. 2.28. There the parameter space of v_0 and β is represented along with the region that, according to (2.87), corresponds to negative energies (shaded area). Also represented are the values that we used in the last section as inputs of our numerical code; point **A** marks the first run, with $\Delta w < 0$ while **B** indicates the second one, with $\Delta w > 0$. In the plot, the phase velocities of the triggered structures are also represented and labeled as v'_{0A} and v'_{0B}. Unfortunately, we do not have a precise enough access to the value of the trapping parameter β from the outcome of the code.

By looking at Fig. 2.28 one is tempted to interpret the numerical results as an indication that the initial conditions in some sense excite a structure with a smaller energy which then grows and is in this way responsible of the instability. This structure would have a larger phase velocity and maybe also a larger β, which could explain why the simulation labeled **B** jumps to a phase velocity that would not have a energy deficit if we keep β fixed. However, the transient process of the excitation and the details on which new mode is chosen would still be unclear.

This explanation is consistent with some laboratory [16] as well as numerical [48] experiments that showed how a plasma hole can suddenly change its velocity and accelerate. We have to admit, however, that the evidences are at the moment not conclusive enough to settle this issue. In any case, from our numerical simulations it can be concluded that holes and, in general, trapping structures have to be taken into account in any complete study of stability in current-carrying plasmas. We infer also that ion kinetics play a decisive role in the outset of plasma instability.

2.7 Concluding remarks

In this chapter we explored self-consistent trapping in classical two-component, current-carrying plasmas. By systematically scanning the parameter space in the small amplitude limit, we showed a complex spectrum of equilibrium solutions to the Vlasov-Poisson system of equations, including some new structures like the chain of alternating electron and ion holes. In a rigorous nonlinear study of current-carrying plasmas, these structures have to complement the linear spectrum of plasma waves.

We also investigated systematically the energies of these electrostatic structures for which we gave an explicit expression. We restricted ourselves to the three most known and easyly describable families of trapping structures, namely electron and ion holes and harmonic (monochromatic) waves. For them we explored their parameter spaces and delimited the areas where energy deficits exist. For ion holes we proved that negative energy structures exist for *any* θ and v_D. This fact as well as the observation in numerical experiments of the spontaneous development and growth of ion holes far below the linear stability threshold led us to believe that a certain connection exists between the possibility of electrostatic structures having an energy deficit and their contribution to a nonlinear destabilization of a current-carrying plasma.

To further investigate this topic we developed a numerical code that, via a Fourier-Hermite decomposition, directly integrates the Vlasov-Poisson system for a two-species current-carrying plasma. We performed two runs of the code inserting as initial conditions respectively a positive and a negative energy small amplitude perturbed ion hole. Then we saw that in both cases the effect of the perturbation was to induce the creation of a new structure that propagates faster than the initial hole. We speculated that this can be explained as the excitation of a new negative energy structure. The difficulty of measuring the trapping parameter as well as the inexistence of drift velocities for which no negative energy modes at all are available, which would allow a decisive test of the hypothesis, are the main obstacles to a more conclusive theory of destabilization by negative energy structures. The way these structures are excited and how they attract the dynamics of the system are also topics deserving further investigation. Our results do not, however, leave any doubt on the utmost importance that self-consistent particle trapping should play in a future complete theory on the nonlinear stability of plasmas.

Therefore, and despite of the mentioned difficulties, we conjecture and in some sense arrive at a new paradigm of stability of current-carrying plasmas in which hole structures of negative energy may play a key role in the understanding of the time evolution of plasmas and the associated anomalous transport. The practical relevance of these findings is better understood in the context of plasma confinement, where improvements in the knowledge of transport phenomena would allow the design of improved devices with longer confinement times.

It is however clear that further refinements and investigations have to be made; first to conclusively settle the issue concerning negative energy structures, later to develop a more formal and general theory that might also allow the extension of our results to three dimensional systems and perhaps also to gradient-driven instabilities. One promising research line is the one provided by the already mentioned availability in the laboratory of pair-plasmas in which, due to the unitary mass ratio, the kinetic equations of electrons and ions are completely symmetric. Such plasmas provide an excellent medium to investigate the importance on the overall stability of the plasma of the ion kinetics, which, according

to our results is decisive in the development of particle trapping instabilitites [49].

CHAPTER 3

Trapping in the quantum domain

The important thing in science is not so much to obtain new facts as to discover new ways of thinking about them.

Sir William Bragg

3.1 Motivation

In the previous chapter we studied thoroughly electrostatic self-consistent structures in classical plasmas. However, trapping can also be seen in Quantum Plasmas [50], a kind of system which has recently received much attention. Non-ideal, dense plasmas generated e.g. in the ultraintense laser-solid interaction certainly belong to this category. However, also ideal plasmas —the addressee of this chapter— can exhibit a quantum behavior. One reason is that the miniaturization of today's micro- and nano-electronic components has reached a level such that the system length becomes comparable with the de Broglie wavelength, in which case tunneling effects are no longer negligible [51, 52, 53, 54, 55]. Also, states in combined traps attained by particles and their anti-particles used to form anti-hydrogen may be modeled by a plasma having quantum features [56]. Other examples can easily be found, and some of them will be mentioned further below. Hence, classical transport models will unlikely be sufficient to describe the plasma behavior in such devices adequately.

Before studying the quantum corrections to such holes let us review some further dilute many particle systems and related disciplines that reveal quantum aspects. Charged-particle beams in particle accelerators are typically dilute systems, so quantum effects are usually disregarded, as we will do in Chap. 4. However, a spectrum of phenomena, which recently became more and more important, reveals the existence of several quantum aspects of beam physics connecting the physics of particle accelerator with the frontiers of several disciplines, such as (for instance) plasma physics, radiation beam

physics, astrophysics, mesoscopic and condensate physics [57, 58]. Most of these phenomena introduce a sort of quantum correction to the leading classical behavior of the system. For example, quantum excitation [59] plays a role for the long-term stability of longitudinal electron beam dynamics in the high-energy circular accelerating machines while the Sokolov-Ternov effect [60] of spin polarization of electron and proton beams is a manifestation, at the macroscopic level, of the single quantum nature of the beam particles. Numerical phase space investigations based on tracking with the quantum map have shown that quantum corrections can substantially affect the particle beam trajectories in the vicinity of the separatrix [61].

Recently quantum-like methodologies [62, 63] have been applied to a number of classical physical situations, in which $\hbar$ is replaced by another characteristic parameter of the problem considered. For instance, they have been applied to accelerator physics [64, 65, 66], to plasma physics [67], to surface gravity wave physics [68, 69, 70, 71] and to nonlinear optics [72, 73, 74, 75] in an attempt to describe linear and nonlinear problems of the dynamics of beams and large amplitude wavepackets.

In principle, all these problems can be formulated, in the configuration space, in terms of a system of Zacharov equations, i.e. nonlinear Schrödinger-like equation coupled with one (or more) equation(s) taking into account the reaction of the environment. The corresponding phase space description is the one provided by the Wigner-Moyal quasidistribution [76, 77, 78] whose evolution equation, the von Neumann equation, plays the role of a kinetic-like equation associated with the system.

Analytically, one framework under which Wigner-Moyal quasidistributions have been considered is that of particles interacting with a given external e.g. parabolic potential to analyze coherent and squeezed states. Also, a quantum-like phase space analysis of a paraxial-charged-particle beam transport, traveling through a quadrupole-like device with small sextupole and octupole aberrations, has been carried out showing a satisfactory agreement with the results of the standard tracking simulations [79] and, consequently, the suitability of using the quantum phase space formalism in particle accelerators. This has been done within the framework of the thermal wave model [64, 65, 66]. Quantum-like corrections involved in the von Neumann equation have been discussed for paraxial beams of both particles and radiation and compared with the standard classical description [80, 81].

Particles in dilute quantum plasmas moving in their own, self-consistent potential, on the other hand, have not been given much attention so far. An exception are self-consistent but linearized solutions of the Wigner-Poisson system, dealing with quantum corrections to Landau damping of Langmuir waves [82] or to the two-stream instability by means of the Nyquist method [83], and the self-consistent linearized solution of the Wigner-Moyal kinetic-like equation for Langmuir wavepackets coupled with the ion-acoustic wave equation [84]. In particular, the Wigner-Moyal kinetic-like description is suitable for describing the Benjamin-Feir instability (modulational instability) as well as predicting the stabilizing effect of a sort of Landau damping. It is well known that the latter cannot be shown in configuration space, where the system is usually described by the Zakharov equations. By using the pure state formalism, a Landau-type damping has been shown for the longitudinal dynamics of both charged-particle coasting beams and electromagnetic wavetrains in high-energy circular accelerators and nonlinear media, respectively [85, 86]. A similar approach has been extended (mixed state formalism) to ensembles of partially-incoherent waves in different physical situations [84, 87, 88].

3.2 Quantum corrections to electron holes

In this chapter we will describe an unmagnetized electron-ion plasma, in which, on the basis of the experimental evidences as well as on theoretical and numerical investigations mentioned above, the quantum nature of the particles is not disregarded. However, it is taken into account only as a weak (perturbative) effect in comparison to the leading classical behavior of the system. Together with the weak quantum effect, we take into account the usual classical electrostatic collective plasma effects coming from the standard meanfield approximation of the Coulombian interaction, in such a way that our system is described by a set of coupled equations comprising the von Neumann equation for the Wigner-Moyal quasidistribution and Poisson's equation. Hereafter, we will refer to this system of equations as WP-system (Wigner-Poisson system). Our goal is to find a self-consistent solution of the WP-system to the lowest order of the quantum correction.

3.2.1 The von Neumann equation

As already mentioned, the most appropriate framework to study quantum correction to electron holes is that of Wigner pseudodistribution functions [76]. But before we start to study its application to electron holes, let us first review some of its properties and the important concept of *pure* and *mixed states*, which will help us understand what we are doing.

Pseudodistribution function for pure and mixed states

Suppose a quantum-mechanical system of N interacting particles. The state of the system at a given time t is completely given by its wave function $|\psi\rangle$ that in the real space representation is a complex function of $3N$ variables plus time $\psi(\mathbf{x}_1, \mathbf{x}_2, \ldots, \mathbf{x}_N; t)$. We can find a pseudodistribution function (Wigner distribution function) f_N defined as [76, 89]

$$\begin{aligned} f_N(\mathbf{x}_1, \ldots, \mathbf{x}_N, \mathbf{p}_1, \ldots, \mathbf{p}_N; t) = \frac{1}{(2\pi)^{3N}} \int d\lambda_1 \ldots d\lambda_N e^{-i\sum \lambda_i \cdot \mathbf{p}_i} \times \\ \times \psi^\star \left(\mathbf{x}_1 - \frac{1}{2}\hbar\lambda_1, \ldots; t \right) \psi \left(\mathbf{x}_1 + \frac{1}{2}\hbar\lambda_1, \ldots; t \right). \end{aligned} \tag{3.1}$$

This function gives us a complete, microscopic description of our system. However, not every real $6N$-variable function corresponds to a complex $3N$-variable wavefunction. In order for f_N to be acceptable, it must satisfy the Tatarskii criterium [89] of separability, i.e. a $|\psi\rangle$ must exist from which we can build f_N. This condition can be expressed as

$$\sum_{ij} \frac{\partial^2 \ln \rho(\mathbf{x}_1^1, \ldots, \mathbf{x}_N^1, \mathbf{x}_1^2, \ldots, \mathbf{x}_N^2; t)}{\partial \mathbf{x}_i^1 \partial \mathbf{x}_j^2} = 0, \tag{3.2}$$

where $\rho(\mathbf{x}_1^1, \ldots, \mathbf{x}_N^1, \mathbf{x}_1^2, \ldots, \mathbf{x}_N^2; t)$ is the probability matrix

$$\begin{aligned} \rho(\mathbf{x}_1^1, \ldots, \mathbf{x}_N^1, \mathbf{x}_1^2, \ldots, \mathbf{x}_N^2; t) = \int \exp\left[i \sum_i \mathbf{p}_i \cdot (\mathbf{x}_i^1 - \mathbf{x}_i^2)/\hbar \right] \times \\ \times f_N \left(\frac{\mathbf{x}_1^1 + \mathbf{x}_1^2}{2}, \ldots, \frac{\mathbf{x}_N^1 + \mathbf{x}_N^2}{2}, \mathbf{p}_1, \ldots, \mathbf{p}_N; t \right) d\mathbf{p}_1 \ldots d\mathbf{p}_N. \end{aligned} \tag{3.3}$$

If the Hamiltonian of the system can be expressed as $H = \sum \frac{p_i^2}{2m} + V(\mathbf{x}_i, \ldots, \mathbf{x}_N; t)$, then the time dependence of f_N is given by

$$\frac{\partial f_N}{\partial t} + \sum \frac{\mathbf{p}_i}{m} \cdot \frac{\partial f_N}{\partial \mathbf{x}_i} - \frac{1}{i\hbar}\left[V\left(\mathbf{x}_1 + \frac{i\hbar}{2}\frac{\partial}{\partial \mathbf{p}_1}, \ldots; t\right) - V\left(\mathbf{x}_1 - \frac{i\hbar}{2}\frac{\partial}{\partial \mathbf{p}_1}, \ldots; t\right)\right] f_N = 0. \tag{3.4}$$

There is, however, too much information in f_N to be an useful representation of the state of the system. As in classical statistical mechanics, we are not interested in the full microscopic description, either because we cannot know the exact state (statistic uncertainty) or because anyway we are concerned only with a more macroscopic behavior.

But (3.4) can also be interpreted in a different way. Suppose that we are not able to determine the exact state of the system at time t and we can only talk about probability ρ_k of finding the system in one of an ensemble of states $|\psi_k\rangle$. Note that this probability has a completely different meaning than the quantum probability. From every $|\psi_k\rangle$ we can construct, using (3.1) a pseudodistribution function f_N^k. Finally, we define

$$f_N = \sum_k \rho_k f_N^k. \tag{3.5}$$

This f_N still depends on $6N$ variables, but it offers no longer a complete description of our system. We can say that this f_N is not a *pure-state* pseudodistribution function and, as it is made up of a lot of different $|\psi_k\rangle$, we cannot expect that it can be decomposed by (3.1) and obtained from a single wave function and, therefore, it should not fulfill the Tatarskii criterium. We call it *mixed-state* pseudodistribution function.

But, in spite of having an absolutely different interpretation, it can be shown that, due to the linear nature of (3.4), and as long as our probabilities ρ_k are time-independent, the equation of evolution for a mixed-state pseudodistribution function is still the same as the one of pure-state functions (3.4).

Quantum BBGKY hierarchy

Up to the moment, we have always dealt with functions of $6N$ variables and, since we have made no approximation, our evolution equation is still exact and includes all orders of correlations between particles. Now we want to make some approximations in order to find an easier although not so precise equation.

As in classical mechanics, we define the *reduced* pseudodistribution functions as

$$f_1(\mathbf{x}_1, \mathbf{p}_1, t) = \int d\mathbf{x}_2 \ldots d\mathbf{x}_N d\mathbf{p}_2 \ldots d\mathbf{p}_N f_N(\mathbf{x}_1, \ldots, \mathbf{p}_1, \ldots, t), \tag{3.6}$$

$$f_2(\mathbf{x}_1, \mathbf{x}_2, \mathbf{p}_1, \mathbf{p}_2, t) = \int d\mathbf{x}_3 \ldots d\mathbf{x}_N d\mathbf{p}_3 \ldots d\mathbf{p}_N f_N(\mathbf{x}_1, \ldots, \mathbf{p}_1, \ldots, t), \tag{3.7}$$

and so forth. Now we integrate (3.4) with respect to the coordinates and momenta of particle N. The first term becomes

$$\frac{\partial}{\partial t} \int d\mathbf{x}_N d\mathbf{p}_N \frac{\partial f_N}{\partial t} = \frac{\partial f_{N-1}}{\partial t}. \tag{3.8}$$

The second term is also easy to calculate:

$$\int d\mathbf{x}_N d\mathbf{p}_N \sum_i^N \frac{\mathbf{p}_i}{m} \cdot \frac{\partial f_N}{\partial \mathbf{x}_i} = \sum_i^{N-1} \frac{\mathbf{p}_i}{m} \cdot \frac{\partial f_{N-1}}{\partial \mathbf{x}_i} + \int d\mathbf{p}_N \frac{\mathbf{p}_N}{m} \cdot \int d\mathbf{x}_N \frac{\partial f_N}{\partial \mathbf{x}_N} \tag{3.9}$$

Now we assume that f_N vanishes whenever any of the coordinates goes to infinity and, therefore the last term of (3.9) is zero.

The third term of the integration of (3.4) is a little bit more complicated. First, we will assume that there exist only pair interactions, this is, we can rewrite the potential as

$$V(\mathbf{x}_1, \ldots, \mathbf{x}_N) = \sum_{i \neq j} v(\mathbf{x}_i, \mathbf{x}_j), \tag{3.10}$$

where $v(\mathbf{x}_i, \mathbf{x}_j) = v(\mathbf{x}_j, \mathbf{x}_i)$. With this assumption, we are now interested in calculating

$$\begin{aligned} &\frac{1}{i\hbar} \int d\mathbf{x}_N d\mathbf{p}_N \sum_{i \neq j} \left[v\left(\mathbf{x}_i + \frac{i\hbar}{2} \frac{\partial}{\partial \mathbf{p}_i}, \mathbf{x}_j + \frac{i\hbar}{2} \frac{\partial}{\partial \mathbf{p}_j} \right) \right. \\ &\left. - v\left(\mathbf{x}_i - \frac{i\hbar}{2} \frac{\partial}{\partial \mathbf{p}_i}, \mathbf{x}_j - \frac{i\hbar}{2} \frac{\partial}{\partial \mathbf{p}_j} \right) \right] f_N := \frac{1}{i\hbar} \int d\mathbf{x}_N d\mathbf{p}_N \sum_{i \neq j} \hat{a}_{ij} f_N. \end{aligned} \tag{3.11}$$

But, as $\hat{a}_{ij} = \hat{a}_{ji}$,

$$\sum_{i \neq j}^{N} \hat{a}_{ij} f_N = \sum_{i \neq j}^{N-1} \hat{a}_{ij} f_N + 2 \sum_{j}^{N-1} \hat{a}_{jN} f_N. \tag{3.12}$$

and

$$\int d\mathbf{x}_N d\mathbf{p}_N \sum_{i \neq j}^{N-1} \hat{a}_{ij} f_N = \sum_{i \neq j}^{N-1} \hat{a}_{ij} f_{N-1}. \tag{3.13}$$

Therefore we can write the full evolution equation for f_{N-1} as

$$\begin{aligned} &\frac{\partial f_{N-1}}{\partial t} + \sum_i^{N-1} \frac{\mathbf{p}_i}{m} \cdot \frac{\partial f_{N-1}}{\partial \mathbf{x}_i} \\ &\qquad - \frac{1}{i\hbar} \left[\sum_{i \neq j}^{N-1} \hat{a}_{ij} f_{N-1} + 2 \sum_j^{N-1} \int d\mathbf{x}_N d\mathbf{p}_N \hat{a}_{jN} f_N \right] = 0 \end{aligned} \tag{3.14}$$

We can also extend these calculations for all $\alpha = 1 \ldots N$ and find evolution equations for every f_α. The set of equations thus obtained may be termed *quantum BBGKY hierarchy*:

$$\frac{\partial f_\alpha}{\partial t} + \sum_i^{\alpha} \frac{\mathbf{p}_i}{m} \cdot \frac{\partial f_\alpha}{\partial \mathbf{x}_i} - \frac{1}{i\hbar} \left[\sum_{i \neq j}^{\alpha} \hat{a}_{ij} f_\alpha + 2 \sum_j^{\alpha} \int d\mathbf{x}_\alpha d\mathbf{p}_\alpha \hat{a}_{j\alpha+1} f_{\alpha+1} \right] = 0 \tag{3.15}$$

We note that if we let $\hbar \to 0$, then

$$\sum_{i \neq j} \hat{a}_{ij} = 2i\hbar \sum_{i \neq j} \frac{\partial v(\mathbf{x}_i, \mathbf{x}_j)}{\partial \mathbf{x}_i} \cdot \frac{\partial}{\partial \mathbf{p}_i}. \tag{3.16}$$

Defining

$$\tilde{V}(\mathbf{x}) = 2\sum_j v(\mathbf{x}, \mathbf{x}_j) \tag{3.17}$$

we find

$$\sum_{i\neq j} \hat{a}_{ij} = i\hbar \sum_i \frac{d\tilde{V}(\mathbf{x}_i)}{d\mathbf{x}_i} \cdot \frac{\partial}{\partial \mathbf{p}_i}. \tag{3.18}$$

and we reobtain the classical BBGKY hierarchy:

$$\begin{aligned} \frac{\partial f_\alpha}{\partial t} + \sum_i^\alpha \frac{\mathbf{p}_i}{m} \cdot \frac{\partial f_\alpha}{\partial \mathbf{x}_i} - \sum_i^\alpha \frac{d\tilde{V}(\mathbf{x}_i)}{d\mathbf{x}_i} \cdot \frac{\partial f_\alpha}{\partial \mathbf{p}_i} \\ -4\sum_j^\alpha \int d\mathbf{x}_\alpha d\mathbf{p}_\alpha \frac{\partial v(\mathbf{x}_j, \mathbf{x}_{\alpha+1})}{\partial \mathbf{x}_j} \cdot \frac{\partial f_{\alpha+1}}{\partial \mathbf{p}_j} = 0 \end{aligned} \tag{3.19}$$

Quantum kinetic equation

Now we must simplify the set of N equations in order to obtain a kinetic evolution equation. In quantum as well as in classical statistical mechanics, the easiest approximation consists in neglecting second and higher order correlations between particles and set

$$f_2(\mathbf{x}_1, \mathbf{x}_2, \mathbf{p}_1, \mathbf{p}_2; t) = f_1(\mathbf{x}_1, \mathbf{p}_1; t) f_1(\mathbf{x}_2, \mathbf{p}_2; t). \tag{3.20}$$

The validity of this approximation is restricted by two conditions: the non-degenerate character of the plasma and the neglection of binary collisions.

The first restriction, namely that we do not treat the particles as identical, thereby assuming the system is completely non-degenerate is justified as long as the mean distance between particles $\lambda_n = \left(\frac{4}{3}\pi n\right)^{-1/3}$ is larger than the thermal de Broglie wavelength:

$$\lambda_n > \lambda_{dB}. \tag{3.21}$$

If we want to consider the degenerate case, where the identity of the particles is treated rigorously, the Fermi-Dirac or the Bose-Einstein statistics have to be taken into account. For this purpose, (3.20) can be modified to read

$$\begin{aligned} f_2(\mathbf{x}_1, \mathbf{x}_2, \mathbf{p}_1, \mathbf{p}_2; t) =& f_1(\mathbf{x}_1, \mathbf{p}_1; t) f_1(\mathbf{x}_2, \mathbf{p}_2; t) \\ &\pm \int d\lambda_1 d\lambda_2 \varrho\left(\mathbf{x}_1 + \frac{1}{2}\hbar\lambda_1, \mathbf{x}_2 - \frac{1}{2}\hbar\lambda_2\right) \times \\ &\times \varrho\left(\mathbf{x}_2 + \frac{1}{2}\hbar\lambda_2, \mathbf{x}_1 - \frac{1}{2}\hbar\lambda_1\right) e^{-i\lambda_1\cdot\mathbf{p}_1 - i\lambda_2\cdot\mathbf{p}_2} \end{aligned} \tag{3.22}$$

where $\varrho(\mathbf{x}_1, \mathbf{x}_2)$ is the second two-particle density matrix and the plus sign applies to bosons and the minus applies to fermions.

The second restriction to the validity of (3.20) is that the binary Coulomb energies are comparatively less important than the mean kinetic energy (i.e. thermal energy) [32, 82] of the plasma. Quantitatively, the relative importance of both processes is measured by the plasma parameter, already introduced in the previous chapter:

$$g := \left(\frac{4}{3}\pi\lambda_D^3 n\right)^{-1} = \left(\frac{\lambda_n}{\lambda_D}\right)^3, \tag{3.23}$$

where λ_D is the Debye length and n is the particle density. The parameter g can be interpreted as the inverse of the average number of particles contained in a Debye sphere. As the neglected terms in (3.20) are of order $\mathcal{O}(g)$, we can safely use (3.20) as long as $g \ll 1$, this is,

$$\lambda_D > \lambda_n. \tag{3.24}$$

This condition is satisfied by low density, high temperature plasmas.

Taking the conditions for the approximation (3.20) as granted, the evolution of f_1 is then given by

$$\frac{\partial f_1}{\partial t} + \frac{\mathbf{p}}{m} \cdot \frac{\partial f_1}{\partial \mathbf{x}} - \frac{2}{i\hbar} \int d\mathbf{x}_2 d\mathbf{p}_2 \hat{a}_{12} f_1(\mathbf{x}_1, \mathbf{p}_1; t) f_1(\mathbf{x}_2, \mathbf{p}_2; t) = 0. \tag{3.25}$$

To cope with this equation we first note that the operator $\hat{a}$ contains partial derivatives of the form $\partial/\partial \mathbf{p}_2$. However, as this partial derivatives operate on $f_1(\mathbf{x}_1, \mathbf{p}_1; t) f_1(\mathbf{x}_2, \mathbf{p}_2; t)$ and are later integrated with respect to $\mathbf{p}_2$, all their contributions will vanish and therefore we can write

$$\begin{aligned} \int d\mathbf{x}_2 d\mathbf{p}_2 \hat{a}_{12} f_1(\mathbf{x}_1, \mathbf{p}_1; t) f_1(\mathbf{x}_2, \mathbf{p}_2; t) = \int d\mathbf{x}_2 d\mathbf{p}_2 \left[v\left(\mathbf{x}_1 + \frac{i\hbar}{2}\frac{\partial}{\partial \mathbf{p}_1}, \mathbf{x}_2\right) - \right. \\ \left. v\left(\mathbf{x}_1 - \frac{i\hbar}{2}\frac{\partial}{\partial \mathbf{p}_1}, \mathbf{x}_2\right) \right] f_1(\mathbf{x}_1, \mathbf{p}_1; t) f_1(\mathbf{x}_2, \mathbf{p}_2; t). \end{aligned} \tag{3.26}$$

Now we will define the average field $\mathcal{V}$ that a particle placed in $\mathbf{x}$ sees as

$$\mathcal{V}(\mathbf{x}; t) = 2 \int d\mathbf{x}_2 d\mathbf{p}_2 v(\mathbf{x}, \mathbf{x}_2) f_1(\mathbf{x}_2, \mathbf{p}_2; t). \tag{3.27}$$

Then, we can write (3.25) as

$$\frac{\partial f_1}{\partial t} + \frac{\mathbf{p}}{m} \cdot \frac{\partial f_1}{\partial \mathbf{x}} + \frac{1}{i\hbar} \left[\mathcal{V}\left(\mathbf{x} + \frac{i\hbar}{2}\frac{\partial}{\partial \mathbf{p}}; t\right) - \mathcal{V}\left(\mathbf{x} - \frac{i\hbar}{2}\frac{\partial}{\partial \mathbf{p}}; t\right) \right] f_1 = 0. \tag{3.28}$$

This equation is formally the same as the evolution equation for a single particle in a given potential $\mathcal{V}$. However, f_1 in (3.28) may not be interpreted as a pseudodistribution function describing the complete state of a single particle, but rather as one that describes a ensemble of many distribution functions f_N. Namely, we can think of f_1 as containing all the different f_N that give rise to f_1 via (3.6) averaged with the same weight.

In quantum statistical mechanics, equation (3.28) plays the same role as Vlasov equation in classical mechanics. We should remember that, as it relies on the assumption (3.20), it corresponds to a non-degenerate gas in the self-consistent field approximation.

3.2.2 Weak quantum corrections to electron holes

Now we can apply the Wigner quasidistribution framework of quantum mechanics to study how an electrostatic structure would be modified when we approach the quantum regime, as was first presented in Ref. 90. The simplest structure we can study is the stationary solitary electron hole as described at the end of Sect. 2.1.4. To do so, we can renormalize (3.28) and, as we will now look for standing structures, make $\partial/\partial t \to 0$ and write it as

$$v\partial_x f + \frac{1}{i\varepsilon} \left[\phi\left(x + \frac{i\varepsilon}{2}\partial_v\right) - \phi\left(x - \frac{i\varepsilon}{2}\partial_v\right) \right] f = 0, \tag{3.29}$$

where ε is the dimensionless Planck's constant

$$\varepsilon = \frac{\hbar}{m_e v_{th} \lambda_D} = \frac{\lambda_{dB}}{\lambda_D}, \tag{3.30}$$

the lengths λ_{dB} and λ_D being thereby the thermal de Broglie wavelength and the Debye screening length. As said before, the validity of (3.29) assumes the absence of degeneracy and of binary collisions.

In the quasiclassical approximation, ε is small, i.e. the quantum effects appear only as corrections to the classical solution, and we can perform a power expansion of the potential operator keeping only the lowest order terms:

$$\begin{aligned}\phi\left(x + \frac{i\varepsilon}{2}\partial_v\right) =& \phi(x) + \frac{i\varepsilon}{2}\phi'(x)\partial_v + \frac{1}{2!}\left(\frac{i\varepsilon}{2}\right)^2 \phi''(x)\partial_v^2 \\ &+ \frac{1}{3!}\left(\frac{i\varepsilon}{2}\right)^3 \phi'''(x)\partial_v^3 f + \mathcal{O}(\varepsilon^4).\end{aligned} \tag{3.31}$$

All even terms are canceled out when we insert this expression into (3.29). Therefore, to include quantum correction of the lowest possible order, we keep terms up to the third order and neglect all other higher order terms. Proceeding this way, we arrive at

$$v\partial_x f + \phi'(x)\partial_v f - \frac{\varepsilon^2}{3!4}\phi'''(x)\partial_v^3 f = 0, \tag{3.32}$$

which is the equation we have to couple with the Poisson's equation (2.2).

Neglecting terms of order $\mathcal{O}(\varepsilon^4)$ is valid as long as the quantum correction to the Vlasov terms dominates over the lowest order collision term, which, as mentioned above, is of order $\mathcal{O}(g)$ with g defined in (3.23). This condition can be written as

$$\left(\frac{\lambda_n}{\lambda_D}\right)^3 < \left(\frac{\lambda_{dB}}{\lambda_D}\right)^2. \tag{3.33}$$

If we summarize all conditions for this approach to be valid, namely (3.21), (3.24), (3.33) we arrive at the set of constraints

$$\lambda_{dB} < \lambda_n < \left(\lambda_{dB}^2 \lambda_D\right)^{1/3} < \lambda_D. \tag{3.34}$$

A picture of the available physical conditions where these approximations are valid is presented in Fig. (3.1). These conditions are met in sufficiently hot and dense plasmas as may be found in the intense laser/particle beam-solid interaction and possibly in the interior of giant planets.

As we keep terms up to $\mathcal{O}(\varepsilon^2)$, we will look for corrections of the same order in the potential and in the distribution function, $f = f_0 + \varepsilon^2 f_1$, $\phi = \phi_0 + \varepsilon^2 \phi_1$, with f_0 and ϕ_0 representing now (2.16) and (2.20) respectively. Inserting this ansatz into (3.32) and (2.2) neglecting again terms of $\mathcal{O}(\varepsilon^4)$ we find

$$\left[v\partial_x + \phi_0'(x)\partial_v\right] f_1 = -\phi_1'(x)\partial_v f_0 + \frac{1}{3!4}\phi_0(x)'''\partial_v^3 f_0, \tag{3.35a}$$

$$\partial_x^2 \phi_1(x) = \int dv f_1. \tag{3.35b}$$

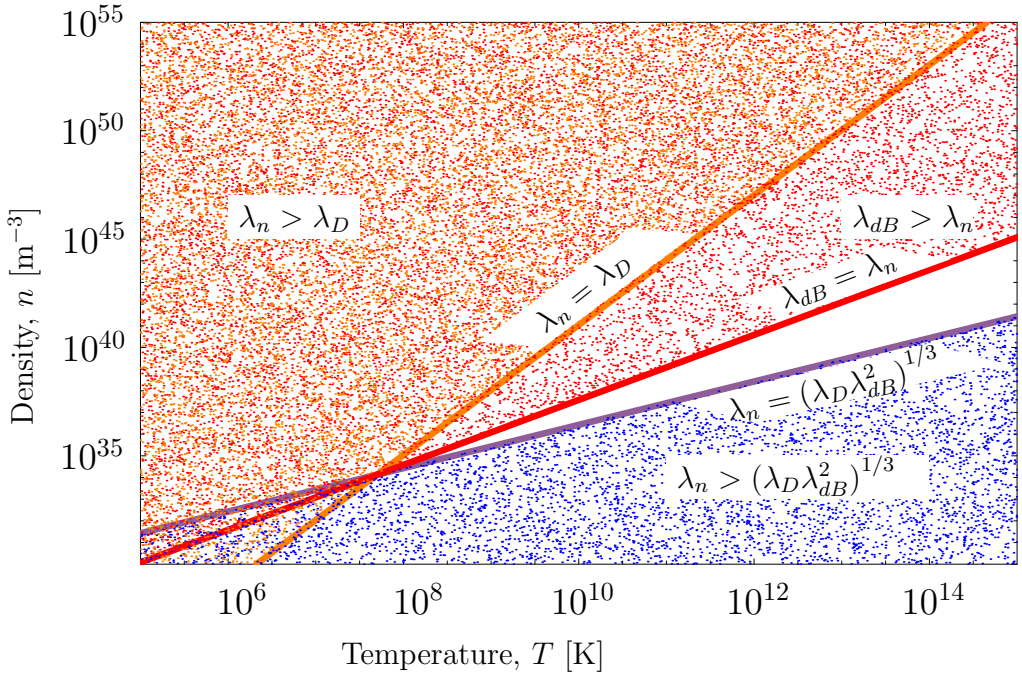

Figure 3.1: (Color) Range of validity of the weak quantum correction presented in the text [see (3.34)]. The shadowed areas represent conditions were one or more of the following constraints are violated: (a) binary collision are negligible ($\lambda_n < \lambda_D$), (b) The plasma is a non-degenerate gas ($\lambda_{dB} < \lambda_n$) and (c) quantum corrections are larger than collisional corrections ($\lambda_n < \left(\lambda_D \lambda_{dB}^2\right)^{1/3}$)

By defining

$$g(x,v) = f_1 + \phi_1 \partial_v f_0, \tag{3.36}$$

we can reduce equations (3.35a) and (3.35b) to the somewhat simpler system

$$[v\partial_x + \phi_0'(x)\partial_v]\, g = \frac{1}{3!4}\phi_0'''(x)\partial_v^3 f_0 =: h(v,x), \tag{3.37a}$$

$$\phi_1''(x) + V''(\phi_0)\phi_1(x) = \int_{-\infty}^{+\infty} dv\, g(x,v), \tag{3.37b}$$

Now it is convenient to switch into a new set of variables defined by $\xi = x$, $E = \frac{v^2}{2} - \phi_0(x)$, $\sigma = \mathrm{sg}(v)$ and rewrite $h(x,v) = H(\xi,E,\sigma)$, $g(x,v) = G(\xi,E,\sigma)$. With these variables, (3.37a) becomes

$$\partial_\xi G(\xi,E,\sigma) = \frac{H(\xi,E,\sigma)}{v(\xi,E,\sigma)}, \tag{3.38}$$

whose general solution is

$$G(\xi,E,\sigma) = G(0,E,\sigma) + \int_0^\xi d\xi'\, \frac{H(\xi',E,\sigma)}{v(\xi',E,\sigma)}, \tag{3.39}$$

where $v(\xi,E,\sigma) = \sigma\sqrt{2\,[E+\phi_0(\xi)]}$. Therefore, in order to find G we only have to integrate $H(\xi,E,\sigma)/v(\xi,E,\sigma)$ along the classical particle trajectories given by $E = const.$. In this expression we have chosen the lower integration limit as $\xi = 0$ because this is the only point which is reached by all trajectories (see below). Note that a trapped particle will move along a closed, bounded trajectory around the origin in phase space.

Now we need to replace $H(\xi,E,\sigma)$ by its full expression. Expressing f_0 in Eq. (2.16) as $f_0(E) = (2\pi)^{-1/2}\,[\exp(-E)\theta(E) + \exp(-\beta E)\theta(-E)]$ we get by differentiation

$$\begin{aligned}
\partial_v^3 f_0 \;&=\; \frac{1}{\sqrt{2\pi}} v \left\{ [3 - 2(E+\phi_0)]\, e^{-E}\theta(E) + \beta^2\,[3 - 2\beta(E+\phi_0)]\, e^{-\beta E}\theta(-E) \right. \\
&\quad \left. - \left[3(1-\beta) - 2\phi_0(1-\beta^2)\right]\delta(E) - 2(E+\phi_0)(1-\beta)\delta'(E) \right\} \\
&=:\; \frac{1}{\sqrt{2\pi}} v(\xi,E,\sigma)\Omega(\xi,E).
\end{aligned} \tag{3.40}$$

For positive energies, we can follow the trajectories up to any ξ in (3.39) and, assuming that the correction vanishes at $\xi \to \pm\infty$, we arrive at

$$G(0,E,\sigma) = \int_{-\infty}^0 d\xi'\, \frac{H(\xi',E,\sigma)}{v(\xi,E,\sigma)} = \frac{1}{3!4\sqrt{2\pi}} \int_{-\infty}^0 d\xi'\, \phi_0'''(\xi')\Omega(\xi',E). \tag{3.41}$$

Note that this expression does no longer depend on σ. For negative energies $G(0,E,\sigma)$ is not determined by such a procedure but, due to the symmetry of the problem we can assume that it will also be σ-independent. On the other side, we can always extend the integration of (3.39) to $-\infty$ for negative energies also as long as we change the integration constant. Therefore we have, for any E,

$$G(\xi,E,\sigma) = G(\xi,E) = \frac{1}{3!4\sqrt{2\pi}} \left[G_0(E) + \int_{-\infty}^\xi d\xi'\, \phi_0'''(\xi')\Omega(\xi',E) \right], \tag{3.42}$$

with $G_0(E) = 0$ for $E > 0$.

Note that $\partial_E f_0$ is discontinuous at $E = 0$. Therefore, $G(\xi, E)$ does not have a definite value at the separatrix. Our approach will be to solve (3.37) for positive and negative energies separately and then put both solutions together imposing the continuity of f_1 at the separatrix.

In order to integrate (3.42), we consider these two different cases:

1. For $E > 0$ we have $G_0(E) = 0$ and

$$\Omega(\xi, E) = [3 - 2(E + \phi_0(\xi))]\, e^{-E}, \tag{3.43}$$

The integral (3.42) can be performed analytically to yield

$$G(\xi, E) \;=\; \frac{1}{3!4\sqrt{2\pi}} \left[\phi_0'(\xi)^2 + (3 - 2E - 2\phi_0(\xi))\, \phi_0''(\xi)\right] e^{-E}.$$

2. If $E < 0$ we must take $G_0(E)$ into account. In this case

$$\Omega(\xi, E) = \beta^2 [3 - 2(E + \phi_0(\xi))\beta]\, e^{-\beta E}. \tag{3.44}$$

and (3.42) reads

$$\begin{aligned} G(\xi, E) =& \frac{1}{3!4\sqrt{2\pi}} \{G_0(E) \\ &+ \left[\beta\phi_0'(\xi)^2 + (3 - 2\beta E - 2\beta\phi_0(\xi))\, \phi_0''(\xi)\right] \beta^2 e^{-\beta E}\}. \end{aligned} \tag{3.45}$$

The continuity of f_1 is now imposed to determine $G_0(E)$. As $f_1 = g - \phi_1 \partial_E f_0$, the discontinuity of $g(x, v) = G(\xi, E)$, namely $\Delta G := G(\xi, 0^+) - G(\xi, 0^-)$ should be equal to $\phi_1 \Delta(\partial_E f_0)$. Since it holds

$$\Delta(\partial_E f_0) = \frac{\beta - 1}{\sqrt{2\pi}}, \tag{3.46}$$

we get

$$\begin{aligned} \Delta G = \; & \tfrac{1}{3!4\sqrt{2\pi}} \quad \left\{\phi_0'(\xi)^2 + (3 - 2\phi_0(\xi))\, \phi_0''(\xi)\right. \\ & \left. -\beta^2 \left[\beta\phi_0'(\xi)^2 + (3 - 2\beta\phi_0(\xi))\, \phi_0''(\xi)\right] - G_0(0)\right\}. \end{aligned} \tag{3.47}$$

Then we can find $\phi_1(\xi)$ as

$$\begin{aligned} \phi_1(\xi) = \; & \tfrac{\Delta G}{\Delta(\partial_E f_0)} = \tfrac{1}{3!4(\beta-1)} \left\{\phi_0'(\xi)^2 + (3 - 2\phi_0(\xi))\, \phi_0''(\xi)\right. \\ & \left. -\beta^2 \left[\beta\phi_0'(\xi)^2 + (3 - 2\beta\phi_0(\xi))\, \phi_0''(\xi)\right] - G_0(0)\right\}. \end{aligned} \tag{3.48}$$

Moreover, as we imposed $\phi_1(\pm\infty) = 0$, we know that $G_0(0) = 0$. Hence, we obtained $\phi_1(\xi)$. Figure 3.2a shows $\phi_1(\xi)$ for $\Psi = 0.1$ and Fig. 3.2b represents the corrected potential. For reference, also the unperturbed potential is drawn. We see that the potential experiences a reduction as a result of quantum correction.

To determine $G_0(E)$ for all negative energies we go back to (3.37b). As we have already determined $\phi_1(x)$, the left hand side is now given. It is convenient to write it in terms of ϕ_0. To do this we note that all derivatives of ϕ_0 can by expressed by ϕ_0 itself via $\phi_0'(\xi) = -\phi_0(\xi)\left(1 - \sqrt{\phi_0(\xi)/\Psi}\right)^{1/2}$, $\phi_0''(\xi) = \phi_0(\xi)\left(1 - 5\sqrt{\phi_0(\xi)/\Psi}/4\right)$ and

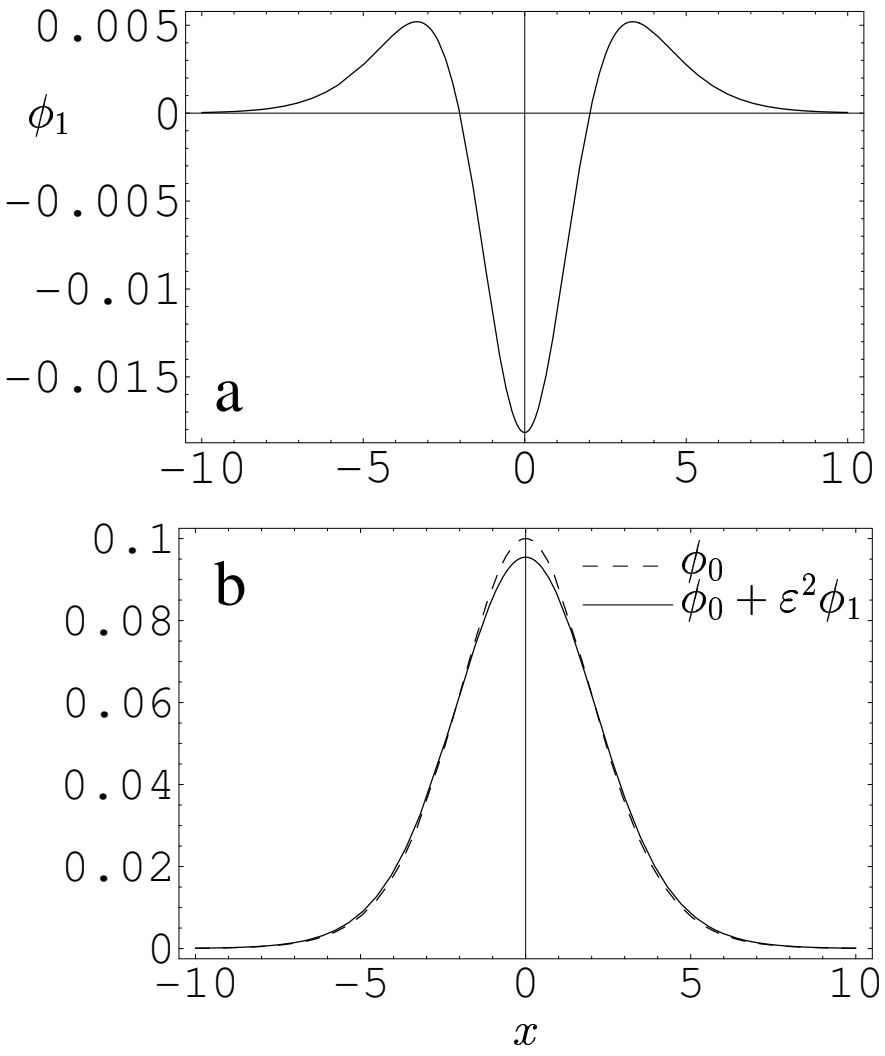

Figure 3.2: Correction to the potential for $\Psi = 0.1$.

also $V''(\phi_0) = -\left(1 - 15\sqrt{\phi_0/\Psi}/8\right)$. Inserting these expressions into (3.37b) we find an expression for its left hand side as a function of ϕ_0 which we call $L(\phi_0)$. It can be expressed as

$$\begin{aligned} L(\phi_0) := \frac{3\phi_0}{16\Psi}\Bigg\{ & 40\left(1+\beta+\beta^2\right)\phi_0^2 + 15\Psi(1+\beta)\sqrt{\frac{\phi_0}{\Psi}} \\ & -\phi_0\left[15 - 16\Psi - 8\beta^2\Psi\left(2 - 7\sqrt{\frac{\phi_0}{\Psi}}\right)\right. \\ & \left. +56\Psi\sqrt{\frac{\phi_0}{\Psi}} + \beta\left(15 - 16\Psi + 56\Psi\sqrt{\frac{\phi_0}{\Psi}}\right)\right]\Bigg\}. \end{aligned} \tag{3.49}$$

On the other side, the right hand side of (3.37b) can be written as

$$\begin{aligned} \int_{-\infty}^{+\infty} dv\, g(x,v) &= \sum_\sigma \sigma \int_{-\phi_0(\xi)}^{\infty} dE\, \frac{G(\xi,E)}{v(\xi,E,\sigma)} \\ &= 2\int_{-\phi_0(\xi)}^{\infty} dE\, \frac{G(\xi,E)}{v(\xi,E,1)}. \end{aligned} \tag{3.50}$$

Making use of (3.42) we can reduce (3.50) to

$$\int_{-\infty}^{+\infty} dv\, g(x,v) = R(\phi_0) + \frac{1}{3!2\sqrt{2\pi}} \int_{-\phi_0(\xi)}^{0} dE\, \frac{G_0(E)}{v(\xi,E,1)} \tag{3.51}$$

The second term of (3.51) can be obtained analytically just by integration of (3.44) and (3.45), and finally we can write it as a function that only depends on ϕ_0:

$$\begin{aligned} R(\phi_0) \;:=\; & \frac{1}{3!2\sqrt{2\pi}} \int_{-\phi_0(\xi)}^{\infty} dE \int_{-\infty}^{\xi} d\xi'\, \frac{\phi_0'''(\xi')\Omega(\xi',E)}{v(\xi,E,1)} \\ =\; & -\frac{1}{3!4\sqrt{4\pi}}\sqrt{\phi_0}\Bigg\{(\beta-1)\left[2\left(2+\phi_0(1+\beta)\right)\sqrt{\frac{\phi_0}{\Psi}} - (3+2(1+\beta))\right]\times \\ & \times\phi_0\left(\beta^2-1\right)\left(5\sqrt{\frac{\phi_0}{\Psi}} - 4\right) \\ & +e^{\beta\phi_0}\mathrm{erf}\left(\sqrt{\beta\phi}\right)\beta\sqrt{\pi}\sqrt{\beta\phi_0}\left[(5+2\beta\phi_0)\sqrt{\frac{\phi_0}{\Psi}} - 2\beta\phi_0 - 4\right] \\ & +e^{\phi_0}\mathrm{erfc}\left(\sqrt{\phi_0}\right)\sqrt{\pi}\sqrt{\phi_0}\left[(5+2\phi_0)\sqrt{\frac{\phi_0}{\Psi}} - 2\phi_0 - 4\right]\Bigg\}. \end{aligned} \tag{3.52}$$

To perform the remaining integral of (3.51), we make a half power expansion of $G_0(E)$:

$$\frac{1}{3!2\sqrt{2\pi}} G_0(E) = a_{1/2}|E|^{1/2} + a_1|E| + a_{3/2}|E|^{3/2} + \ldots \tag{3.53}$$

With this ansatz, we have

$$\frac{1}{3!2\sqrt{2\pi}} \int_{-\phi_0(\xi)}^{0} dE\, \frac{G_0(E)}{v(\xi,E,1)} = \sqrt{\phi_0}\sqrt{\frac{\pi}{2}} \sum_{n=1}^{\infty} \frac{\Gamma\left(1+\frac{n}{2}\right)}{\Gamma\left(\frac{3}{2}+\frac{n}{2}\right)} a_{n/2}\phi_0^{n/2}. \tag{3.54}$$

And we can finally reduce (3.37b) to

$$L(\phi_0) = R(\phi_0) + \sqrt{\phi_0}\sqrt{\frac{\pi}{2}}\sum_{n=1}^{\infty}\frac{\Gamma\left(1+\frac{n}{2}\right)}{\Gamma\left(\frac{3}{2}+\frac{n}{2}\right)}a_{n/2}\phi_0^{n/2}. \tag{3.55}$$

Therefore, if we define $\rho(t)$ as

$$\rho(t) := \frac{1}{t}\left(L(t^2) - R(t^2)\right), \tag{3.56}$$

we can find all $a_{n/2}$ as

$$a_{n/2} = \frac{1}{n!}\sqrt{\frac{2}{\pi}}\frac{\Gamma\left(\frac{3}{2}+\frac{n}{2}\right)}{\Gamma\left(1+\frac{n}{2}\right)}\left.\frac{d^n\rho(t)}{dt^n}\right|_{t=0} \tag{3.57}$$

With this expression for $a_{n/2}$ we can sum $G_0(E)$ and then find $G(\xi, E)$ and f_1. The correction of the distribution function, $f_1(x, v)$ is plotted in Fig. 3.3, while the final, corrected distribution function $f = f_0 + \varepsilon^2 f_1$ is represented at fixed x in Fig. 3.5.

We clearly recognize a partial filling of the phase space within the separatrix being maximum at the hole center. An interpretation may be given in terms of refraction or tunneling: in the classical solution nearby its separatrix, the region of untrapped electrons is populated stronger than that of trapped electrons. In the quantum domain when tunneling becomes effective this gives rise to a net influx of particles resulting in a less dilute distribution of trapped electrons.

We, therefore, conclude that the overall effect of a quantum correction to a classical e-hole is the tendency of the system to reduce the coherent excitation by both a diminution of the amplitude and a partial filling of the trapped particle region by refraction (tunneling), bringing the system closer to the thermal state.

Open questions are how these semiclassical corrections are modified in case of finite amplitudes $\Psi \gtrsim \mathcal{O}(1)$, of finite quantum corrections $\varepsilon \gtrsim \mathcal{O}(1)$, of hole propagation $v_0 > 0$, of nonlocality of structures such as periodic wave trains (cnoidal waves). In fact, first numerical simulations of a two-stream unstable WP-plasma [91] suggest the existence of propagating holes of finite amplitude in the fully quantum regime.

3.3 Quantum-like systems

In the last section we developed a method to study small quantum corrections to electrostatic structures in plasmas. However, there exist many other quantum-like physical systems which we can investigate following a very similar approach, in particular in the field of nonlinear optics.

In the following pages, we will show that self-consistent trapping is not a phenomenon affecting only real particles. In fact, quasi-particles such as photons or phonons can also become trapped when they interact nonlinearly with their medium. As an appropriate framework, the Wigner method will be used, which has already been applied to the study of trapped BGK-like modes in the incoherent light propagation of wavepackets in nonlinear media [87], but only for long enough wavelengths that the quantum-like effects could be completely disregarded. Linearization of the von Neumann equation has also been used to investigate a kind of quantum-like Landau damping of electromagnetic wavepackets [86]. Here we will deal with a fully nonlinear weak quantum treatment of this phenomenon.

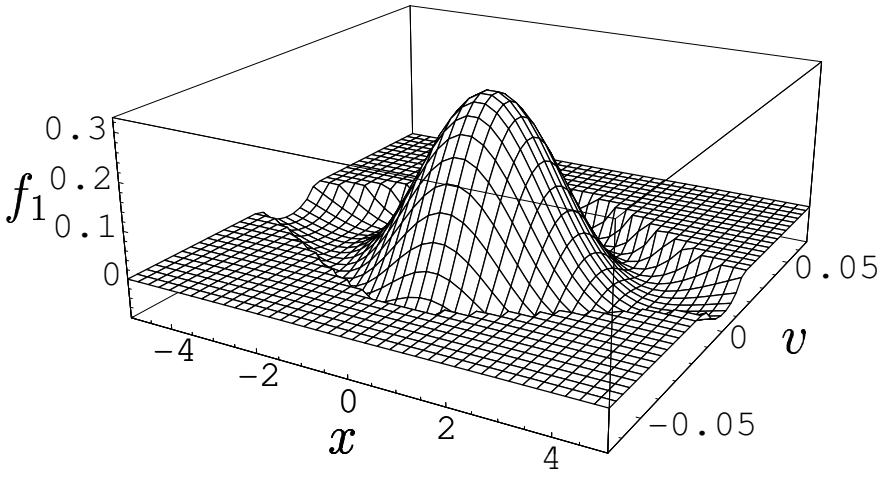

Figure 3.3: Correction of the distribution function $f_1(x, v)$.

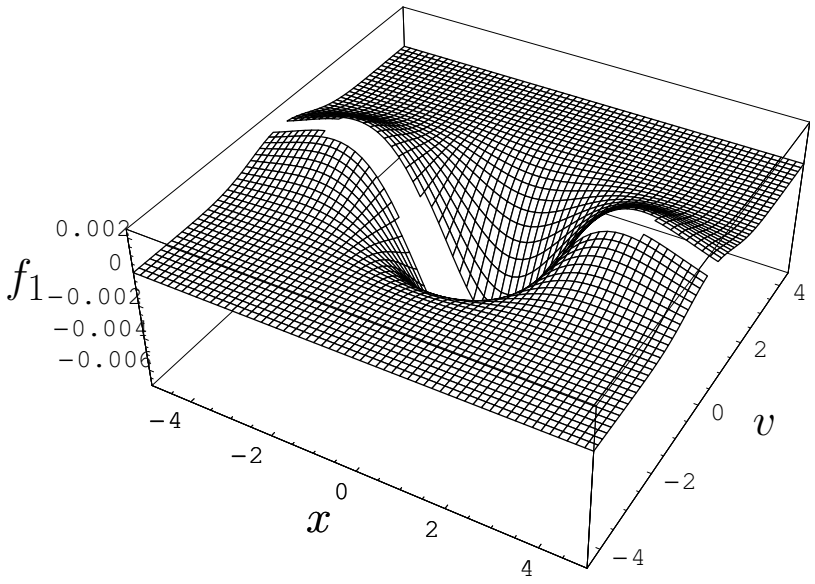

Figure 3.4: Correction of the distribution function $f_1(x, v)$. The correction for positive energies is much smaller that that for negative energies. Therefore, to appreciate the former, negative energies have to be kept out of the graph, as presented here.

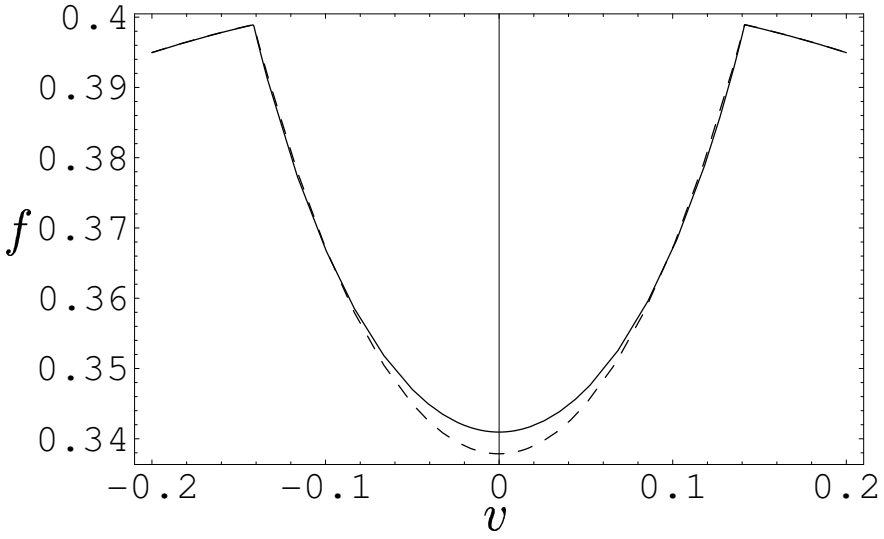

Figure 3.5: Corrected distribution function ($f_1(x, v)$) at $x = 0$. For $\Psi = 0.01$, $\varepsilon = \sqrt{\Psi} = 0.1$. The dashed line represents the original (unperturbed) distribution function.

The key is that whenever we face a Schrödinger-like equation with a self-consistent potential, we can perform a Wigner transformation and, if some parameter that plays the role of Planck's constant is small enough, arrive at an equation identical to (3.32) coupled with some other *Poisson-like* equation. Based on the solution we found for quantum plasmas, in this section we will provide a more general method to solve equations like these. In particular, we will study the *Nonlinear Schrödinger Equation (NSE)* for which we will provide approximate solutions for its well known cubic form as well as a method to face arbitrary nonlinearities.

The application of the Wigner method to nonlinear optics has several advantages and gives us new insights into the underlying physics of such systems. First of all, it allows us, as we will do here, to draw parallelisms and find new connections to standard plasma physics, and other mesoscopic physical systems. It also allows the formulation of conceptually new problems regarding the dynamics of incoherent waves and beams.

3.3.1 The Nonlinear Schrödinger Equation

The propagation of an electromagnetic wavepacket through a nonlinear medium can be described by a Schrödinger-like equation for the (complex) wave amplitude where $\hbar$ and potential energy are replaced by the inverse of the wavenumber $1/k = \lambda/2\pi$ and refractive index, respectively [92]. In general, the refractive index depends on the wave amplitude and the describing equation becomes the Nonlinear Schrödinger equation [93, 94]. The longitudinal dynamics of the wavepacket predicted by such an equation has received much attention. In particular, modulational instability and soliton formation deserved careful studies as they are regarded as crucial phenomena in the design of optical fibers for the communication industry [75, 93, 95].

In general, the Nonlinear SchrödingerEquation can be written as [86]

$$i\frac{\partial\psi}{\partial t} + \frac{\alpha^2}{2}\frac{\partial^2\psi}{\partial x^2} - U\psi = 0, \tag{3.58}$$

where α^2 is a parameter proportional to the inverse of the wave number which accounts for the diffraction effects while x and t play the role of configurational space coordinate (longitudinal coordinate relative to the wavepacket center) and time-like variable (longitudinal coordinate of the wavepacket center), respectively. The potential U is in general a functional of $|\psi(x,t)|^2$ representing the refractive index. The relationship between U and $|\psi(x,t)|^2$ is given by the nonlinearity of the medium. A possible form of this dependence is given by [86]

$$U\left[|\psi|^2\right] = -\chi\left(|\psi|^2 - |\psi_0|^2\right) - \mathcal{R}\int\left(|\psi|^2 - |\psi_0|^2\right)dx. \tag{3.59}$$

An equation similar to this one has been considered for studying the nonlinear stability in nonlinear media [95] as well as in the thermal wave model [66]. Here, χ accounts for the nonlinear frequency shift and $\mathcal{R}$ accounts for a sort of resistive effect. In the case $\mathcal{R} \to 0$, $\psi_0 \to 0$ we arrive to the well-known cubic form of the NSE:

$$i\frac{\partial\psi}{\partial t} + \frac{\alpha^2}{2}\frac{\partial^2\psi}{\partial x^2} + \chi|\psi|^2\psi = 0. \tag{3.60}$$

The cubic NSE given by (3.60) has been called "the master equation of nonlinear optical fibers" [93] and has deserved thoroughful investigations since the seventies. A proof of its integrability as well as a general solution were provided using the *inverse scattering method* [96]. Without loss of generality, we will deal here with $\chi > 0$, and the boundary conditions $|\psi(x,t)| \to 0$ when $x \to \pm\infty$. Under these conditions, the general solution is constructed from one or several *bright soliton* solutions given by [93, 96]

$$\psi(x,t) = \eta e^{i\sigma(x,t)}\mathrm{sech}\left(\eta\sqrt{\frac{\chi}{\alpha^2}}(x - x_0) + \kappa\chi t\right), \tag{3.61a}$$

$$\sigma(x,t) = -\sqrt{\frac{\chi}{\alpha^2}}\kappa x + \frac{1}{2}(\eta^2 - \kappa^2)\chi t + \varphi, \tag{3.61b}$$

where η, κ, φ and x_0 are real arbitrary constants. Note that the solitons provided by this particular solutions are moving with a velocity $-\kappa\alpha\chi^{1/2}/\eta$ and therefore we can also find standing structures by setting $\kappa = 0$. General solutions are composed of several soliton solutions via inverse scattering. Although this method allows us to solve exactly the NSE, it has the drawback that N-soliton solutions do not have explicit analytical expressions.

Several analytical as well as numerical approaches, among them the variational method [97], have succeeded in sheding a new light on the NSE and bringing in a great amount of information about the properties of the cubic NSE and some of its extensions, including different nonlinearities and space dependent damping or amplification [98]. In the next section we will take a different view and emphasize the role of the NSE as an equation describing the trapping of (pseudo)particles in nonlinear media. For this reason we will introduce pseudodistribution functions and deal with them in a way that resembles the pseudo-potential method in classical plasmas.

Most of the literature about the NSE deals with coherent waves, described by (3.60). Coherence means that knowing the phase at a given point on the beam one can predict the phase at any point across that beam. In recent years, however, the subject of *incoherent* or partially incoherent waves has received attention in the nonlinear optics community, both experimentally [99] and theoretically [87, 100, 101]. Incoherent waves are composed

by a statistical ensemble of waves satisfying the coherent NSE. The nonlinear excitation of the medium is in the cubic case given by $\chi\langle|\psi|^2\rangle$, where $\langle\dots\rangle$ represents the average over the statistical ensemble (Klimontovich average). The equation for these incoherent waves then reads

$$i\frac{\partial\psi}{\partial t}+\frac{\alpha^2}{2}\frac{\partial^2\psi}{\partial x^2}+\chi\langle|\psi|^2\rangle\psi=0. \tag{3.62}$$

In the Wigner-Moyal framework of quasidistribution functions, equations (3.60) and (3.62) receive a formally equivalent treatment. However, not all the quasidistribution functions that solve the corresponding von Neumann equation can be transformed back into a single wavefunction that satisfies (3.60). Therefore, if we are interested in finding solutions to this equation, we must disregard all pseudodistribution functions that violate the Tatarskii criterium, as they do not represent pure states. Equation (3.62) do not present this problem and all solutions arising from the von Neumann equation are legitime. Our approach here will be to find a general family of incoherent solutions and then look among them for a solution as close as possible to coherence, thereby finding a partially incoherent state.

3.3.2 Wigner transform and quasi-classical solutions

Now we can apply the Wigner transformation method [76] to the NSE (3.60) and again look for standing structures with $\partial f/\partial t\to 0$. Then we arrive to a von Neumann equation like (3.29), where the role of the adimensionalized Planck's constant ϵ is now played by α, that contains information about the wavepacket carrying wavelength. If it is small enough (i.e. we are interested only on structures much larger than one wavelength) an expansion with respect to α^2 can be made and we will finish in an equation similar to (3.32):

$$v\partial_x f+\phi'(x)\partial_v f-\frac{\alpha^2}{3!4}\phi'''(x)\partial_v^3 f=0. \tag{3.63}$$

The role of the potential is now played by the medium refractive index, which depends on $|\psi(x)|^2=\int dv f(x,v)$. In the cubic NSE case, the Poisson-like equation reads

$$-U=\phi(x)=\chi\int dv f(x,v)\equiv\chi|\psi|^2. \tag{3.64}$$

Although equation (3.63) is in fact mathematically identical to (3.32), a straightforward application of the method we developed in section 3.2.2 is here prevented by (3.64). To see this, just suppose we find two nonzero functions $f_0(x,v)$ and $\phi_0(x)$ given by (2.16) that satisfy (3.63) with $\alpha=0$. Then we would have a known function $n(\phi)=\int dv f(x,v)$ and (3.64) would result in $\phi=\chi n(\phi)$, which is a closed equation in ϕ that can therefore be only solved by $\phi=const.$ Furthermore, we also require $\phi\to 0$ as $|x|\to\infty$ which implies that no other solution than the trivial $\phi=0$ would be found. Therefore this direct naive approach must be rejected.

Note also that the boundary conditions that we are imposing require

$$\lim_{x\to\pm\infty}\phi(x)=\chi\lim_{x\to\pm\infty}\int dv f(x,v)=0, \tag{3.65}$$

and they will not be met if we look for quasidistribution functions close to (2.16), which have $\int dv f(x,v)\to 1$ when $\phi\to 0$.

There is, however, a path to circumvent these difficulties. First suppose we have $f_0(x,v)$ and $\phi_0(x)$ that satisfy the unperturbed Vlasov equation corresponding to (3.63) with $\alpha = 0$ where f_0 is not given by (2.16) but

$$f_0(x,v) = A\theta(-E)\left[e^{-\beta E} - 1\right] \tag{3.66}$$

where A is a arbitrary normalization constant and $E = v^2/2 - \phi_0(x)$. Note that for small E (3.66) can be written as $f_0(x,v) \approx -A\theta(-E)\beta E$. In fact, we could have used this simpler expression, and obtain exactly the same results, but we kept (3.66) to make the analogy with (2.16) apparent. Note that at this point we do not know what $\phi_0(x)$ and therefore $f_0(x,v)$ are.

The pseudodistribution function defined by (3.66) should be interpreted as one in which only trapped particles are present. This makes sense because we are looking for bright soliton solutions, being formed by solitary structures where the amplitude vanishes at infinity. Note also that nothing in (3.66) restricts us to standing solitons: on the contrary, the following development might be also made for propagating structures. Only for simplicity and without loss of generality we will in the following deal only with standing solutions.

We will now look for solutions of (3.63) and (3.64) that are close enough to certain f_0 and ϕ_0 to be written as $f = f_0 + \alpha^2 f_1$, $\phi = \phi_0 + \alpha^2\phi_1$ with f_1 and ϕ_1 being of order unity. Inserting this expressions into (3.63) and neglecting terms of order $\mathcal{O}(\alpha^4)$ we find the equivalent of (3.35a)

$$\left[v\partial_x + \phi_0'(x)\partial_v\right] f_1 = -\phi_1'(x)\partial_v f_0 + \frac{1}{3!4}\phi_0(x)'''\partial_v^3 f_0. \tag{3.67}$$

To avoid the problem mentioned above, we make the ansatz

$$\int f_1(x,v)dv = \gamma\phi_0''(x) + \frac{\phi_1}{\chi}, \tag{3.68}$$

where γ is an arbitrary introduced constant. If we make use of (3.68) in (3.64) we obtain

$$\phi_0(x) = \chi\int f_0(x,v)dv + \chi\alpha^2\gamma\phi_0''(x). \tag{3.69}$$

But from (3.66) we also know

$$\int f_0(x,v)dv = \frac{4A\beta\sqrt{2}}{3}\phi_0^{3/2} + \mathcal{O}(\phi_0^{5/2}) =: \lambda(\phi_0). \tag{3.70}$$

Therefore, we can write the following equation for ϕ_0:

$$\phi_0 = \chi\lambda(\phi_0) + \chi\alpha^2\gamma\phi_0'', \tag{3.71}$$

that we can solve by defining a classical potential

$$-V'(\phi_0) = \phi_0'' = \frac{1}{\chi\alpha^2\gamma}\left[\phi_0 - \chi\lambda(\phi_0)\right], \tag{3.72}$$

that integrated yields

$$-V(\phi_0) = \frac{1}{\chi\alpha^2\gamma}\frac{\phi_0^2}{2}\left(1 - \frac{8A\beta\sqrt{2}}{15}\chi\phi_0^{1/2}\right). \tag{3.73}$$

If, as usual, we call Ψ the maximum value of ϕ_0, we can find a nonlinear dispersion relation by imposing $V(\Psi) = 0$. This is,

$$\sqrt{\Psi} = \frac{15}{8A\beta\chi\sqrt{2}}, \tag{3.74}$$

which, as we are assuming $\chi > 0$, implies $A\beta > 0$. Thus we can write the classical potential as

$$V(\phi_0) = -\frac{r\phi_0^2}{2}\left(1 - \sqrt{\frac{\phi_0}{\Psi}}\right), \tag{3.75}$$

where $r = 1/\chi\alpha^2\gamma$. Note that r has to be positive and, therefore $\gamma > 0$. If we make use of this expression of the classical potential to obtain the actual shape of $\phi_0(x)$ we arrive at

$$\phi_0(x) = \Psi \mathrm{sech}^4\left(\frac{x\sqrt{r}}{4}\right). \tag{3.76}$$

At this point we can follow the approach developed in Sect. 3.2.2 to solve (3.35a) this time coupled with (3.68), which will now play the role of a Poisson-like equation. If we introduce again $g(x, v) := f_1 + \phi_1\partial_E f_0$ equation (3.68) will read

$$\gamma\phi_0''(x) + \frac{\phi_1(x)}{\chi} + V''(\phi_0)\phi_1(x) = \int g(x, v)dv, \tag{3.77}$$

which plays the same role as (3.37b) in our previous derivation.

We must however keep in mind that now we are dealing with a different f_0 that is exactly null for all the untrapped range. This implies that $G(\xi, E, \sigma)$, as defined in (3.38), will now be zero for $E > 0$. Taking all this into account, the correction to the potential results as shown in Fig. 3.6 for an arbitrary γ. The correction f_1 to the distribution function can also be obtained by the direct application of the procedure sketched above for electron holes in quantum plasmas.

Finding an almost pure (coherent) state

Up to this point we have found valid solutions of equations (3.63) and (3.64). Note that the parameter γ introduced in (3.68) has been left arbitrary and therefore for a given amplitude Ψ we have obtained a whole family of solutions. On the other side, not every pseudodistribution function $f(x, v)$ can be transformed back into a coherent complex wavefunction $\psi(x)$, this is, not any $f(x, v)$ represents a coherent state. This problem did not arise in the case of plasmas because there we assumed that $f(x, v)$ represents a mixture of many different pure states, combined according to some statistical ensemble. In the case of optical beams, incoherence can also be allowed, but only up to some extent and only in inertial media. If we are interested in coherent or only partially incoherent states, we must look at (3.60), for which only pure states can be accepted. The obvious way to proceed now is to look for pure states in the space of solutions which we obtain by varying γ.

The standard check to know if a pseudodistribution function represents a pure state is given by Eq. 3.2. This is however too mathematically involved to make any analytical progress and even numerical approaches would be unnecessarily complicated. Instead we will use a much easier method to test how close a given solution is to a pure wavefunction.

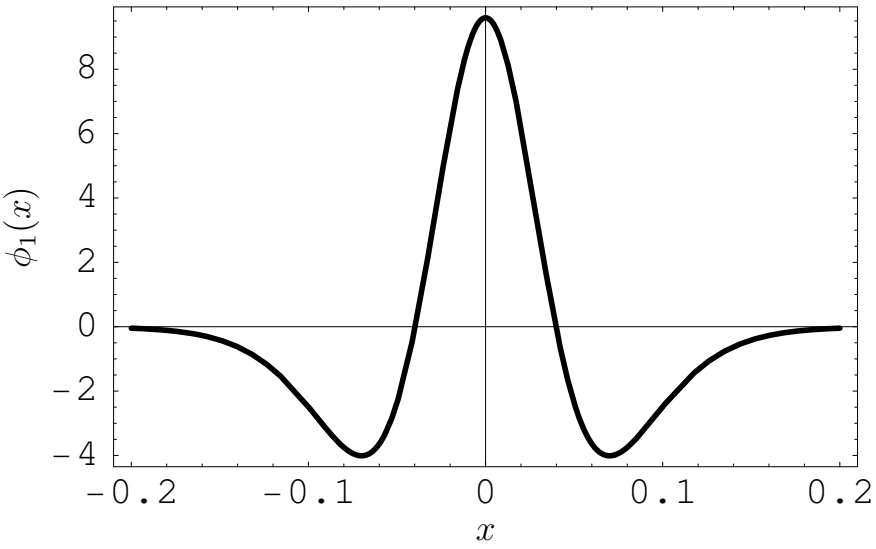

Figure 3.6: Correction to the potential for $\psi = 0.08$. As can be observed, the qualitative shape of $\phi_1(x)$ is here similar to that found before for the quantum correction to electron holes, but with a sign inversion.

Suppose that for a given γ we have already calculated $\phi = \phi_0 + \alpha^2\phi_1$. Then if it were a valid solution of (3.60), it must hold $\phi = |\psi|^2$. To simplify the notation let us define $\rho(x) := \sqrt{\phi(x)}$. We are looking for a function

$$\psi(x,t) = \rho(x)e^{i\sigma(x,t)}. \tag{3.78}$$

that solves the NSE. We make the ansatz $\sigma(x,t) = Kx - \Omega t$ with K and Ω being real constants related to the width in wavenumber and frequency domains in Fourier space of the wavepacket. Inserting it into (3.78) and then into (3.60), taking the real and imaginary parts, we arrive at

$$2K\alpha^2\rho'(x) = 0, \tag{3.79a}$$

$$2\Omega\rho(x) + 2\chi\rho^3(x) + \alpha^2\left(\rho''(x) - K^2\rho\right) = 0. \tag{3.79b}$$

From the first equation we derive $K = 0$. The second one, on the other hand, can be rewritten as

$$\Omega = -\frac{2\chi\rho^3(x) + \alpha^2\rho''(x)}{2\rho(x)} := s(x). \tag{3.80}$$

But as we know $\rho(x)$, we already have an explicit form of $s(x)$; we can therefore check whether it is a constant and if it is, the potential ϕ is compatible with a pure state. However, we have solved the von Neumann equation only perturbatively: nothing assures us that an *exact* solution is included in the family of solutions we have found so far. We can however test how far any particular solution is from being an exact solution if we note that (3.80) is equivalent to

$$\int_{-\infty}^{+\infty}\left(\frac{ds}{dx}\right)^2 dx = 0. \tag{3.81}$$

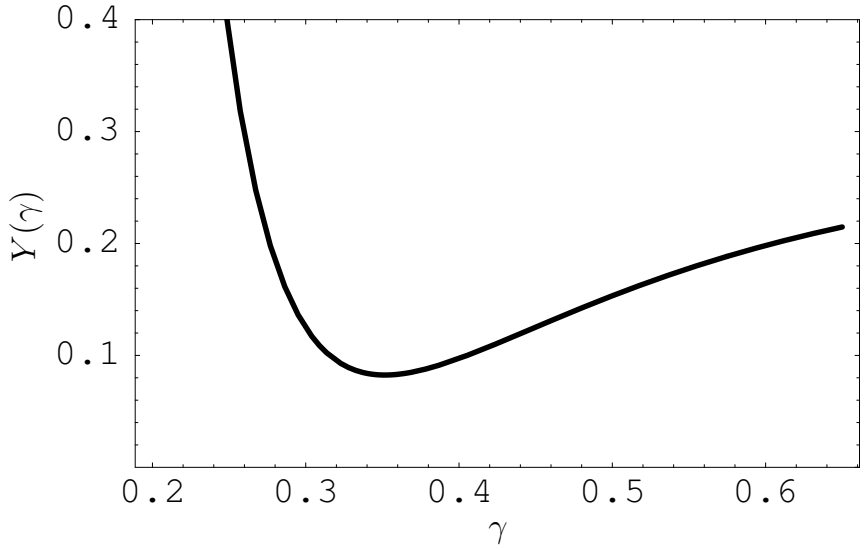

Figure 3.7: Dependence of the function $Y(\gamma)$, as defined in Eq. (3.82) with respect to γ. The solution corresponding to the minimum of $Y(\gamma)$ is the closest to a pure state. Figure 3.8 shows how this solution looks like and compares it to the exact analytical solution.

Thus, we may say that the best solution contained in the parametric family of solutions is the one that minimizes the function

$$Y(\gamma) = \int_{-\infty}^{+\infty} \left(\frac{ds}{dx}\right)^2 dx. \tag{3.82}$$

A typical representation of the function $Y(\gamma)$ is given in Fig. 3.7. Choosing γ through the procedure just sketched, we arrive to a final potential ϕ as represented in Fig. 3.8.

3.3.3 Generalization to an arbitrary nonlinearity

In the last section we found an approximate solution to the cubic NSE, of which an exact analytical solution already exists. The purpose of such development was twofold: (a) show how self-consistent trapping appears also in fields quite different from plasma physics and give some hints as to how trapping in the quantum domain can be faced and (b) provide a general, albeit only approximate, procedure to solve the NSE with any arbitrary nonlinearity. In this section we will focus on (b) and show how the steps we took in the last section can be generalized when the potential (resp. refractive index) of a given material depends on the field amplitude as

$$\phi = F[|\psi|^2], \tag{3.83}$$

where the only property required to F is being a continuous, derivable and invertible function. As long as α is a small parameter, when transformed into the Wigner representation, (3.83) can be written as

$$\phi(x) = F\left[\int dv f_0(x,v)\right] + \alpha^2 F'\left[\int dv f_0(x,v)\right] \int dv f_1(x,v). \tag{3.84}$$

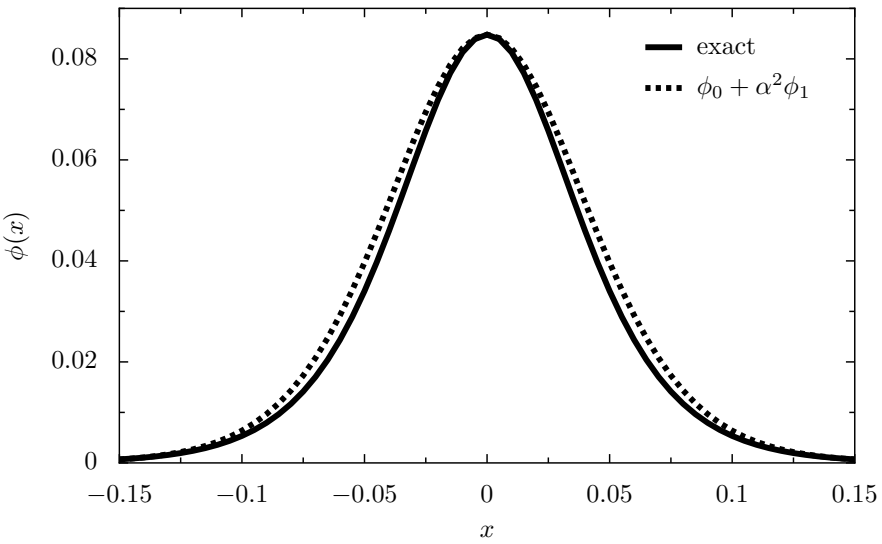

Figure 3.8: Approximate and exact solutions of the cubic NSE. The exact solution is given by (3.61) with $\kappa = 0$. The amplitudes are selected such that the maximum of the corrected (approximate) solution coincides with the top of the exact solution.

Where f_0 has been defined again according to (3.66). The ansatz we should make now being equivalent to (3.68) reads

$$\int f_1(x,v)dv = \gamma\phi_0''(x) + \frac{\phi_1}{F'[\lambda(\phi_0)]}, \tag{3.85}$$

with $\lambda(\phi_0)$ still defined by (3.70). The equation for ϕ_0 yields

$$\phi_0 = F[\lambda(\phi_0)] + \gamma\alpha^2 F'[\lambda(\phi_0)]\phi_0''. \tag{3.86}$$

This is an ordinary equation that can in general be solved directly through e.g. the pseudo-potential method. Once we have obtained a suitable ϕ_0 we only need to go again through the same steps as for plasmas and the cubic NSE and then find ϕ_1 and f_1. Looking then for a solution closest to a pure state is also straightforward because we have demanded F to be invertible and therefore, given ϕ we can know $|\psi|$. The parameter γ can be fixed in this way.

Note that in (3.85) nothing prevents us from including more derivatives of ϕ_0 along with more parameters $\gamma_1, \ldots, \gamma_n$. In general, the more terms we add, the larger the freedom we have later when looking for pure states. The price we pay is that the resulting equation for ϕ_0 might then not be analytically solvable.

3.4 Concluding remarks

In this chapter we have extended the theory of self-consistent trapping to quantum and quantum-like systems. This extension was based on the use of the Wigner method and on a perturbative expansion of the von Neumann evolution equation. We presented, therefore, a *fully nonlinear approach to the study of self-trapping in dilute, weakly quantum plasmas*, which to our knowledge is new.

The first part of the chapter was devoted to the study of quantum corrections to electron holes. There we saw how to introduce the quantum character of particles, which means a finite de Broglie wavelength and the possibility of diffraction and tunneling effects, and which resulted in bringing the system closer to thermodynamical equilibrium. This effect was expected because it is a typical phenomenon met for any quantum correction. Drawbacks of the method we used are that it is only applicable to certain systems with some constraints with respect to density and temperature and that we are limited to strictly standing structures. This is due to the fact that in the way we construct the unperturbed, classical solutions, infinite derivatives are involved with respect to the velocity as we approach the separatrix from the outside. A possible path to circumvent this problem would be to use some kind of intermediate layer theory in which we introduce a special treatment of the equation near the separatrix. This extension lies, however, beyond the scope of this thesis.

In the second part we dealt with the self-consistent trapping of (pseudo)particles that interact nonlinearly with the medium and whose behavior is described by the nonlinear Schrödinger equation (NSE). There we presented an approach to the study of such systems based on a phase space representation of the trapping via Wigner pseudodistribution functions. In the particular case of Kerr media, governed by the cubic NSE, we derived an approximate solution that successfully compares with the exact one-soliton solution. An interesting point that this derivation raises is the comparison with some other methods of facing the cubic NSE, such as the already mentioned variational method, that do not rely on a phase space representation.

Our procedure is based on the introduction of the closure relation (3.68), that allows us to treat the problem as a perturbative one. The exact form of this closure relation is to a certain extent arbitrary, but it is intended to emphasize the relationship between self-consistent trapping in plasmas and in other nonlinear systems, thus giving us a deeper understanding of the physics involved in such processes.

In summary, from this chapter we can conclude that strong connections exists between the trapping of particles in an electrostatic potential and the trapping of pseudo-particles in a self-modulated nonlinear medium. The methods outlined here seem to be appropriate to shed light on this connection and to cope with similar problems in both fields as well as to formulate conceptually new problems.

CHAPTER 4

Trapping in charged particle beams

. . . y hasta los cerebros electrónicos se estremecen
en las noches de luna llena
cuando una lívida lucidez ilumina los ficheros
donde las ecuaciones sonríen petulantes
afilando los ángulos de sus raíces cúbicas.

Ángel González

4.1 Motivation

The third and last kind of physical system that we will study is that of beams of charged particles in storage rings and accelerators. Long-lived coherent structures due to particle trapping have been observed since a long time in coasting beams [102, 103] and an analytical theory [104, 105] has been developed. Similar coherent structures have also been recently observed in bunched beams in the Super Proton Synchrotron (SPS) at CERN [106, 107] and the Tevatron at Fermilab [108, 109] as well as in the Relativistic Hadron-Ion Collider (RHIC) in the Brookhaven National Laboratory [110, 111]. In this chapter we will address the study of these phenomena showing how their longitudinal dynamics can also be described by a system of a Vlasov equation and a Poisson-like equation. In particular, we will deal here with trapping in bunched beams, a phenomenon in which, due to the boundary conditions, different to these of infinite plasmas, analytical solutions are not known for the Vlasov-Poisson system and therefore we must rely heavily on numerical approaches. However, before proceeding with this task, we will shortly review the fundamental physics of modern synchrotrons and storage rings.

A synchrotron [112] is a circular particle accelerator similar to a cyclotron in which the magnitude of the magnetic field and of the accelerating rf voltage are changed in time to keep the diameter of the designed trajectory constant. As the space where the fields are created is confined to a circular ring, this design is much more efficient than

a cyclotron. The machine is designed in such a way that a given *ideal particle* which follows the design trajectory always enters the rf cavities with the same phase and the energy it receives is hence maximized. However, the energy spread of all the particles in the beam and the self-consistent interaction between them (so called space-charge forces) makes it difficult to predict the trajectories of real particles and optimize the machine to give them the maximum possible amount of energy. The characteristics of the machine and the injection conditions of the particles have to be carefully chosen to assure that particles close to the design trajectory do not get further apart as time evolves. These desired conditions are commonly referred as *focusing* and are usually associated with the existence of bunches and hotspots in the particle distributions.

4.2 Electrostatic structures in coasting beams (a review)

Stable long-lived coherent electrostatic structures superimposed on the designed beam have been long observed in coasting beams [102, 103] and a theoretical explanation has been given [104, 105] based in a kinetic description of the longitudinal beam dynamics which leads for a purely reactive wall impedance to the Vlasov-Poisson system of equations [105, 113]

$$[\partial_t + p\partial_z - \epsilon\partial_p]\, f = 0, \tag{4.1}$$

$$\epsilon'' = \bar{\mu}\epsilon + \bar{\alpha}\lambda_1', \tag{4.2}$$

where λ_1 is the perturbation of the line density $\lambda = \int dpf$ over the designed one. The notation defined in Ref. 105 is followed here, which means that the constants $\bar{\mu}$ and $\bar{\alpha}$ in (4.2) are given by

$$\bar{\mu} = \frac{\mu}{1-L}, \qquad \bar{\alpha} = \alpha\frac{g_0 - L}{1-L}, \tag{4.3}$$

where L is the dimensionless wall inductance and g_0 represents the capacitive space charge impedance of the beam. The parameters μ and α, where μ is proportional to $(\gamma R_0/b)^2$ and α proportional to ηN, are typically very large, so that one is tempted to solve (4.2) approximately by letting both terms on the right hand side balance each other. Note that R_0 is the large radius of the design trajectory, b the radius of the circularly shaped cross section of the toroidal vessel, N the total number of particles in the beam and η is the slip factor [112].

A rigorous study of equations (4.1) and (4.2) and the focusing properties of beams that can be derived from them has already been performed in Ref. 113. The results are summarized in Fig. 4.1.

4.3 Bunched beams

4.3.1 Experimental evidences

Long-lived coherent structures (solitons) have been observed in the SPS, the Tevatron and in the RHIC. They were first apparent in reported observations of "rf activity" during stochastic cooling studies. Later they have been clearly seen in current monitor data at RHIC. This data measures the current induced at a certain point of the wall by the beam and is commonly assumed to be proportional to the instantaneous line density

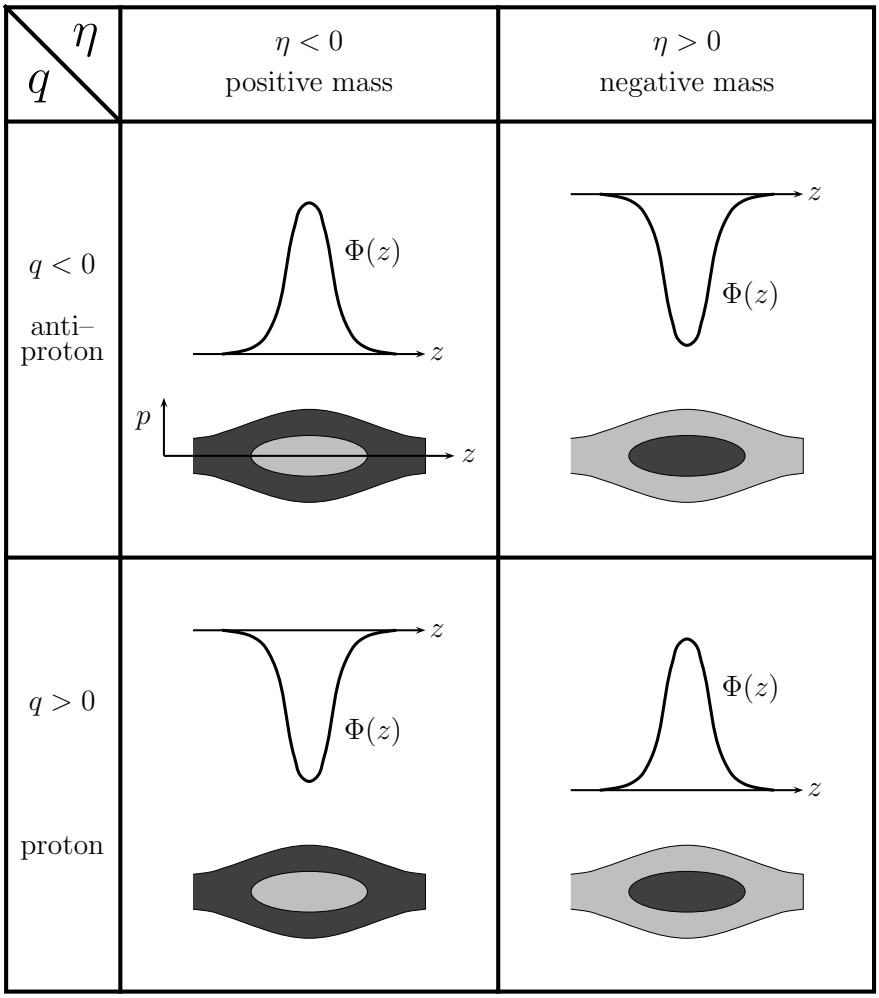

Figure 4.1: Standard (de)focusing properties of impedances for coasting (debunched) beams, valid for $L < 1 < g_0$. Represented at each cell is the shape of the electric potential (above) and the schematic distribution function, where a darker color means larger particle densities. When $1 < L$ the chart must be changed by reversing columns and rows, which means e.g. that for $\eta < 0$ (positive mass) the system is focusing, showing a positive potential for $q < 0$.

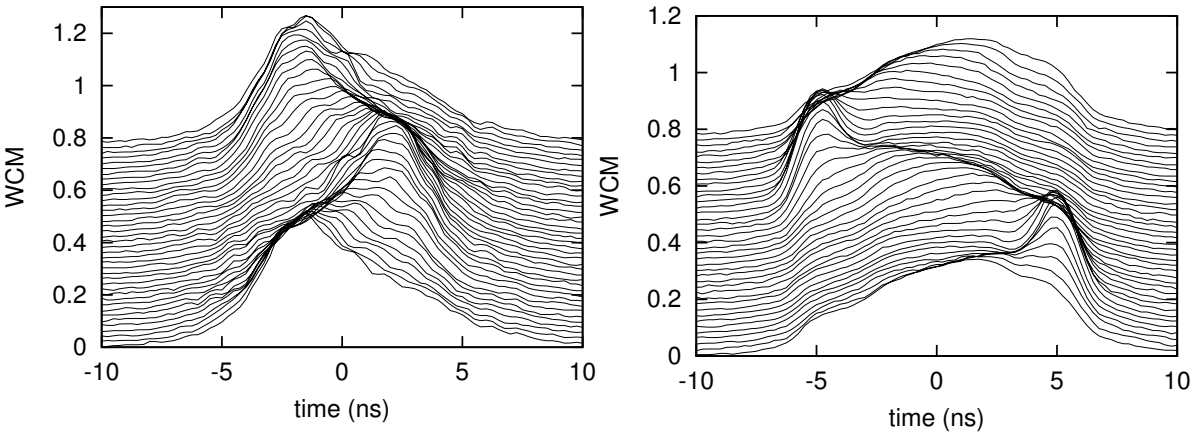

Figure 4.2: Wall current monitor data for a freshly injected (left) bunch of protons with $\gamma = 35.9$ at RHIC and the same bunch 17 min later, still at injection energy (right).

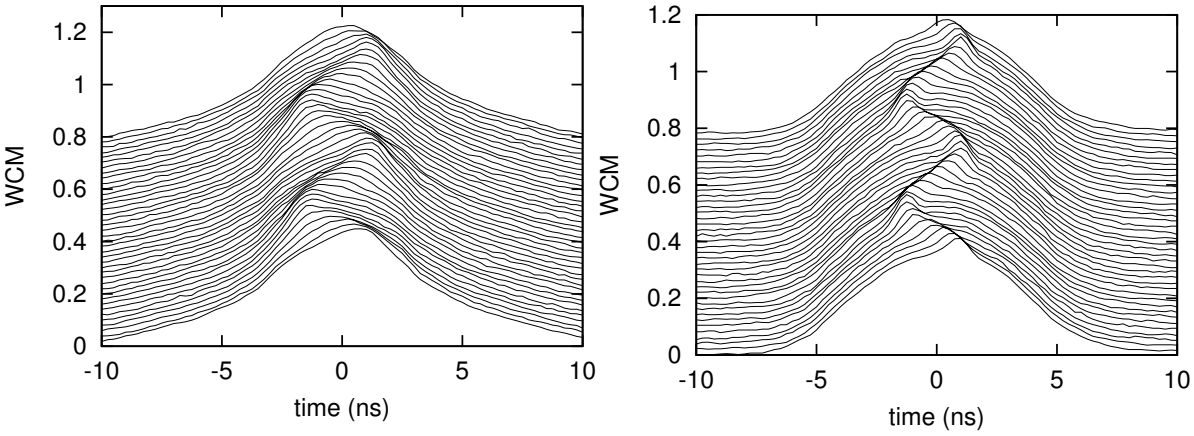

Figure 4.3: Wall current monitor data for two different bunches at flattop. Both have $\gamma = 107$.

carried by the beam at this point. The wall current monitor (WCM) data gives us therefore an image of the density profile of particles in the beam. Thus, if we take different measures as the beam passes through different monitors or through the same monitor at different cycles, we can have a picture of how the line density evolves. Figure 4.2 shows an example of the mountain range plot of observations at RHIC where a bunch can be seen with a superimposed oscillating soliton manifest as a hump (hotspot) in the line density. Figure 4.3 show two other bunches at flattop with a larger energy. In all cases, only the 28MHz accelerating cavities were operating and the total acquisition time was 4000turns $\approx$ 50ms. The transition energy [112] of RHIC is $\gamma_T = 23.8$, so all the measures were above transition. There exists also data showing humps in deuteron beams with $\gamma = 10.7 < \gamma_T$. All this observations are commonplace at RHIC but a stable hole (a depression in the line density) has never been observed.

Humps have always been observed with impedances that for a coasting beam will be thought as defocusing and lead to holes. It is therefore clear that a new approach has to be taken to model bunched beams. Due to the strong nonlinear nature of the phenomenon, perturbative analytical approaches have few chances to succeed.

4.3.2 Bunched beam model

Following Ref. 111, a theoretical model for bunched beams can be developed which relies on the approximation of assuming that the two terms to the right of (4.2) are much larger than the left hand side ϵ'' which can be thus neglected. This simplification corresponds to what in Ref. 113 is called *quasineutrality (QN) assumption*. For bunched beams a *bunching* rf voltage has also to be included in the beam equations of motion. Let φ be the position in the bunch measured in radians, $\omega_{s,0}$ be the small amplitude angular synchrotron frequency and use $s = \omega_{s,0}t$ as the evolution variable. Let $\lambda(\varphi, s)$ be the normalized line density of particles

$$\int_{-\pi}^{+\pi} d\varphi \lambda(\varphi, s) = 1 \tag{4.4}$$

The rf voltage is $V(t) = V_{rf} \sin\varphi$ and ω_{rf} is the angular rf frequency. The effect of transition energy is included in the sign of the rf voltage with $V_{rf} > 0$ below transition and $V_{rf} < 0$ above. Let Q denote the total charge in the soliton, which is assumed to be positive. The single particle equation of motion is then

$$\frac{d^2\varphi}{ds^2} + \sin\varphi = \ell \frac{\partial \lambda(\varphi, s)}{\partial \varphi}, \tag{4.5}$$

where to simplify notation we have set

$$\ell = -\frac{LQ\omega_{rf}}{V_{rf}}. \tag{4.6}$$

If we introduce now $p = d\varphi/ds$, we can rewrite (4.5) in canonical coordinates as

$$\frac{dp}{ds} = -\sin\varphi - \ell \frac{\partial \lambda(\varphi, s)}{\partial \varphi}. \tag{4.7}$$

This equation can be generated from the Hamiltonian

$$H(\varphi, p, s) = p^2/2 + 1 - \cos\varphi + \ell\lambda(\varphi, s). \tag{4.8}$$

Consider a canonical transformation of Goldstein's [114] first type with a generator given by

$$F_1(\varphi, \Psi) = \frac{\varphi^2}{2} \cot(\Psi + s) \tag{4.9}$$

where Ψ is the new position coordinate and J is the new momentum coordinate. They are related to the old coordinates via

$$p = \sqrt{2J}\cos(\Psi + s) \qquad \varphi = \sqrt{2J}\sin(\Psi + s). \tag{4.10}$$

Performing a phase average defined as

$$\langle h(J, \Psi, s)\rangle_s = \frac{1}{2\pi}\int_0^{2\pi} h(J, \Psi, s) ds, \tag{4.11}$$

we arrive at the following averaged Hamiltonian, valid as long as the coherent frequency of the soliton is close to the small amplitude synchrotron frequency:

$$H_1(J, \Psi) = \alpha(J) + \frac{\ell}{\pi}\int d\Psi_1 dJ_1 \frac{f(\Psi_1, J_1, s)}{\left[2J + 2J_1 - 4\sqrt{JJ_1}\cos(\Psi - \Psi_1)\right]^{1/2}}, \tag{4.12}$$

where $f(\Psi_1, J_1, s)$ is the distribution function of particles and $\alpha(J) := -J/2 + 1 - J_0(\sqrt{2J}) \approx -J^2/16$, $J_0(x)$ being the Bessel function.

The corresponding Vlasov equation for this Hamiltonian is

$$\frac{\partial f}{\partial s} + \{f, H\} = 0, \tag{4.13}$$

with the Poisson bracket $\{f, H\}$ defined as

$$\{f, H\} = \frac{\partial f}{\partial \Psi}\frac{\partial H_1}{\partial J} - \frac{\partial f}{\partial J}\frac{\partial H_1}{\partial \Psi}. \tag{4.14}$$

The solitons will appear as solutions uniformly rotating in the phase space defined by (Ψ, J), $f(\Psi, J, s) = g(\Psi + \tilde{r}s, J)$, where $\tilde{r}$ is a constant. Inserting this into (4.13) we obtain

$$\left[\tilde{r} + \frac{\partial H_1}{\partial J}\right]\frac{\partial g}{\partial \Psi} - \frac{\partial H_1}{\partial \Psi}\frac{\partial g}{\partial J} = 0. \tag{4.15}$$

It is useful to transform back to Cartesian phase space coordinates

$$A = \sqrt{2J}\sin\Psi, \qquad B = \sqrt{2J}\cos\Psi. \tag{4.16}$$

As we got rid of the time dependence, the density $g(A, B)$ satisfies now the time-independent Vlasov equation

$$\frac{\partial K}{\partial B}\frac{\partial g}{\partial A} - \frac{\partial K}{\partial A}\frac{\partial g}{\partial B} = 0, \tag{4.17}$$

with the new Hamiltonian

$$K = R(A, B) + V(A, B), \tag{4.18}$$

where the single particle motion is generated by

$$R(A, B) = \alpha\left([A^2 + B^2]/2\right) + \frac{\tilde{r}}{2}(A^2 + B^2) \tag{4.19}$$

and collective effects are due to the self-consistent potential

$$V(A, B) = \frac{\ell}{\pi}\int dA_1 dB_1 \frac{g(A_1, B_1)}{\sqrt{(A - A_1)^2 + (B - B_1)^2}} \tag{4.20}$$

4.3.3 Self-consistent numerical solutions

It is well known that the Vlasov equation (4.17) can be solved if the contours of constant particle density in phase-space coincide with those of constant energy K. However, due to the possible existence of separatrices, this does not imply that there exists a single function $G(K)$ such that $g(A, B) = G\left(K(A, B)\right)$ in all the phase space. In principle, there can be as many different G_i functions as regions in which the separatrices divide the phase-space.

In Fig. 4.4 (left) a schematic plot of K is presented along the line $B = 0$. Note that for a given value of K there can be as much as four different points with this same energy. The value of K at the separatrix, which in this picture can be identified with the local maximum to the left, is denoted by K_s. In the same figure to the right, a phase-space

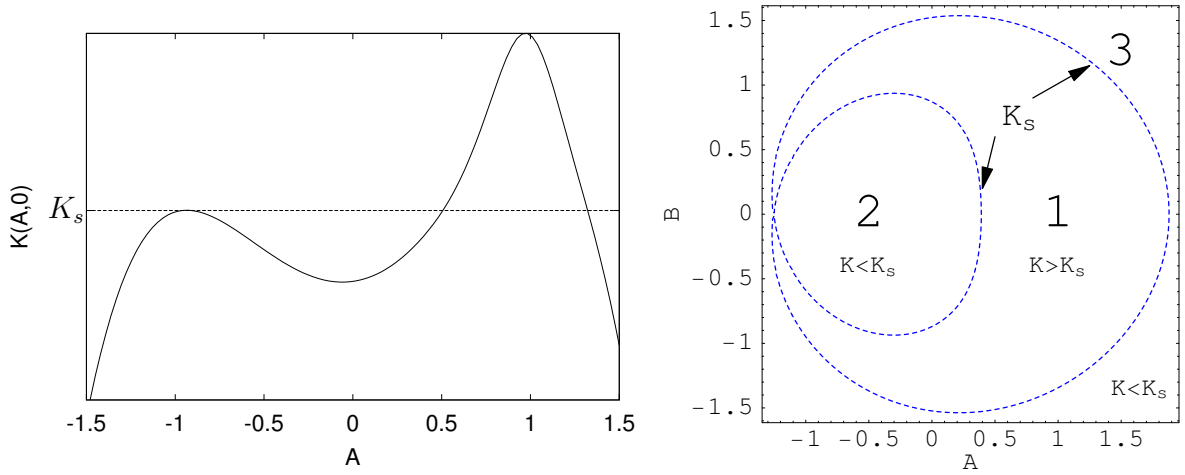

Figure 4.4: Schematic plot of $K(A, B = 0)$ for $\ell > 0$ (left) and typical phase-space map (right) when a soliton is present. The dashed line represents the separatrix $K = K_s$. The particles are divided into three different groups: particles that belong to the soliton and that rotate around a certain O-point located at $(A_0 > 0, 0)$ (region 1), particles inside the inner separatrix which rotate around a different O-point at $(A_0' < 0, B)$ (region 2) and particles outside the outer separatrix which turn around the whole structure (region 3).

map symmetric around the $B = 0$ axis is presented with a typical shape of the separatrix that differentiates three areas in each one of which, a different dependence of K on the density can be assumed.

We can solve the Vlasov-Poisson-like system composed by (4.17) and (4.20) by prescribing the functions $G_i(K)$ at each one of the three regions of the phase-space. There are limitless possibilities, but we take the fairly simple

$$g(A,B) = C_3 \begin{cases} G_1(x) = C_0 x^2 + C1, & \text{in region 1,} \\ G_2(x) = C_1 + \sqrt{C_2 - x} - \sqrt{C_2}, & \text{in region 2,} \\ G_3(x) = C_1 - \sqrt{C_2 - x} + \sqrt{C_2}, & \text{in region 3,} \end{cases} \tag{4.21}$$

with $x = K - K_s$, and $C_0, \ldots, C_3$ being arbitrary constants.

Any $g(A, B)$ given by (4.21) will automatically satisfy Vlasov equation. But at this point nothing assures us that it will also be consistent with the potential satisfying (4.20). To find self-consistent solutions with $\ell > 0$ and containing a hotspot we use the following numerical procedure[1]:

1. Choose $\tilde{r}$. Set n, the iteration counter, as zero. Choose initial parameters C_0^0, C_1 and C_2. Set up an initial distribution function $g^0(A, B)$ which is symmetric around $B = 0$.

2. Use $g^n(A, B)$ to calculate $K^n(A, B)$ through (4.20). Find the separatrix, on which $K^n(A, B) = K_s^n$. We can easily do this as the symmetry imposed by the initial conditions will be kept all along the procedure, so the X-point contained in the separatrix will have $B = 0$ and can be found as a local maximum of $K(A, 0)$.

   Define the electrostatic amplitude $\psi^n = K^n(O) - K_s$ where $K^n(O)$ is the value of K at the O-point in region 1 (and also the absolute maximum of K).

[1]The code that implements this algorithms and that was used to produce the results of this chapter can be downloaded from `http://www.phy.uni-bayreuth.de/~btpa16/downloads.html`.

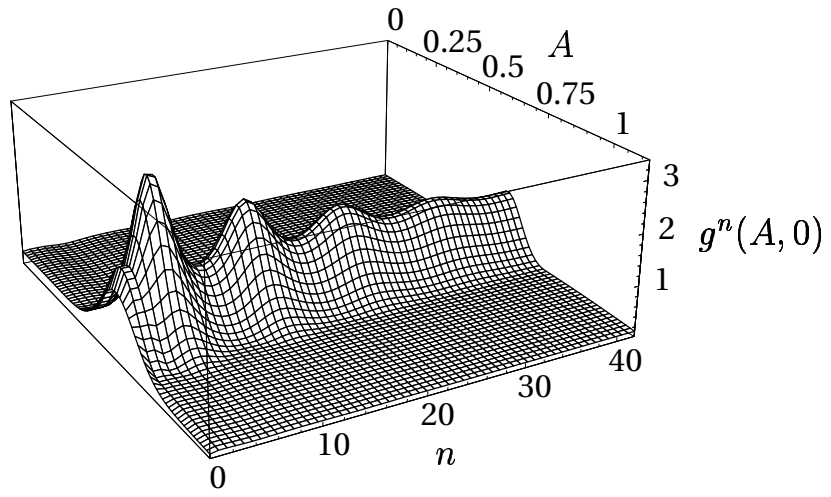

Figure 4.5: Evolution of the density along $B = 0$ during the iteration. Convergence is reached after about 30 iterations.

3. If $n > 0$ change C_0 through the formula

$$C_0^{n+1} = C_0^n \left(1 - \alpha \frac{\psi^n - \psi^{n-1}}{\psi^n}\right), \tag{4.22}$$

   where α is an input parameter. If $n = 0$ use $C_0^1 = C_0^0$.

4. Calculate g^{n+1} using (4.21) with $K^n(A, B)$ and C_0^n. Calculate the global normalization constant C_4 and increase n.

5. Repeat the iteration steps 2-4 until $g^n(A, B)$ converges.

The variation in C_0 defined through Eq. 4.22 is introduced because an iterative scheme with fixed C_0 was proven to be largely unsuccessful, as the initial density had to be so close to a final self-consistent solution that the whole procedure was of small utility. The exact form of (4.22) was chosen because in the numerical investigation it proved robust, leading almost always to interesting, nontrivial solutions. When convergence is achieved, the parameter α ceases to play any significant role. It can be therefore regarded as an additional "initial condition". Typically, $\alpha \sim 1$. Figure 4.5 shows the evolution of the density as the iteration proceeds. Depending on the initial parameters (including α), a large range of stable solutions can be obtained. An outcome of this numerical procedure is that there is a definite relationship between $\tilde{r}$ and the converged quantities C_0 and ψ, denoted by $F(\psi, C_0, \tilde{r}) = 0$ and shown in Fig. 4.6. It can be regarded as a nonlinear dispersion relation (NDR) that plays a similar role than the one played in standard particle-trapping theory by the relationship between the trapping parameter β, potential amplitude Ψ and the propagating velocity v_0, shown e.g. in Eq. (2.52).

As seen from (4.21), C_0 can be expressed by

$$C_0 = \frac{g(O) - g(X)}{N\psi}, \tag{4.23}$$

where $g(O)$ $[g(X)]$ is the distribution function at the stable (unstable) fixed point. It is clear that C_0 is positive for a hump in region 1 of Fig. (4.4), zero for a flattoped and

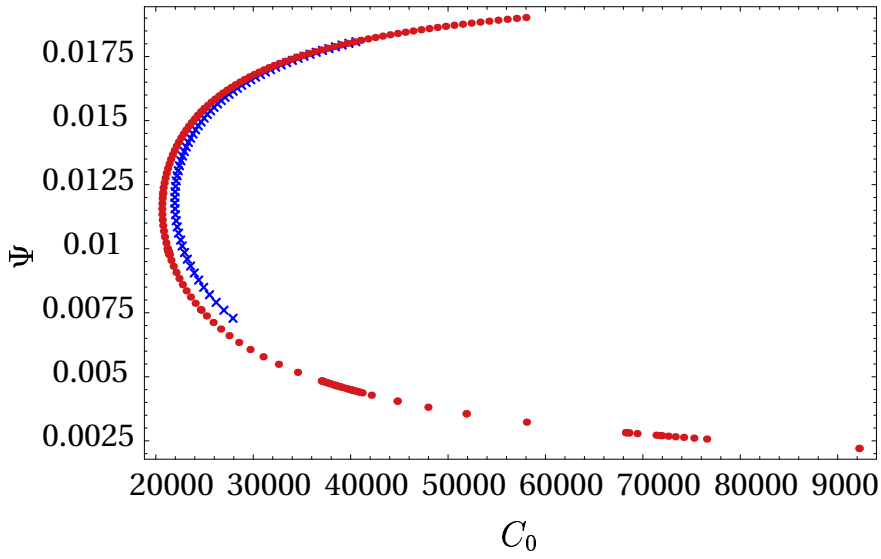

Figure 4.6: Relationship between C_0 and the soliton potential ψ. The red circles (outer curve) correspond to $\tilde{r} = 0.025$ and the blue crosses (inner curve) to $\tilde{r} = 0.030$.

negative for a notch, and hence C_0 reflects the status of trapped particles. We learn from Fig. 4.6 that C_0 is strictly positive, corresponding to a hump (hotspot), and that there are two different values of ψ for given $\tilde{r}$ and C_0. For the larger one (upper branch), most of the particles are residing in the hotspot, this is, region 1 (as in Fig. 4.7), whereas for the smaller value of ψ (lower branch) the majority of the particles id residing in the background.

Figure 4.7 shows the phase space density and accompanying line density for a bunch with most of the beam trapped in the soliton, while Fig. 4.8 presents a small soliton, similar to the observations shown in Fig. 4.3. Both solutions have $\ell = 0.01$ and $A_0 = 0.025$ showing the broad range of solutions that are possible for the same bunch charge and machine impedance. This is qualitatively consistent with Figs. 4.2 and 4.3.

To cross-check the results obtained by the iterative procedure, they were inserted in a time-dependent drift-kick code that directly simulates equations (4.13) and (4.20). The results are presented in Fig. 4.9: the plot on the left shows the mountain range plot (simulated WCM) for the initial conditions taken as the outcome of the iterative procedure. On the right the line density after 100 synchrotron oscillation is presented. As can be seen, the soliton proves to be quite robust and long-lived, with only small quantitative change that may be due to numerical inaccuracies.

4.3.4 Holes in bunched beams

Although long-lived holes have not yet been observed in bunched beams [111], the theory we have developed can also be successfully applied to find hole solutions as long as $\ell < 0$.

One is tempted to blindly apply the iterative procedure just described but set an initial density $g^0(A, B)$ with a hole instead of a jump and $C_0^0 < 0$. There are several difficulties that would then arise:

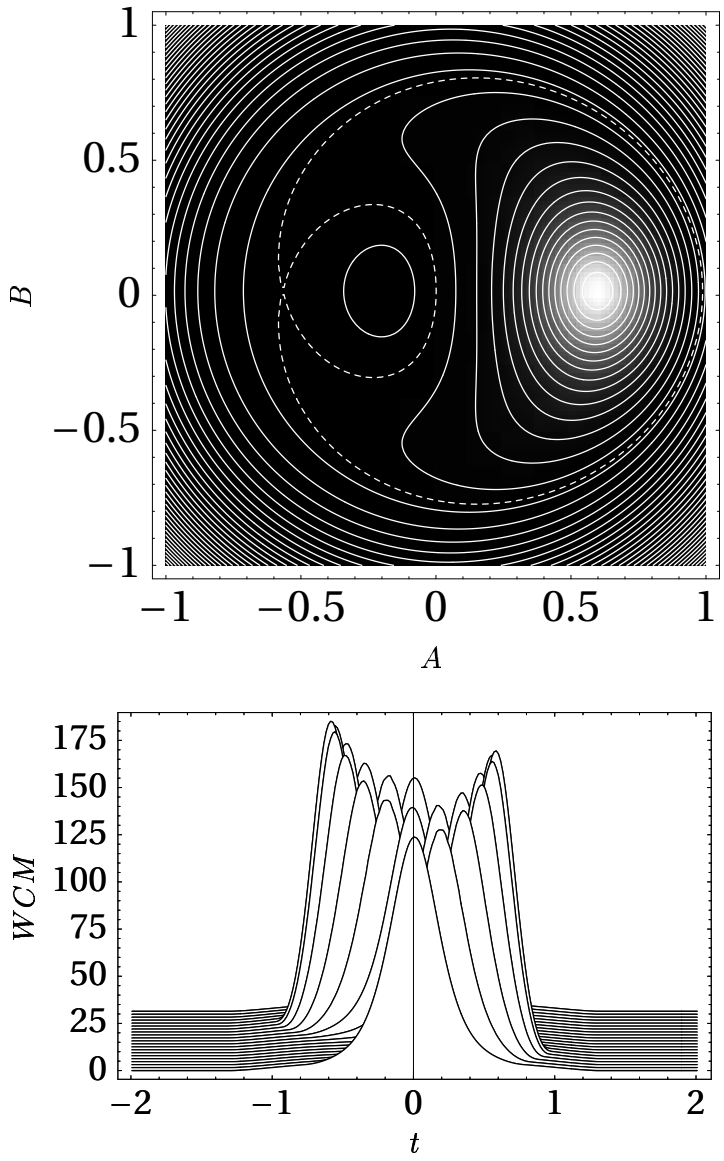

Figure 4.7: (a) Phase space density (gray scale) and contours of constant energy $K(A, B)$ (particle trajectories). (b) Line density (simulated WCM data). The solution was obtained with $\alpha = 0.3$, $\tilde{r} = 0.025$, $C_1 = 0.1$, $C_3 = 0.005$, $\ell = 0.01$, $C_0 = 21975$ and $\psi = 0.014$. This solution consists in a large soliton with a little background, i.e., almost all particles are trapped in the soliton.

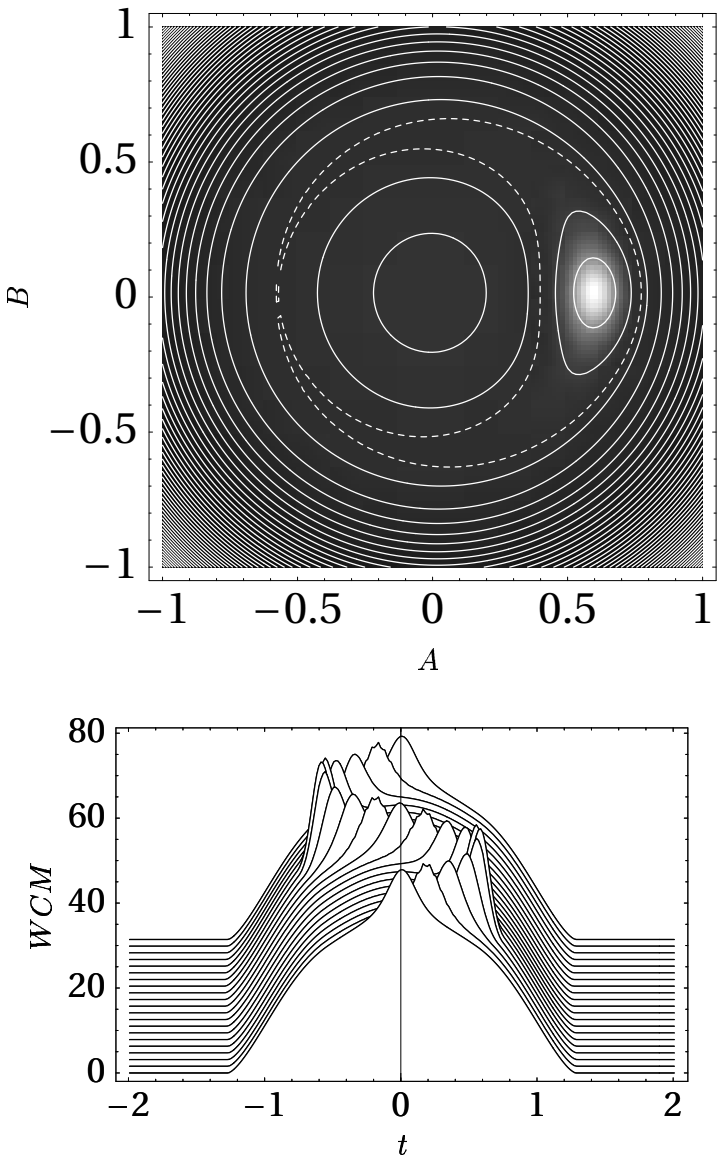

Figure 4.8: (a) Phase space density (gray scale) and contours of constant energy $K(A, B)$ (particle trajectories). (b) Line density (simulated WCM data). The solution was obtained with $\alpha = 1.2$, $\tilde{r} = 0.025$, $C_1 = 0.1$, $C_3 = 0.005$, $\ell = 0.01$, $C_0 = 92191$ and $\psi = 0.0022$. This solution has comparable density in the soliton and the background.

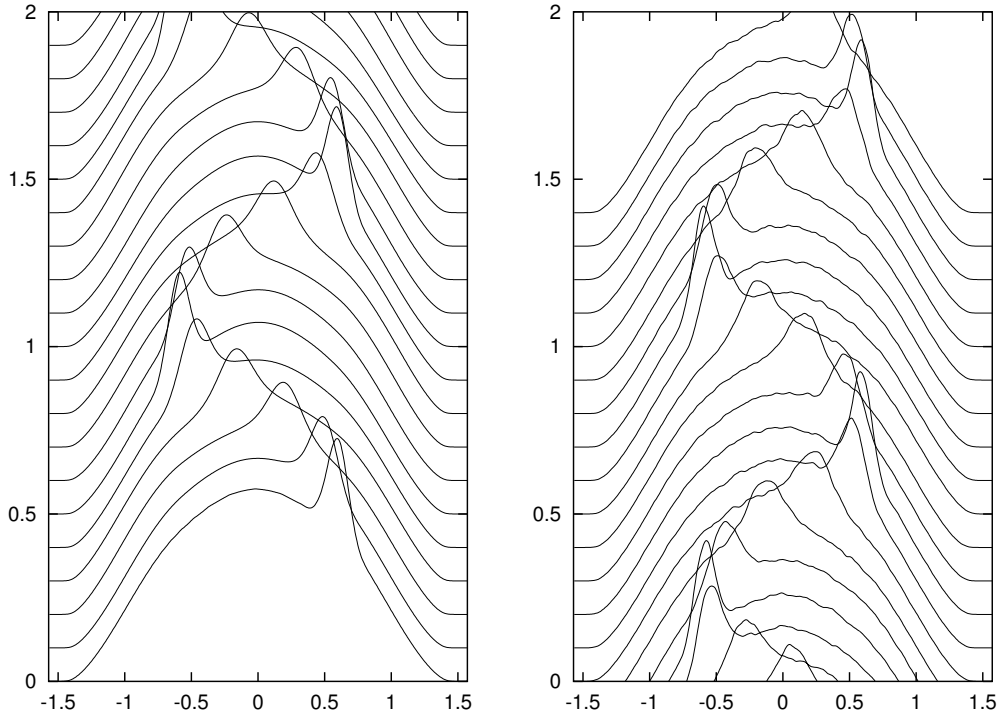

Figure 4.9: Simulation of a bunched beam with initial conditions provided by the outcome of the iterative procedure. On the left the line density for the first oscillation is shown, whereas the plot on the right corresponds to the line densities after 100 synchrotron oscillations. Only small quantitative variations probably due to numerical errors, can be observed, which proves that the solution obtained by the iterative code is a solution to the time-independent Vlasov equation.

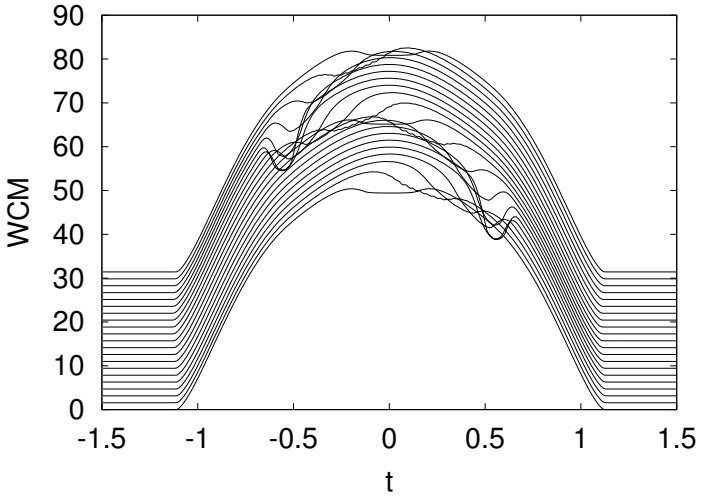

Figure 4.10: Mountain range plot or WCM of a hole solution with $\ell = -0.01$, $C_0 = -144208$.

1. From Eq. 4.21 we see that a negative C_0 can lead to negative particle densities which have no physical sense. This can be avoided by setting

$$G_1(x) = \max(0, C_0 x^2 + C1). \tag{4.24}$$

2. The attempts made to find hole solutions by using (4.24) instead of (4.21) proved that convergent nontrivial solutions are very hard to obtain. In almost all cases, one arrives either to a standard bunch without any superimposed structure or to vacuum solutions with $g(A, B) = 0$. To overcome this further problem, a "trial and error" schema can be devised. To assure the convergence, we set an *amplitude window* defined by a minimum and a maximum ψ, denoted ψ_- and ψ_+ respectively. Then we apply the iterative steps described in the former section but with the restriction that if $\psi_- < \psi^n < \psi_+$ does not hold, then C_0 is modified according to (4.22) but the density $g^n(A, B)$ (and therefore, also the energy) is held constant. Then the code will evolve and vary C_0 until a acceptable nontrivial solution (usually in the very margin of the window) is obtained.

Through this modified iterative approach, hole solutions can easily be obtained as long as $\ell < 0$. An example of a possible mountain range plot is given in Fig. 4.10

4.4 Concluding remarks

This chapter was concerned with trapping phenomena in the longitudinal dynamics of charged particles beams. After reviewing the status of the topic of coasting beams, we concentrated on investigating solitons on bunched beams. For this purpose we developed a simplified model in which some terms of the fields equation were neglected in a quasi-neutral approach.

Within this model we applied an iterative numerical procedure to find self-consistent solutions consisting of hotspots sitting on top of the bunch. A relationship between the parameters determining the shape of the distribution function and the soliton amplitude

was also found. A comparison with the actual data show a good qualitative agreement with our results. Later we slightly modified the code to search also for holes in the particle densities. We concluded that holes are in principle possible but only for $\ell < 0$, a condition which has not yet been available in the experimental machines.

Many improvements could be made to the present theory. First of all a more rigorous derivation of the field equations should be made to take fully into account the local charge densities and the quasi-cylindrical geometry, leaving aside the quasi-neutrality approximation. A theory that continuously connects the coasting beam scenario with the bunched beam one would also be helpful in the understanding of soliton phenomena in particle beams. This theory might be constructed by starting from a coasting beam solution and then using finite amplitude expressions to derive solutions where almost all the particles are contained in the soliton.

CHAPTER 5

Summary and conclusions

Überhaupt ist es für den Forscher ein guter Morgensport, täglich vor dem Frühstück eine Lieblingshypothese einzustampfen – das erhählt jung.

Konrad Lorenz

In the introduction to this thesis we mentioned that its main purpose was to present an account on the role self-consistent trapping phenomena are playing in many different areas of modern physics. We investigated three topics which we were able to study within a similar framework of Vlasov-Poisson-like systems of equations and we showed that self-consistency and trapping are the keys to the understanding of a plethora of nonlinear physical phenomena.

A large part of plasma physics is concerned with transport theory and stability issues; in some sense we can say that progress in plasma physics is measured by the increasing ability to avoid unstable regimes and control the flow of particles, momentum and energy through the system. The lack of understanding of some of these processes, commonly known as *anomalous transport* processes, has impeded many of the desired progresses e.g. in the confinement times of fusion reactors. But it has been shown[27, 35] that the existence of electrostatic structures greatly affects the transport coefficients. Furthermore, as we showed in this thesis, these electrostatic structures can be excited out of thermal noise and therefore have to be taken into account from the very beginning of the calculations. Therefore a general framework for the study of self-consistent trapping like the one presented in this work seems to provide a helpful resource for the research in this important field.

On the other hand, the extension of the concept of nonlinear self-consistent trapping into the quantum domain further proves that these phenomena have to be always taken into account when one deals with dilute systems of interacting particles. It also allows to show connections between seemingly distant parts of physics, such as hot plasmas and nonlinear optical fibers. The concept of approaching a nonlinear equation (in our case

the Nonlinear Schrödinger Equation) by going into a kinetic description and then applying some variation of the pseudo-potential method appears to be appropriate for other equations as well thereby allowing the formulation of conceptually new and challenging problems and providing a deeper understanding on the physics involved in nonlinear wave phenomena in different media.

Finally, charged particle beams show another example of the successful application of the methods and knowledge about nonlinear trapping that stem from plasma physics. The investigations on solitons on bunched beams had however to rely strongly on numerical methods, due to the lack of reliable analytical unperturbed solutions. This problem might be overcome in the future if a theory that continuously connects coasting and bunched beam physics succeeds.

Many open questions deserve further investigation in this field. The properties of negative energy modes seem to be the most outstanding one among them: a new paradigm of stability based on the idea of nonlinear self-consistent trapping appears to be at hand that would be a breakthrough in plasma physics, a point that could eventually be applied also to quantum systems as well as to beam dynamics. In the corresponding chapter we mentioned also the value of extending the description of holes in a weak quantum plasma to propagating electron holes and finite amplitudes. Also the topic of trapping in accelerators and storage rings presents challenging problems that still need to be solved, e.g. the use of an improved field equation for bunched beams.

In summary, we can say that the topic of self-consistent collective nonlinear particle trapping has achieved a better understanding on many relevant nonlinear problems in plasma physics and related areas. It is, on the other hand, far from being exhausted, for it still provides challenging problems and promises to play a key role in many forthcoming investigations on a large variety of subjects mainly contained in, but not restricted to plasma physics.

APPENDIX A

Particle–in–cell simulation of two–stream nonlinear instabilities

A.1 Motivation

In a landmarking work, R.H. Berman, D.J. Tetreault and T.H Dupree [39, 40] presented computer simulations showing instability well below the predicted linear ion-acoustic threshold. In particular, they observed how eddies typical of a Bernstein-Greene-Kruskal equilibrium were formed even without any initial macroscopic (i.e. collective) excitation. These structures in phase space, that can be better described as holes, tended to last for relatively long times while they grew and were decelerated.

By showing how a system conventionally regarded as stable against small perturbations was destabilized even by thermal fluctuations, these results focused the attention of the plasma physics community onto the limitations of linear stability theory. These numerical works were presented two decades ago and, although they used very optimized algorithms and computer capabilities quite impressive for that time, progress in the available hardware has been so fast that an average desktop computer of nowadays can easily outperform the computational power they used. It is therefore timely and convenient to reexamine such results and check them using modern equipment to test whether they stand up when using more realistic conditions for the simulations (i.e. a larger number of simulated particles).

A.2 Particle-in-cell simulation: a short review

Besides the Vlasov and Fokker-Planck codes like the one we introduced in section 2.4, the other family of simulation techniques that take into account the kinetic behavior of the particles is that of *Particle-in-cell (PIC)* codes [115]. Unlike Vlasov and Fokker-Planck codes, which integrate a statistical kinetic equation to predict the evolution of a

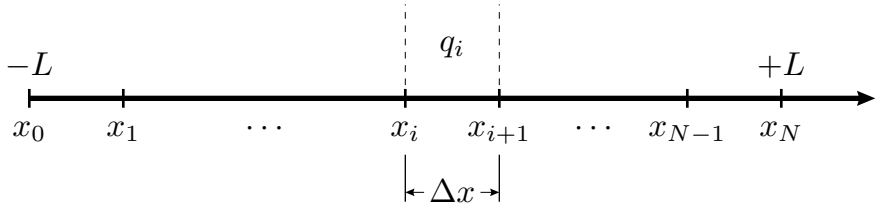

Figure A.1: Division of the system length into several sub-intervals (cells). The electric field is calculated at every x_i and later interpolated for all intermediate positions.

distribution function, PIC codes just follow the trajectory of every plasma particle while self-consistently calculating the generated fields.

The name *Particle-in-cell* comes from the procedure used to calculate the field. Simply using the complete Coulomb expression to calculate the interaction between every pair of particles turns usually out to be far too computationally expensive to be useful. A different approach is used instead which can be regarded as the numerical equivalent to what in statistical mechanics is called a *mean-field approximation*. The procedure for a one-dimensional system with periodic boundary conditions is as follows[1] : as represented in Fig. A.1, one can divide the simulated system lenght, that we suppose spans from $-L$ to $+L$, into N sub-intervals or *cells* of length $\Delta x = 2L/N$. Let q_i be the net charge contained between points x_i and x_{i+1}, this is,

$$q_i = n_i^i - n_e^i, \tag{A.1}$$

with n_i^i and n_e^i being, respectively the number of ions and electrons present in cell i. If we apply the Gauß theorem we find the variation of electric field between points x_i and x_{i+1}:

$$E(x_{i+1}) - E(x_i) = q_i. \tag{A.2}$$

Then, supposing we know the field at the boundary $E(x_0) = E(x_N)$, we would be able to calculate the field at any x_j as

$$E(x_j) = E(x_0) + \sum_{i=0}^{j-1} q_i. \tag{A.3}$$

Note that the periodicity is granted if we assume quasineutrality, this is $\sum_{i=0}^{N-1} q_i = 0$. The field at the boundary can be related with the average electric field $\langle E \rangle$. Usually $\langle E \rangle = 0$, in which case

$$E(x_0) = -\frac{1}{N} \sum_{j=0}^{N-1} \sum_{i=0}^{j-1} q_i. \tag{A.4}$$

Once we have calculated the electric field at every grid point, we can also calculate by interpolation the forces acting on each particle and then integrate the field equations by a straightforward leap-frog algorithm.

[1]Here we describe a direct integration of the field equations via a finite differences method. Most of the actual PIC codes use *Fast Fourier Transforms (FFT)* to compute the fields, which has the advantages of smoothing the solutions and providing immediate access to spectral information. As we are only interested in a handy repetition of previous results, the exposed procedure yields a sufficiently reliable outcome. For a detailed review on further refinements on PIC codes, see Ref. 115.

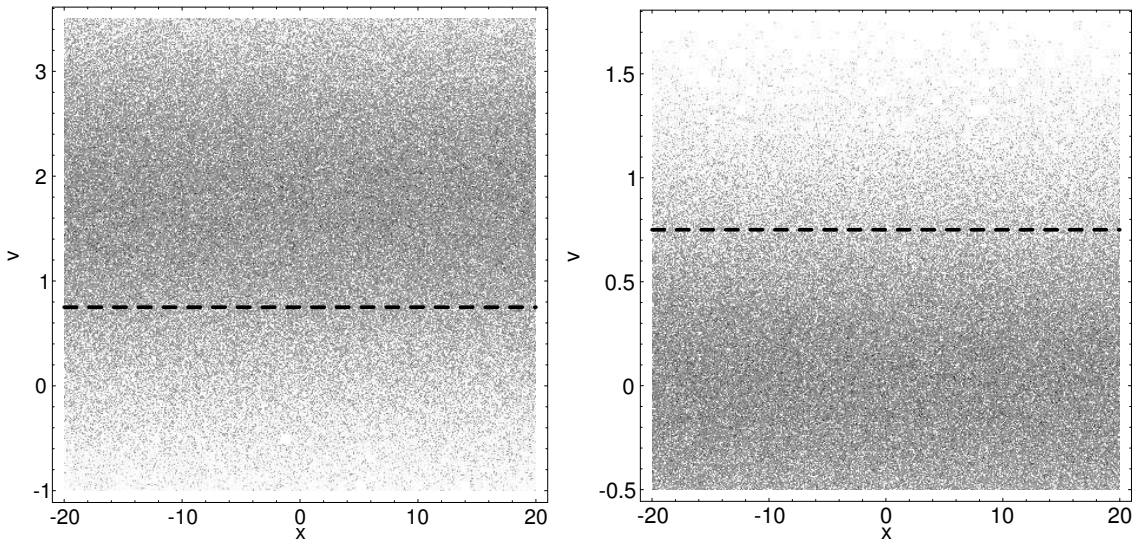

Figure A.2: Initial phase space densities of electrons (left) and ions (right). Note that no initial excitations are present, the local variations in the density being due only to random (incoherent) fluctuations. The dashed line is located at $v = 0.75$ and represents the limit of negative energies for ion holes when $\beta = 0$.

A.3 Nonlinear instability and formation of phase-space vortices

A PIC code that works as sketched in the past section[2] can be used to prove that nonlinear instability exists far below the linear threshold. To do so, we can initialize the code with a very large number of particles with an initial thermal distribution and without any macroscopic excitation (what Berman and coworkers called *random start*). As physical parameters we will use the same as we did in section 2.6.2 which, in turn, are the same used by Berman and coworkers: the mass ratio is set to $\delta = m_e/m_i = 1/4$, the temperature ratio is set to unity ($T_e = T_i$) and the drift between electrons and ions is set to $v_D = 1.75$ (remember that the linear threshold for stability for this parameters is located at $v_D^\star = 1.96$). We will simulate 1024000 particles whithin 1024 cells (i.e. ten times more particles and double as many cells as in Ref. 40).

The outcome of the simulations is summarized in Figs. A.2 - A.5. The first conclussion we can extract from looking at such pictures is that the system is actually far from stable, thus contradicting the linear stability theory. We conclude also that the onset of instability is clearly related with the development of vortices in phase space that usually appear as electron and ion holes (depressions in the particle densities). Figure A.5 shows also that after the interaction and coalescence of structures, some of them seem to survive for long times.

We can also study the influence of negative energy modes on the nonlinear destabilization of the system. On this purpose we plotted in our figures the boundary $v^\star = 0.75$ between positive and negative energy ion holes for the used temperature ratio and drift velocity and $\beta = 0$ (see (2.77) and also Fig. 2.28). The selection of $\beta = 0$ seems not to be

[2]The PIC code which was used to generate the results presented here can be downloaded from the same internet address as all the codes with which we deal in this thesis: `http://www.phy.uni-bayreuth.de/~btpa16/downloads.html`.

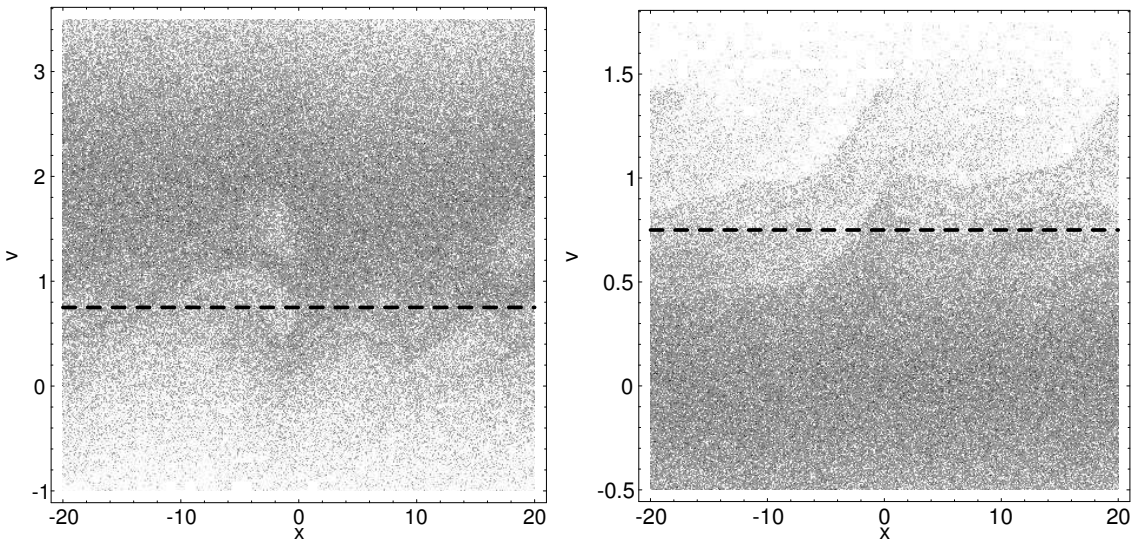

Figure A.3: Phase space densities of electrons (left) and ions (right) at $t = 255$. This is approximately the instant when nonlinear instability is first macroscopically visible. Note how small vortices, seen as depressions in phase space density, start to develop.

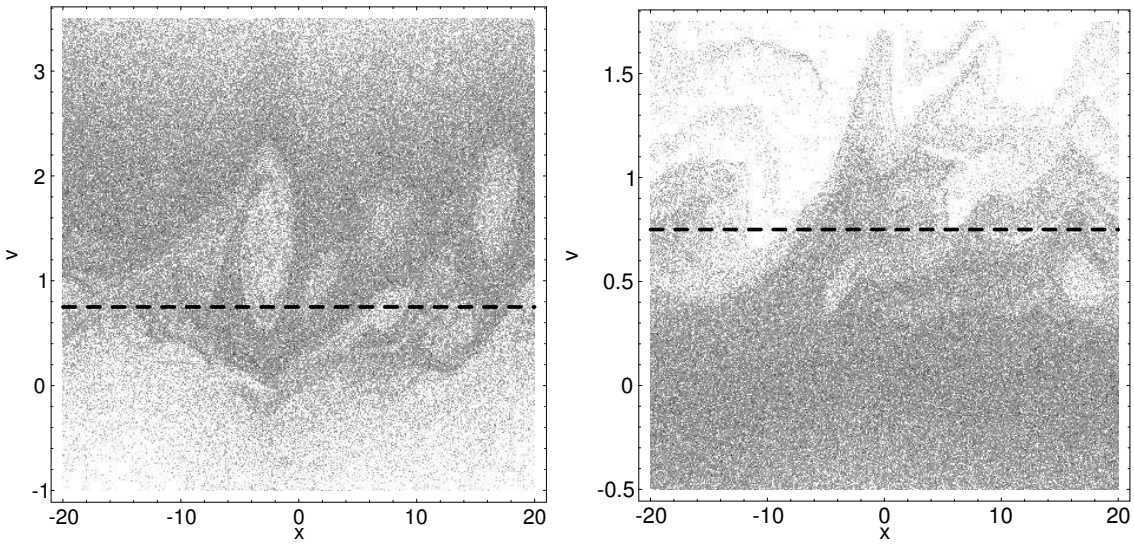

Figure A.4: Phase space densities of electrons (left) and ions (right) at $t = 350$. Note how instability has led to the formation of clusters of trapping structures, mostly visible in the electron phase space.

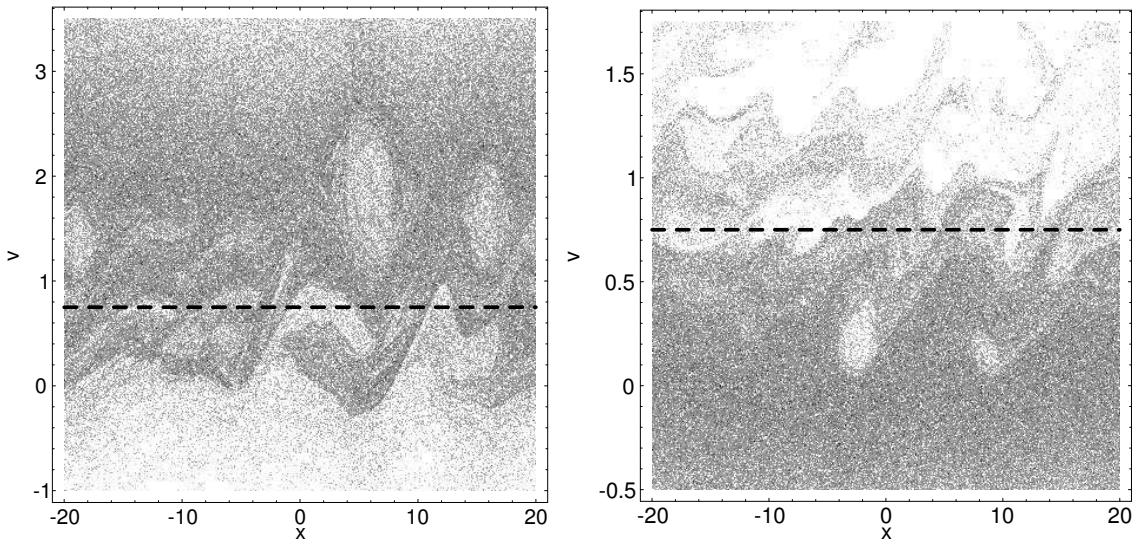

Figure A.5: Phase space densities of electrons (left) and ions (right) at $t = 400$.

unphysical, as one would expect that when structures arise out of thermal fluctuations, they start with distribution functions more or less flat at the trapped range. Figure A.3 suggests that initially electrostatic structures start to develop in the negative energy range while later (perhaps due to the interaction between them) the are decelerated. If we go to much larger times (Fig. A.5) and we look at the ion phase space densities we see that the distribution function has suffered a large amount of filamentation mostly above the negative energy threshold. Some solitary surviving holes are found however in the postive energy range.

From our simulations we conclude that the results of Berman and coworkers remain unchanged when the number of particles in the simulation is highly increased, thereby proving to be robust and reliable evidences of the importance of trapping and holes in the nonlinear stability of current-carrying plasmas. The results support also the claim of Refs. 19, 18 according to which ion holes arise spontaneously in the negative energy range, which is one of the arguments on which the conjecture of a destabilization through negative energy holes is based.

Bibliography

[1] A. A. Vlasov, J. Phys. U.S.S.R. **9**, 25 (1945).

[2] L. D. Landau, J. Phys. U.S.S.R. **10**, 25 (1946).

[3] I. B. Bernstein, J. M. Greene, and M. D. Kruskal, Phys. Rev. **108**, 546 (1957).

[4] H. L. Berk and K. V. Roberts, Phys. Fluids **10**, 1595 (1967).

[5] R. L. Morse and C. W. Nielson, Phys. Rev. Lett. **23**, 1087 (1969).

[6] A. V. Gurevich, Sov. Phys. JETP **26**, 575 (1968).

[7] H. L. Berk, C. E. Nielsen, and K. V. Roberts, Phys. Fluids **13**, 980 (1970).

[8] M. Kako, T. Taniuti, and T. Watanabe, J. Phys. Soc. Jpn. **31**, 1820 (1971).

[9] H. Schamel, Plasma Phys. **14**, 905 (1972).

[10] H. Schamel, J. Plasma Phys. **9**, 377 (1973).

[11] H. Schamel, J. Plasma Phys. **13**, 139 (1975).

[12] H. Schamel, Phys. Plasmas **7**, 4831 (2000).

[13] H. Schamel, Physics Reports **140**, 161 (1986).

[14] Y. Omura, H. Matsumoto, T. Miyake, and H. Kojima, J. Geophys. Res. **101**, 2685 (1996).

[15] Y. Omura *et al.*, J. Geophys. Res. **104**, 14627 (1999).

[16] C. Franck, T. Klinger, A. Piel, and H. Schamel, Phys. Plasmas **8**, 4271 (2001).

[17] A. Luque, H. Schamel, and J.-M. Grießmeier, Phys. Plasmas **9**, 4841 (2002).

[18] J.-M. Grießmeier, A. Luque, and H. Schamel, Phys. Plasmas **9**, 3816 (2002).

[19] J.-M. Grießmeier and H. Schamel, Phys. Plasmas **9**, 2462 (2002).

[20] H. Schamel, Physica Scripta **20**, 336 (1979).

[21] H. Schamel, Symposium on plasma double layers, Roskilde, Denmark 1982; Risø Report **472**, 13 (1982).

[22] H. Schamel, Physica Scripta **T2/1**, 228 (1982).

[23] H. Schamel and S. Bujarbarua, Phys. Fluids **26**, 190 (1983).

[24] H. Schamel, Z. Naturforsch. **38a**, 1170 (1983).

[25] H. Schamel and S. Bujarbarua, Phys. Fluids **23**, 2498 (1980).

[26] D. L. Newman, M. V. Goldman, and R. E. Ergun, Phys. Plasmas **9**, 2337 (2002).

[27] J. Korn and H. Schamel, J. Plasma Phys. **56**, 307 (1996).

[28] B. D. Fried and R. W. Gould, Phys. Fluids **4**, 139 (1961).

[29] N. A. Krall and A. W. Trivelpiece, *Principles of Plasma Physics* (McGraw-Hill, New York, 1973).

[30] P. Bhatnagar, E. Gross, and M.Krook, Phys. Rev. **94**, 511 (1954).

[31] D. R. Nicholson, *Introduction to Plasma Theory* (Wiley, New York, 1983).

[32] R. Balescu, *Transport Processes in Plasmas* (North–Holland, Amsterdam, 1988).

[33] W. Press, S. Teukolsky, W. Vetterling, and B. Flannery, *Numerical Recipes in C : The Art of Scientific Computing* (Cambridge University Press, Cambridge, 1988), available at `http://www.nr.com`.

[34] J. Korn, Doktorarbeit, Universität Bayreuth, 1996.

[35] J. Korn and H. Schamel, J. Plasma Phys. **56**, 339 (1996).

[36] T. O'Neil, Phys. Fluids **8**, 2255 (1965).

[37] G. Manfredi, Phys. Rev. Lett. **79**, 2815 (1997).

[38] T. P. Armstrong and D. Montgomery, Phys. Fluids **12**, 2094 (1969).

[39] R. H. Berman, D. J. Tetreault, T. H. Dupree, and T. Boutros-Ghali, Phys. Rev. Lett. **48**, 1249 (1982).

[40] R. H. Berman, D. J. Tetreault, and T. H. Dupree, Phys. Fluids **28**, 155 (1985).

[41] W. Oohara and R. Hatakeyama, Phys. Rev. Lett. **91**, 205005 (2003).

[42] R. G. Greaves, M. D. Tinkle, and C. M. Surko, Phys. Plasmas **1**, 1439 (1994).

[43] J. Zhao, I. Sakai, and K. Nishikawa, Phys. Plasmas **3**, 844 (1996).

[44] R. G. Greaves and C. M. Surko, Phys. Rev. Lett. **75**, 3846 (1995).

[45] in *Pulsars: Problems and Progress*, edited by S. Johnston, M. A. Walker, and M. Bailes (ASP Conference Series, San Francisco, 1996), Vol. 105.

[46] *Active Galactic Nuclei*, edited by H. R. Miller and P. J. Wiita (Springer–Verlag, Berlin, 1998).

[47] *The Very Early Universe*, edited by G. W. Gibbons, S. W. Hawking, and S. Siklos (Cambridge University Press, Cambridge, 1983).

[48] B. Eliasson and P. K. Shukla, Phys. Rev. Lett. **92**, 045001 (2004).

[49] H. Schamel and A. Luque, to be published.

[50] R. Redmer, Phys. Rep. **282**, 35 (1997).

[51] N. Kluksdahl, A. Kriman, D. Ferry, and C. Ringhofer, Phys. Rev. B **39**, 7720 (1989).

[52] A. Driskill-Smith, D. Hasko, and H. Ahmed, Appl. Phys. Lett. **75**, 2845 (1999).

[53] D. Frank *et al.*, Proc. IEEE **89**, 259 (2001).

[54] S. Wind *et al.*, Appl. Phys. Lett. **80**, 3817 (2002).

[55] J. R. Barker, in *Physics of Non-linear Transport in Semiconductors*, edited by D. K. Ferry, J. R. Barker, and C. Jacoboni (Plenum, New York, 1980).

[56] M. H. Holzscheiter, Hyperfine Interactions **109**, 1 (1997).

[57] P.Chen, in *Proc. of Advanced ICFA Beam Dynamics Workshop on "Quantum Aspects of Beam Physics", Monterrey, California, USA, 4–9 January 1998*, edited by P.Chen (World Scientific, Singapore, 1999).

[58] P.Chen, in *Proc. of 18th Advanced ICFA Beam Dynamics Workshop on "Quantum Aspects of Beam Physics", Capri, Italy, 15–20 October, 2000*, edited by P.Chen (World Scientific, Singapore, 2002).

[59] M. Sands, *Physics with Intersecting Storage Rings* (Aademic Press, New York, 1971).

[60] A. Sokolov and I. Ternov, Sov. Phys. Dokl. **8**, 1203 (1964).

[61] S. Heifets and Y. Yan, in *Proc. of Advanced ICFA Beam Dynamics Workshop on "Quantum Aspects of Beam Physics", Monterey, California, USA, 4–9 January 19*, edited by P.Chen (World Scientific, Singapore, 1999).

[62] *Quantum-like Models and Coherent Effects*, edited by R. Fedele and P. Shukla (World Scientific, Singapore, 1995).

[63] *New Perspectives in the Physics of Mesoscopic Systems – Quantum-like Descriptions and Macroscopic Coherence Phenomena*, edited by S. De Martino *et al.* (World Scientific, Singapore, 1997).

[64] R. Fedele and G. Miele, Nuovo Cimento **D13**, 1527 (1991).

[65] R. Fedele, G.Miele, L.Palumbo, and V.G.Vaccaro, Phys. Lett. A **179**, 407 (1993).

[66] D. Anderson *et al.*, Phys. Lett. A **258**, 244 (1999).

[67] P. Shukla, Phys. Rep. **138**, 1 (1986).

[68] I. Alber, Proc. Royal Soc. London A Mat. **363**, 525 (1978).

[69] D. Crawford, P. Saffman, and H. Yuen, Wave Motion **2**, 1 (1980).

[70] P. Janssen, J. Fluid. Mech. **133**, 113 (1983).

[71] P. Janssen, in *The Ocean Surface*, edited by Y. Toba and H. Mitsuyasu (Reidel, Dordrecht, Holland, 1985), p. 39.

[72] M. Leontovich, Izv. Akad. Nauk SSSR **8**, 16 (1944).

[73] V. Fock and M. Leontovich, Zh. Éksp. Teor. Fiz. **16**, 557 (1946).

[74] D. Gloge and D. Marcuse, J. Opt. Soc. Am. **59**, 1629 (1969).

[75] G. Agrawal, *Nonlinear Fibre Optics* (Academic Press, San Diego, 1995).

[76] E. Wigner, Phys. Rev. **40**, 749 (1932).

[77] E. P. Wigner, in *Perspectives in Quantum Theory*, edited by W. Yourgrau and A. van der Merwe (World Scientific, Singapore, 1979).

[78] J. Moyal, Proc. Cambridge Philos. Soc. **45**, 99 (1949).

[79] R. Fedele, F. Galluccio, V. Man'ko, and G. Miele, Phys. Lett. A **209**, 263 (1995).

[80] R. Fedele and V. Man'ko, Phys. Rev. E **58**, 992 (1998).

[81] R. Fedele and V. Man'ko, Phys. Rev. E **60**, 6042 (1999).

[82] Y. Klimontovich and V. Silin, Sov. Phys. Usp. **3**, 84 (1960).

[83] F. Haas, G. Manfredi, and J. Goedert, Phys. Rev. E **64**, 026413 (2001).

[84] R. Fedele *et al.*, Phys. Lett. A **303**, 61 (2002).

[85] R. Fedele, D. Anderson, and M. Lisak, Physica Scripta **T84**, 27 (2000).

[86] R. Fedele and D. Anderson, J. Opt. B: Quantum Semiclass. Opt. **2**, 207 (2000).

[87] B. Hall *et al.*, Phys. Rev. E **65**, 035602(R) (2002).

[88] M. Onorato, A. Osborne, R. Fedele, and M. Serio, Phys. Rev. E **67**, 046305 (2003).

[89] V. Tatarskii, Sov. Phys. Usp. **26**, 311 (1983).

[90] A. Luque, H. Schamel, and R. Fedele, Phys. Lett. A **324**, 185 (2004).

[91] F. Haas, G. Manfredi, and M.Feix, Phys. Rev. E **62**, 2763 (2000).

[92] V. Karpmann, *Nonlinear Waves in Dispersive Media* (Pergamon, Oxford, 1975).

[93] A. Hasegawa and M. Matsumoto, *Optical Solitons in Fibers* (Springer, Berlin, 1989).

[94] A. Hasegawa and F. Tappert, Appl. Phys. Lett. **23**, 142 (1973).

[95] K. Blow and D. Wood, IEEE Trans. Quantum Electron. **25**, 2665 (1989).

[96] V. Zakharov and A. Shabat, Sov. Phys. JETP **34**, 62 (1972).

[97] D. Anderson and M. Lisak, in *Quantum-like Models and Coherent Effects*, edited by R. Fedele and P. K. Shukla (World Scientific, Singapore, 1995), p. 345.

[98] D. Anderson, A. Berntson, and M. Lisak, Physica Scripta **T82**, 42 (1999).

[99] M. Mitchell, Z. Chen, M. Shih, and M. Segev, Phys. Rev. Lett. **77**, 490 (1996).

[100] D. N. Christodoulides *et al.*, Phys. Rev. E **63**, 035601 (2001).

[101] V. V. Shkunov and D. Z. Anderson, Phys. Rev. Lett. **81**, 2683 (1998).

[102] S. Koscielniak, S. Hancock, and M. Lindroos, Phys. Rev. ST Accel. Beams **4**, 044201 (2001).

[103] P. L. Colestock and L. K. Spentzouris, in *The Tamura Symposium Proceedings, Austin, TX, 1994*, edited by T. Tajima (AIP Conf. Proc., Springer–Verlag, Berlin, 1996), Vol. 356.

[104] H. Schamel, Phys. Rev. Lett. **79**, 2811 (1997).

[105] H. Schamel and R. Fedele, Phys. Plasmas **7**, 3421 (2000).

[106] D.Boussard, in *Proc. Joint US-CERN Acc. School, Texas, 1986*, Vol. 296 of *Lecture Notes on Phys.* (Springer Verlag, Berlin, 1987), p. 289.

[107] F.Caspers and D. Mohl, CERN Report No. CERN/PS 98-051 (D1), 1998.

[108] R. Pasquinelli, in *Proceeding of the PAC 1995, Dallas* (JACoW, CERN, Geneva, 1995), p. 2379.

[109] L. Spentzouris, J.-F. Ostiguy, and P. Colestock, Phys. Rev. Lett. **76**, 620 (1996).

[110] M. Blaskiewicz *et al.*, in *Proceeding of the PAC 2003, Portland* (JACoW, CERN, Geneva, 2003).

[111] M. Blaskiewicz, J. Wei, A. Luque, and H. Schamel, Phys. Rev. ST Accel. Beams **7**, 044402 (2004).

[112] S. Humphries, *Principles of Charged Particle Acceleration* (John Wiley and Sons, New York, 1999).

[113] H. Schamel and A. Luque, New J. Phys. **6**, 113 (2004).

[114] H. Goldstein, *Classical Mechanics* (Addison–Wesley, Philippines, 1980).

[115] C. K. Birdsall and A. B.Langdon, *Plasma Physics Via Computer Simulation* (McGraw–Hill, New York, 1985).

Acknowledgments

First of all, I would like to express my gratitude to my *Doktorvater* Prof. Dr. H. Schamel. Although obvious, it is necessary to say that without him, this thesis would have never been possible. His patient and kind guidance over the last years as well as his scientific enthusiasm and encouragement provided me the greatest help that one could expect from a supervisor.

Of course, I could also not forget to thank my parents for the support and advice that I have always found in them and for teaching me, among all other essential things, the importance of pursuing my studies. **¡Gracias!**

I want also to mention Aberto de Lózar and Carmen Pérez León, with whom I came to Bayreuth, for their standing friendship and continuous support. To Pavel Akimov I am grateful for the assistance he provided me in my first days here and for being always there whenever I needed something. Martin Riedel was also a big help thanks to his patience with my German and, not to forget, his lessons on cooking. But I could also not leave out the members of the *spanish community* in Bayreuth, which gave me their friendship and were always ready for juicy debates, sometimes as sharp as Martin's cooking, in the *Cafeteria*: Mar García, Luis Miguel Fernández, Alberto Rivera, Laura Torre and many others.

And, last but not least, I would like to thank all my friends and partners in Sevilla, in the Faculty of Physics and in any other place, because they were so nice to believe in me and because they have the virtue of, just due to their being there, make the world a little bit warmer.